CDF/ANAL/TOP/CDFR/9589
February 20, 2009
Version 1.2

Measurement of the single top production cross section in the $\not\!\!E_T$ plus jets sample

A. Apresyan[1], D. Bortoletto[1], F. Margaroli[1], K. Potamianos[1]

[1] *Purdue University*

Abstract

Top quarks are produced mostly in pairs at the Tevatron through the strong force. The production of one top quark per process is allowed through electroweak processes, with its cross section being half the size of the former. In addition, the less distintinctive signature makes it much harder to observe. Tevatron experiments looked until now only in events where one high energy electron or muon has been identified, in order to suppress the huge QCD background and achieve a reasonable signal over background ratio. We look here for the first time at events where no electron or muon has been identified, and where tau leptons decay hadronically and are reconstructed as calorimetric jets. Multivariate analysis techniques are used to discriminate the single top signal against the dominant backgrounds, and we use a likelihood profile of this discriminant to measure the production cross section of single top events, reaching the expected sensitivity of $\sigma^{exp}_{s+t} = 2.7^{+2.3}_{-2.1}$ pb. Once looking at the first $2.1\,\mathrm{fb}^{-1}$ of data recorded by CDF, we measure a cross section of $\sigma^{obs}_{s+t} = 4.9^{+2.5}_{-2.2}$ pb. We also measure the V_{tb} element of the CKM matrix: $|V_{tb}| = 1.24^{+0.34}_{-0.29} \pm 0.07$(theory). We also find that $|V_{tb}| > 0.36$ at 95% confidence.

Contents

1 Introduction

The top quark is a very interesting particle in the Standard Model, and it has been studied extensively at the Tevatron since its discovery in 1994 [1, 2] which happened looking at events where top quarks are produced in pairs. The top has a lifetime shorter than the hadronization time, and as such it is the only quark which decays before hadronizing. The Standard Model predicts that the top quark decays to a W boson and a b quark almost 100% of the times, and the W subsequently decays hadronically or leptonically. Events with top pair production appear as events with high multiplicity of energetic objects (jets and leptons) and as such are relatively easy to isolate. In addition, the presence of b-jets allows us to use b-tagging algorithms to further suppress backgrounds.

On the other hand, the single top production is one of the rarest Standard Model processes produced at the Tevatron. It is a source of 100% polarized quarks. Most importantly, the single top cross-section is a direct measure of V_{tb} since the former is proportional to the square of the latter. A good measure of the elements CKM matrix is important in understanding CP violation.

It is produced mostly through the t-channel with a cross section of 1.98 pb, or through the s-channel with a cross section of 0.88 pb [3, 4, 5]. Events with an hadronically decaying W are especially hard to isolate, as the characteristic signature is 4 quarks in the final state, and so four hadronic jets, and the QCD processes which give rise to the same signature have a production cross section many orders of magnitude higher. The CDF and D0 collaborations focused then on events where the W decays leptonically, hoping to improve the signal-over-background ratio by looking the more distinct signature of ≥ 2 jets out of which at least one is b-tagged, a high P_T lepton and a neutrino [7, 8]. Unfortunately, the efficiency of e or μ identification is not 100%, and the coverage of both electron and muon detection in η is pretty limited at CDF. Moreover, τs are usually detected only through their leptonic decays, and the three-prong τ identification algorithms are not widely used.

The cross section being so low, and the processes that mimic the signal so abundant, CDF and D0 are having hard times to reach the observation level on this interesting process. We look here at events discarded by other analysis, i.e. events where there are no identified leptons, thus relying solely on the signature of high P_T jets and missing transverse energy.

This analysis stems from the event selection implemented for the latest search for the Standard Model Higgs boson in the same channel, which is described in note 9393 [9]. In that analysis, particular attention has been dedicated to increasing acceptance to events where the Higgs is produced toghether with a W boson, which has a very similar signature to the events which are here of interest. In order to reach such a goal, particular care has been devoted also to the background composition understanding and modeling. Measuring the single top cross section in this sample, would also give us more confidence in the tools and techniques used for the Higgs search. We describe in this note how starting from the event selection used in the Higgs analysis, we focused here on the single top properties to isolate it from the remaining backgrounds.

Having no leptons identified in the final state, this channel is peculiar in the fact that backgrounds are many orders of magnitude higher than the signal even after requiring the final state topology of missing transverse energy plus b-jets. It is thus necessary to develop an event selection which reduces backgrounds to a more manageable size before trying to build a discriminant to measure the single top cross section. The QCD multijet production is peculiar in the sense that it is the only background where the $\not\!\!E_T$ is mainly instrumental. We study the dynamical properties of these events and implement a multivariate technique with the goal of cutting out the dominant QCD multijet background as much as possible, separating it from the signal. We then use again a machine learning technique to discriminate the signal from the surviving backgrounds, and finally scan its output distribution to measure the production cross section of the single top processes in the $\not\!\!E_T$+jets final state. This sample being statistically independent from the one used till now by CDF, it will provide independent measurements of $\sigma_{singletop}$ and V_{tb} which can be regarded as a consistency check; moreover, these measurements can be combined to the existing measurements to increase the precision in the $\sigma_{singletop}$ and V_{tb} determinations.

2 The trigger requirements

The events analyzed here are recorded using the missing E_T plus jets trigger path. This trigger has been changed along time in order to accommodate higher instantaneous luminosity regime while keeping the bandwidth low.

The data used in this analysis is collected with MET35_&_TWO_JETS trigger. It triggers on $\not\!\!E_T$ and two jets (this trigger was changed several times during 0i data taking period, differences are described in[9]).

The events collected by these triggers can be found in the emet0d, emet0h, emet0i and emet0j data sets. In this analysis we process 2.1 fb^{-1} of data in these samples.

Trigger efficiency were initially obtained using 1.0 fb^{-1}[12] and recently updated using 2.1 fb^{-1} of data [20]. For this version of analysis we use the latter trigger parameterization summarized in the following:

$$\epsilon_{L1}(\not\!\!E_T) = \frac{1}{1 + e^{\frac{31.2-\not\!\!E_T}{6.6}}} \tag{1}$$

$$\epsilon_{L3}(\not\!\!E_T) = \frac{1}{1 + e^{\frac{37.0-\not\!\!E_T}{6.6}}} \tag{2}$$

and the uncertainties (on the whole trigger path) are provied by:

$$\Delta\epsilon/\epsilon(\not\!\!E_T) = \begin{cases} 0.01 \times \frac{(80-\not\!\!E_T)}{10} + 0.25 \times \left(\frac{80-\not\!\!E_T}{50}\right)^4 & \text{if } \not\!\!E_T < 80 \text{ GeV}, \\ 0. & \text{if } \not\!\!E_T \geqslant 80 \text{ GeV}. \end{cases} \quad (3)$$

3 The event selection

Most of the content of this paragraph is taken from CDF note 9358 [9], where all the details and motivation of the current choices can be found. Events passing the trigger are required to comply with the following additional requirements. First of all we require the v19 Good Run List with good EM and Silicon, to ensure that all the necessary subdetectors were operational during data taking. We exclude run ranges 217990-220272 and 245448-246231 due to the presence of hot towers in this periods of data-taking. In addition to this we modify the good-run-list following the instructions on the official web-page, to remove the runs with missing beam-lines.

Due to a hardware problem in L1MET calculation, events with a high $\not\!\!E_T$ might be discarded by the $\not\!\!E_T$+JETS trigger. This happens when the energy deposited in a single tower at Level 1 exceeds 127 GeV in which case only 127 GeV is used in the $\not\!\!E_T$ calculation. These type of events should be automatically accepted, but it has not been happening until very recently when the problem was fixed. We recover these events by collecting them from Jet100 sample, as described in [19]

We do not need a high purity lepton sample, but indeed the opposite, so we use a set of loose identification cuts to reject events with isolated leptons. We use a slightly modified version of the commonly used CMIO muon identification cuts for the track isolation[9]. We constructed these cuts to be loose enough to prevent double-counting the single top signal already considered in the channel with identified leptons.

Jets are reconstructed offline using the JetClu algorithm with a cone in the $\eta - \phi$ space of radius R=0.4. We denote as “tight” jets with $|\eta| < 2.4$ and uncorrected transverse energy $E_T > 10$ GeV. We correct a jet four momentum using the latest energy corrections, applied up to level 5. We further correct jets by reconstructing their four-momenta according to the H1 prescription [11]. The H1 algorithm was chosen for the Higgs analysis because it provides a slight ($\sim 10\%$) increase in jet energy resolution; we decided for simplicity to keep the same definition here. Tight jets are finally required to have H1-corrected $E_T > 15$ GeV. In order to improve the signal to background ratio further, we need to identify jets originating from a b quark. We do so employing both the SECVTX and JetProb b-tagging algorithms. We subdivide the sample into three orthogonal tagging categories: 1 SECVTX tag “tight”, 1 SECVTX tag “tight” plus 1 JetProb ($< 5\%$) tag and 2 SECVTX tag “tight”. While in single top events it is hard to tag both jets, and so the 2 tags samples have poor sensitivity to single top presence, for semplicity we kept the same configuration used in the corresponding Higgs analysis.

Previous studies found that the trigger becomes fully efficient only at high values of the $\not\!\!E_T$ and the two leading jets E_T; in this analysis we loosen those cuts to the following values: $\not\!\!E_T > 50\,\mathrm{GeV}$, $E_T(j1) > 35\,\mathrm{GeV}$, $E_T(j2) > 25$ GeV. Since with such a choice the selected events are no longer in the the plateau of the trigger efficiency, we need to apply the trigger parametrization to our Monte Carlo simulations. It was observed that the trigger efficiency depends also on the difference in R space between the two jets. We preserve this choice which maintain the trigger fully efficient: $\Delta R > 1$ (to avoid cluster merging at L2, which would result in a loss of efficiency). The two leading jets are required to be not very forward: $|\eta(j_i)| < 2$, while the leading jet is required to be very central to match the trigger requirements $|\eta(j_{1,2})| < 0.9$.

We accept events with 2 or 3 tight jets. We expect events with mostly 2 jets in the s-channel, while single top appears as events with three jets in the NLO t-channel events, or where the charged lepton coming from the W is reconstructed as a jet[1].

In fact, in some cases the W decays to $e\nu$ and the electron fails the CDF electron identification algorithm, but is reconstructed as a jet by JetClu; or when the W decays to $\tau\nu$ and $\tau \to hadrons$. Finally, we accept events where one of the quarks from the final state radiates a quark or a gluon. We checked the acceptance to hadronic decays of the W from single top events, which resulted very small (less than 2%). As can be seen in Tab. 1,2, we have acceptance roughly half of the time to events where the W decays to taus, and the rest split in electrons and muons. Since electrons and taus leave energy in the calorimeter, they can be reconstructed as jets by JetClu. As seen again in Tab. 1,2, this happens roughly 40% of the time (but mostly taus). Fig. 1 shows the distribution of the Eta direction of the lepton from $W \to l\nu$ decay, in s-channel.

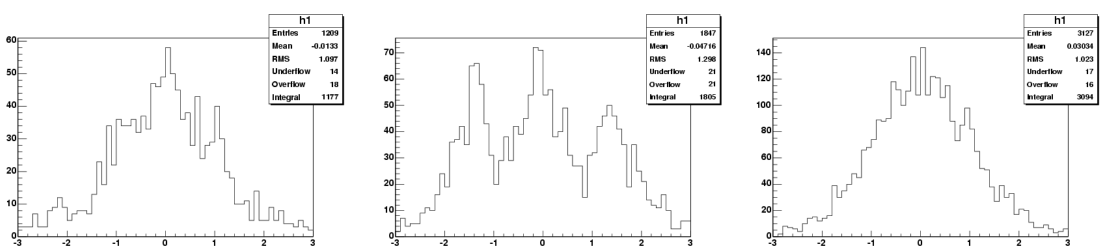

(a) $W \to e\nu$ (b) $W \to \mu\nu$ (c) $W \to \tau\nu$

Figure 1: Distribution of Eta direction of the lepton from $W \to l\nu$ decay, in s-channel.

Most of background processes considered in this analysis do produce real high $\not\!\!E_T$, e.g. W/Z decays to neutrinos or muons, which escape detection in the calorimeter. Additionally b-quarks produced in an event can decay semi-leptonically, which also produce real $\not\!\!E_T$. Mis-measurements in the calorimeter, on the other hand, can cause a QCD multijet event which has no real $\not\!\!E_T$ to appear with energy imbalance in transverse plane. Since QCD multijet production has a very large cross-section, these events constitute a big fraction of $\not\!\!E_T$+jets data sample. With the relatively low $\not\!\!E_T$ cut and no leptons, most of the data at this analysis stage is composed of QCD production of

[1] Or just whenever there is additional radiation from the initial or final state.

s-channel	$W \to e\nu$	$W \to \mu\nu$	$W \to \tau\nu$
all events	19%	30%	51%
2 jet events	20%	34%	46%
lepton-matched	1.2%	–	4.4%
3 jet events	17%	24%	59%
lepton-matched	5.4%	–	31%

Table 1: Contributions to 2/3 jet events from different leptonic decay modes of the W-boson in single top s-channel events

t-channel	$W \to e\nu$	$W \to \mu\nu$	$W \to \tau\nu$
all events	19%	29%	51%
2 jet events	21%	32%	47%
lepton-matched	3.3%	–	6.9%
3 jet events	17%	23%	61%
lepton-matched	6.5%	–	36%

Table 2: Contributions to 2/3 jet events from different leptonic decay modes of the W-boson in single top t-channel events

two or three jets, where one of the jets is poorly measured, resulting in a large transverse energy imbalance. Due to this mismeasurement, most of the time the poorly measured jet will be the second highest E_T jet; the $\not\!\!E_T$ will as a consequence be aligned to it in the transverse plane. We label events having $\Delta\phi(\not\!\!E_T, j2) < 0.4$ as our QCD control region as in the past analysis; this events are used to derive a data-driven background modeling [14] and to check the same technique on a very pure QCD region. For the preselection we are describing in this note, where we want to isolate a signal, the above cut is reversed. After that cut, QCD events where the $\not\!\!E_T$ is purely instrumental, and so aligned with the jets, remain the dominant background. Therefore we cut on $\Delta\phi(\not\!\!E_T, j1) > 1.5$ and $\Delta\phi(\not\!\!E_T, j3) > 0.4$ to further suppress the QCD background. As can be seen in Tab. 3, those cuts remove $\sim 10\%$ of the signal while reducing the backgrounds almost of a order of magnitude.

As a way to get a better estimate of the event true missing energy we calculate the $\not\!p_T^{tr}$, which is defined as negative vector sum of track p_T's:

$$\not\!p_T^{tr} = \left| - \sum_{tracks} \vec{p}_T^{\,i} \right| \tag{4}$$

For true $\not\!\!E_T$ events $\not\!p_T^{tr}$ is highly correlated with Calorimeter $\not\!\!E_T$, while for QCD events with mismeasured jets it is not. This criteria has been already used first by D0 [15], and then in all following analyses by CDF [17] [18] and D0 [16] collaborations.

Thus, $\not\!p_T^{tr}$ would provide an additional handle to separate mismeasurements from real $\not\!\!E_T$ events.

The direction of $\not\!p_T^{tr}$ is calculated similar to $\not\!\!E_T$

$$\varphi_{\not p_T^{tr}} = \arctan\left(\frac{\not\!p_y^{tr}}{\not\!p_x^{tr}}\right) \tag{5}$$

where $\not{P}_x^{tr}$ and $\not{P}_y^{tr}$ are sums of track momenta in x and y directions respectively.

We found that the most discriminating variables that we can extract out of tracking are, ranked in order of separation power, the $\Delta\phi(\not{P}_T^{tr}, \not{E}_T)$, the absolute amount of $\not{P}_T^{tr}$, the $\Delta\phi(\not{P}_T^{tr}, j_i)$, and use them all in the following.

Selection cut	#Events s-channel	Acc.(%)	# Events t-channel	Acc.(%)	# Events DATA
Trigger driven selections	131.3	100%	200.4	100%	523207
Electron veto	102.9	78.3%	154.6	77.1%	512383
Isolated track veto	71.3	54.2%	110.0	54.8%	500813
$\not{E}_T$ not collinear to any jet	63.6	48.4%	101.0	50.3%	56301
Tight+Tight	8.4	13.1%	1.9	1.8%	190
Tight+JetProb (Excl to TT)	7.1	11.1%	1.9	1.8%	300
Tag (Excl to TT&TJ)	18.5	29.1%	37.3	36.9%	3520

Table 3: Acceptance of signal and backgrounds after sets of cuts in 2.1 fb^{-1}. The acceptance is relative to the events surviving the trigger requirements. The events were weighted by cross-section and efficiencies after applying the final selection.

More details can be found in the CDF note dedicated to the event selection for the corresponding Higgs search [9].

After the event selection listed above, the number of signal events, subdivided in the three tagging categories, are presented in Table 3.

4 Signal and Background Simulation

We present here the modeling of our signal and background. We use MC samples from Pythia or MadEvent for all the backgrounds but QCD multijet production, where a data-driven model has been developed. This modeling has already been used in the Higgs analysis in the same $\not{E}_T$+jets channel. The only differences concern the modeling of the top-related processes (Single Top & Top Pair), for which we use the official CDF top samples.

All samples are reconstructed with CDF-soft version 6.1.4mc set to realistic (run-dependent) mode. Later the production output is ntuplized to Standard Ntuples with dev243 under CDF-soft version 6.1.4.

4.1 Single top Monte Carlo samples

To model the single top dynamics, we use a sample generated with MadGraph/MadEvent with the parton showering performed by Pythia; the latter is the official sample used in CDF, as it allows the description of the polarization of the outgoing top quark. The official sample is actually composed of three subsamples, one s-channel sample, and a LO and a NLO t-channel sample, whose matching has been performed following instruction from the single top group. Training, acceptance studies, expected sensitivity of the technique, control sample studies and the final measurement are all performed using the official single top sample.

4.2 Background Simulation

In the signal events under study the single top events appear as two or three jets, and a W boson which decays to undetected e or μ, or τ reconstructed as a jet. The most important characteristics of these events are the large intrinsic missing transverse energy, relatively low jet multiplicity, and the lack of (detectable) isolated leptons. There are numerous Standard Model processes that can produce this signature. In this section, we list all the backgrounds considered in the analysis.

4.2.1 Multijet backgrounds

The most significant background at the first stage of the analysis is the QCD multijet processes. QCD jet production has a large cross-section (μb), which is about 9 orders of magnitude greater than the signal before requiring the first b-tag. Although, these processes generally do not have intrinsic $\not{E}_T$, mismeasured jets do cause imbalance in the total transverse energy by which the QCD events can pass the basic selection cuts if one of the jets is mis-tagged. Furthermore, QCD b-quark pair production yields taggable jets and if one b undergoes a semi-leptonic decay large $\not{E}_T$. In both cases, the missing transverse energy tends to be aligned parallel or anti-parallel to the first or second most energetic jet. This topology provides us one of the most effective devices against the QCD background.

Due to the large cross-section, it is practically impossible to generate enough statistics to simulate all QCD processes. In the past version of the analysis we have used Monte-Carlo simulation to estimate Heavy Flavor QCD production.

We have developed a new method to estimate QCD background from data, which is documented in [14]. This technique allows us to estimate not only heavy flavour QCD production, but also processes with a light flavour jet falsely tagged as a b-quark. Additionaly it allows us to model Single SecVTX tagged data sample, which adds additional sensitivity to the analysis.

4.2.2 Top pair production

The top pair-production yield a measurable contribution to the background in the signal region. Due to its large mass and the semi-leptonic decay of the top, these events are energetic, bear large $\not{E}_T$ and high jet multiplicity. We use Monte Carlo samples generated for the Top Group. The $t\bar{t}$ events were generated with Pythia at 175 GeV and normalized with $6.73^{+0.71}_{-0.79}$ pb (*Cacciari et al.* [6]) to the luminosity.

4.2.3 Di-boson and W/Z backgrounds

The electroweak backgrounds were all generated with Pythia. All the W and Z samples were filtered for a b- or c-quark at generator level with the exception of $W \rightarrow \tau\nu$ and $Z \rightarrow \tau\bar{\tau}$. In some cases, the events were also $\not{E}_T$ filtered, after the event reconstruction whenever it resulted in a significant reduction of the event number.

In both cases of the Z + h.f. and W + h.f. backgrounds, we normalized using the inclusive cross-sections measured by the EWK group. These samples were generated to be identical to the ones used in the EWK group for those measurements with the exception of the filters; therefore we correct the cross-sections with the filtering efficiencies. The measurements this way, correspond to a k-factor of 1.4 with respect to the Pythia LO predictions. There are no cross-section measurements for $W \rightarrow \tau\nu$ and $Z \rightarrow \tau\bar{\tau}$, therefore we use the LO Pythia cross-section corrected by 1.4.

In this way, Z/W samples have the correct normalization regarding their inclusive production. However, the heavy flavor production simulated by Pythia provides a possible source of systematic error. We assign a 40% uncertainty based on the total error of the Z + h.f. cross-section measurement in CDF (CDF Note 7780). The analysis we quote, measured the cross-section ratio between inclusive Z and Z + h.f. processes and found that the LO Pythia prediction scaled by a k=1.38 well reproduces the Z + h.f. seen in data. This analysis also used a b/c-filtered Pythia simulation identical to ours.

In the diboson simulations, the bosons' decays are all-inclusive. We use the LO Pythia cross-sections scaled by a k-factor corresponding to the ratio between the NLO and LO cross-section prediction in MCFM. The LO MCFM predictions are also consistent with those from Pythia and are reported to be in good agreement with the data. An 11.5% uncertainty of on the MCFM cross-section is assigned for the diboson normalization.

5 The search for the signal

In this section we present the strategy used to obtain the discrimination between the signal and the background. We present our two step approach using multivariate analysis to form the final discriminant, whose output distribution will be scanned to measure the production cross section of the single top processes in the $\not\!\!E_T$+jets final state.

5.1 Discrimination of background QCD multijet events from the signal

As stressed before, the main background at this stage of the selection is the QCD production of two or three jets, and events with mistags. We investigated the dynamic of the events in the sample, using the QCD plus mistags modeling derived from applying a tag rate parametrization to the data. Looking at a large set of variables, we keep here only the ones for which those events have a very different behaviour with respect to the signal.

The single top signal used for the training is a mixture of 50% s-channel events and 50% t-channel events, which is roughly what we expect to accept after the event selection described in the previous paragraph. We use only events with at least one tight tag. The background is pre-tag data weighted by a tag rate parameterization function, wich is a first approximation of the QCD multijet background.

The multivariate technique used here is an artificial neural network (ANN or NN). We use a MultiLayerPerceptron (MLP) as implemented inside the TMVA[2] package. Our network has 2 hidden layers. The number of nodes of each layer are 15:30:15:1. The neuron activation function is the hyperbolic tangent. We use a LearningRate of 0.01 and a TestRate of 5. The other parameters are set do the default in TMVA. We train for 500 epochs and check the convergence plots for overtraining.

The 15 input variabels are (from left to right and top to bottom in fig. 2):

- Absolute amount of the missing transverse momentum, $\not\!\!P_T^{tr}$;
- Absolute amount of the missing transverse energy, $\not\!\!E_T$;
- Difference in ϕ between missing transverse energy $\not\!\!E_T$ and missing transverse momentum $\not\!\!P_T^{tr}$, $\Delta\phi(\not\!\!E_T, \not\!\!P_T^{tr})$;
- Maximum of the difference in the R space between two jets, taking two jets at the time;
- Minimum of the difference in ϕ between the $\not\!\!E_T$ and each jet j_i, considering all two or three $(\not\!\!E_T, j_i)$ pairings;
- Minimum of the difference in ϕ between the $\not\!\!P_T^{tr}$ and the jets, considering all two or three $(\not\!\!P_T^{tr}, j_i)$ pairings;

[2] http://tmva.sourceforge.net/

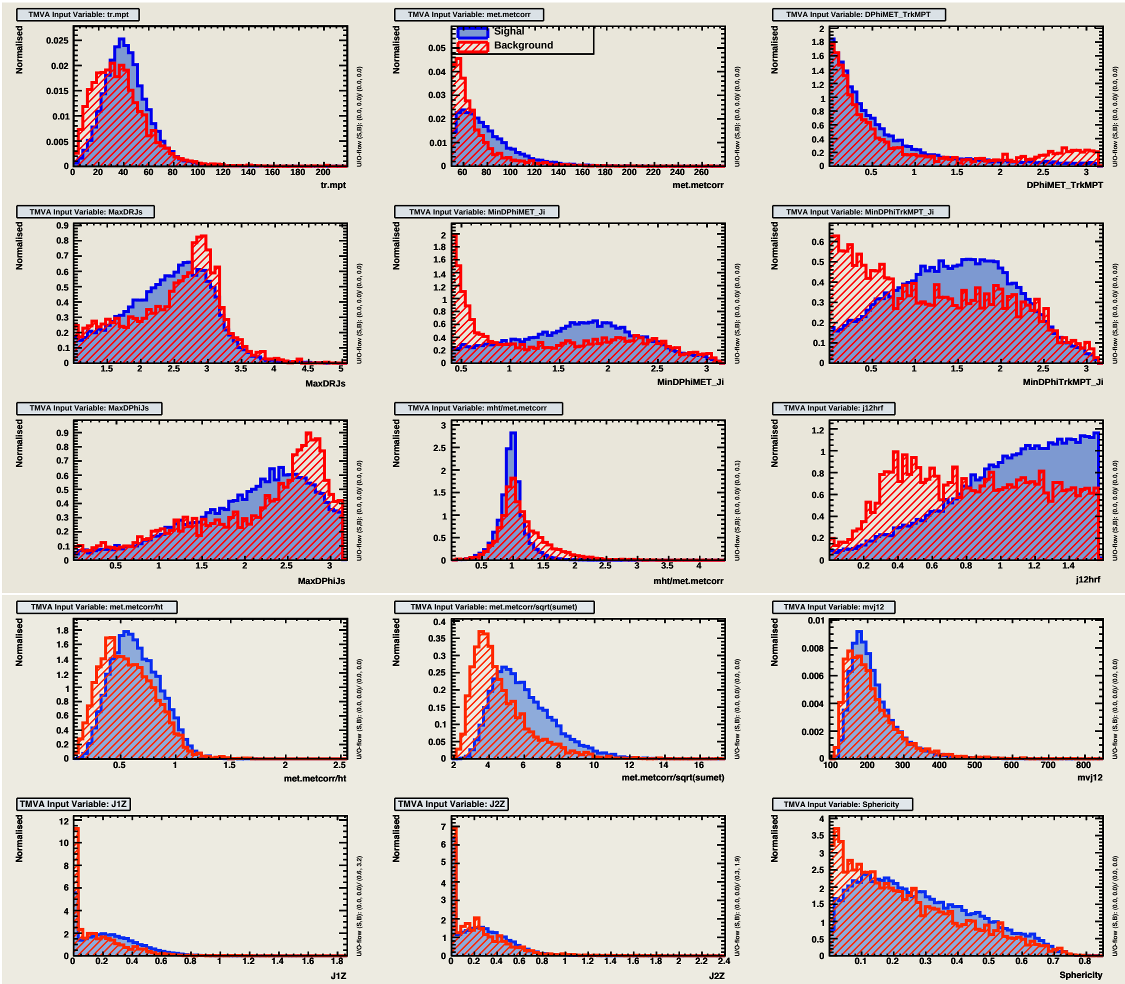

Figure 2: QCDNN input variables for signal and background mixtures

- Maximum of the difference in ϕ between two jets directions, taking two jets at the time;
- Ratio of $\not{H}_T$ (vector sum of tight jet E_Ts) and the $\not{E}_T$;
- $\Delta\phi$ between the direction of the leading jets in two-jet rest frame and the direction of the boost;
- $\not{E}_T$/HT: $\not{E}_T$ over scalar sum of the two leading jets MET;
- $\not{E}_T$ significance : $\not{E}_T$ over square root of sum E_T (all calorimetric activity);
- Invariant mass of $\not{E}_T$, j_1 and j_2;
- Z($j_{1(2)}$) : Ratio of the sum of Pass 1 track P_Ts to the $P_T(j_{1(2)})$;
- Event sphericity : S $= 1.5\ \times(\lambda_2+\lambda_3)$, where $\lambda_1 \geq \lambda_2 \geq \lambda_3$ are the eigenvalues of the sphericity tensor.

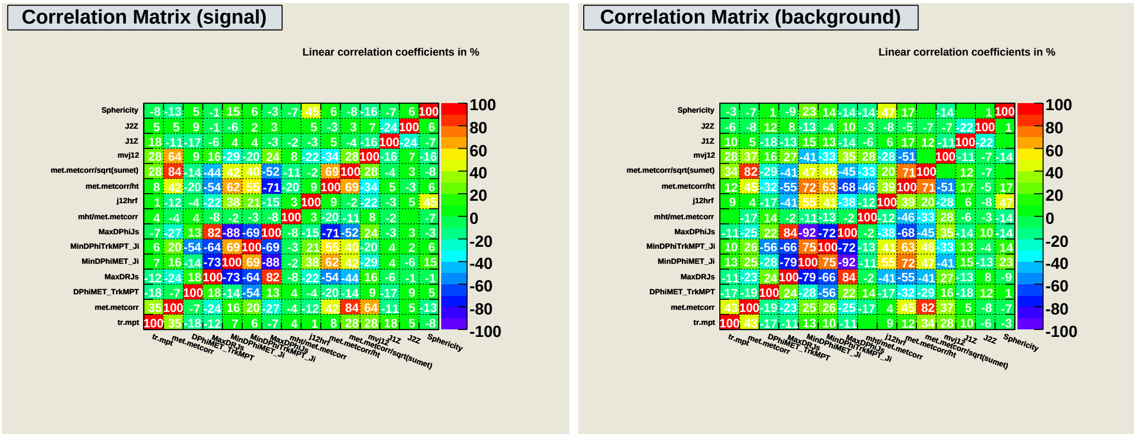

Figure 3: Correlations between the QCDNN input variables, for signal and background mixtures

The Fig. 2 shows the distributions of the input variables for the training sample under use. Fig. 3 shows the different correlation pattern between the input variables for the signal and background training samples.

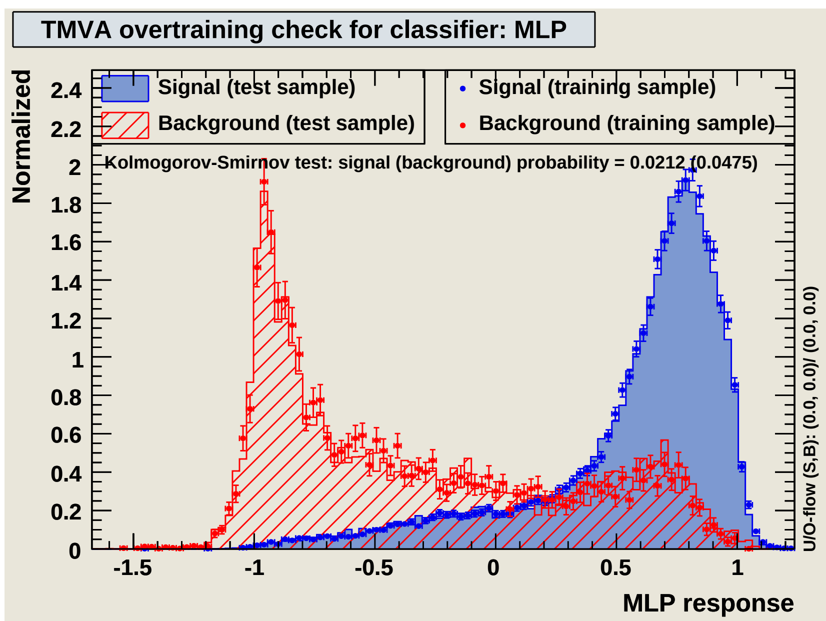

Figure 4: QCDNN output for the testing and training samples

Fig. 4 shows the NN output for the training and testing sample. Fig. 5 shows the QCDNN output, where it can be seen that this NN does a good job at discriminating multijet events, while keeping the signal to the right. We cut on this output at QCDNN > -0.1, to form the signal region. Doing so removes most the the QCD multijet background (77.2%) while keeping most of the signal (90.7%). When considering the total amount of background, we are removing 64.79% of it. This cut allows

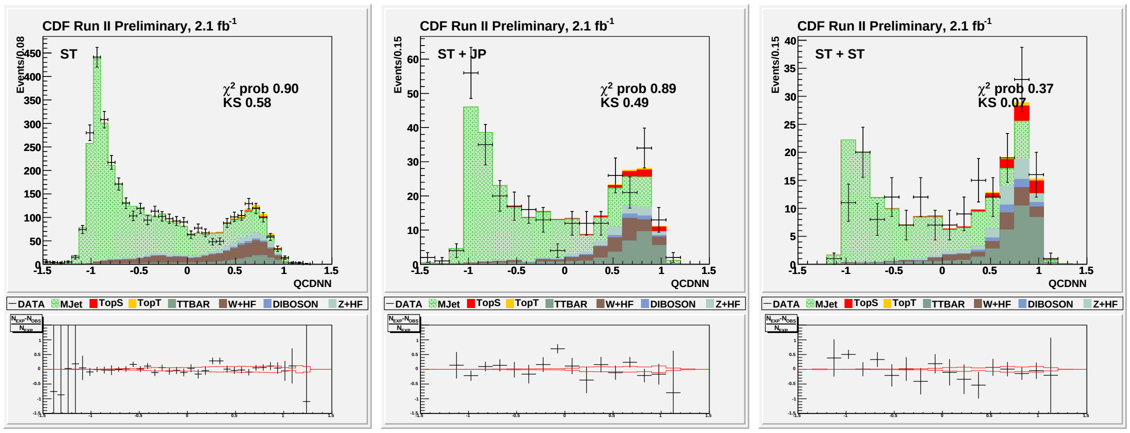

(a) Excl. ST (b) ST+JP (c) ST+ST

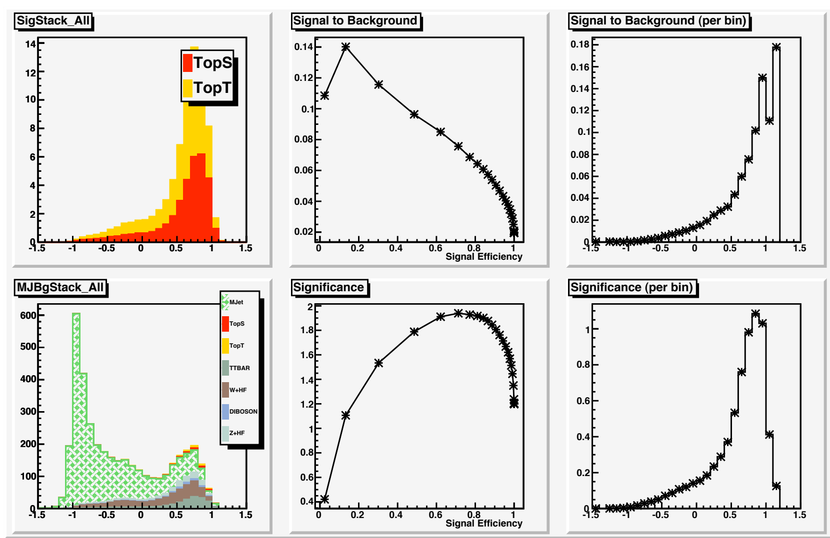

(d) At least 1 tight tag

Figure 5: QCDNN output in the pre-selection region

us to bring the overall S/B ratio of the events with at least one tight tag (i.e. the sum of our three tagging categories) from 1/50 to 1/20 (+150%) and the significance ($S/\sqrt{S+B}$) from 1.2 to 1.8 (+50%). The remaining events, with QCDNN < -0.1, form a new control region: CR3. This QCD-rich region will be used to extract the normalization scale factor for the QCD multijet.

5.2 The final discrimimant

The QCDNN mentioned above does a good job at separating the QCD events and the mistags. We are now going to address the other major backgrounds (on top of QCD multijet, which is still the biggest background): top pair, W+h.f. & Z+h.f.

The single top signal used for the training is a mixture of 33% s-channel events and 67% t-channel events. We again use only events with at least one tight tag. The background consists of 58% pre-tag data weighted by a tag rate parameterization function, 20% $W \to \tau\nu$, 13% top pair & 9% $Z \to \nu\nu$. For the three latter, we use only events with at least one tight tag. The proportions are those from the exclusive single tag category, considering only processes contributing individually for more than 5% of the total background in that tagging category and re-weighting such as to constitute a full background (100%).

The multivariate technique used here is again MLP. Our network has 2 hidden layers. The number of nodes of each layer are 11:22:11:1. The neuron activation function is the hyperbolic tangent. We use a LearningRate of 0.01 and a TestRate of 5. The other parameters are set do the default in TMVA. We train for 500 epochs and check the convergence plots for overtraining.

The 11 variables used are (from left to right and top to bottom in fig. 6):

- Invariant mass of the second jet and missing transverse energy; the second jet in the $W \to \tau\nu$ events is often a τ, thus this variable is the reconstructed W transverse mass for the background events;
- Scalar sum of transverse energy of the two or three leading jets, H_T^3;
- Minimum of the difference in ϕ between the $\not{E}_T$ and each jet j_i, considering all two or three $(\not{E}_T, j_i)$ pairings;
- Z($j_{1(2)}$) : Ratio of the sum of Pass 1 track P_Ts to the $P_T(j_{1(2)})$;
- Absolute amount of the missing transverse energy, $\not{E}_T$;
- Absolute amount of the missing transverse momentum, $\not{P}_T^{tr}$;
- $\Delta\phi$ between the direction of the leading jets in two-jet rest frame and the direction of the boost;
- $\not{E}_T/H_T$;
- Invariant mass of $\not{E}_T$, j_1 and j_2;
- Invariant mass of all tight jets in the event, m_{3j};

The Fig. 6 shows the distributions of the input variables for the training sample under use.

Fig. 7 shows the different correlation pattern between the input variables for the signal and background training samples.

Fig. 8 shows the MLP output, where it can be seen that it still does a good job at discriminating the signal from the background.

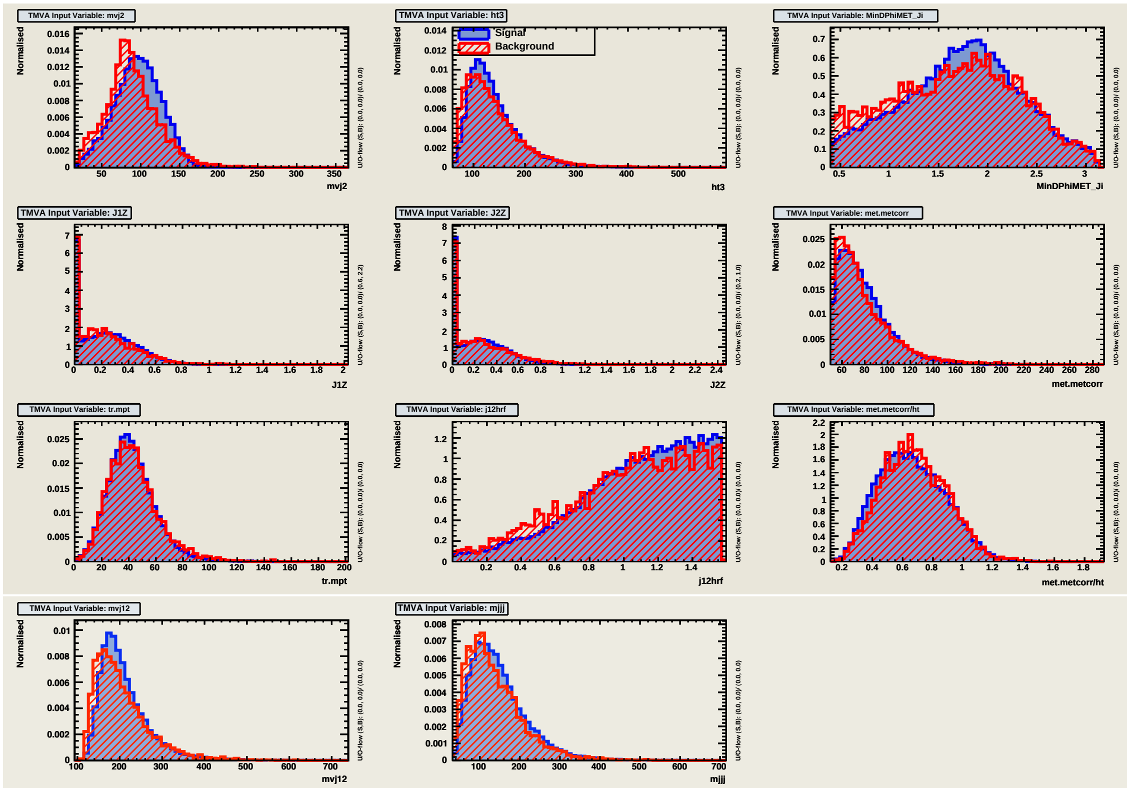

Figure 6: Final MLP input variables for signal and background mixtures

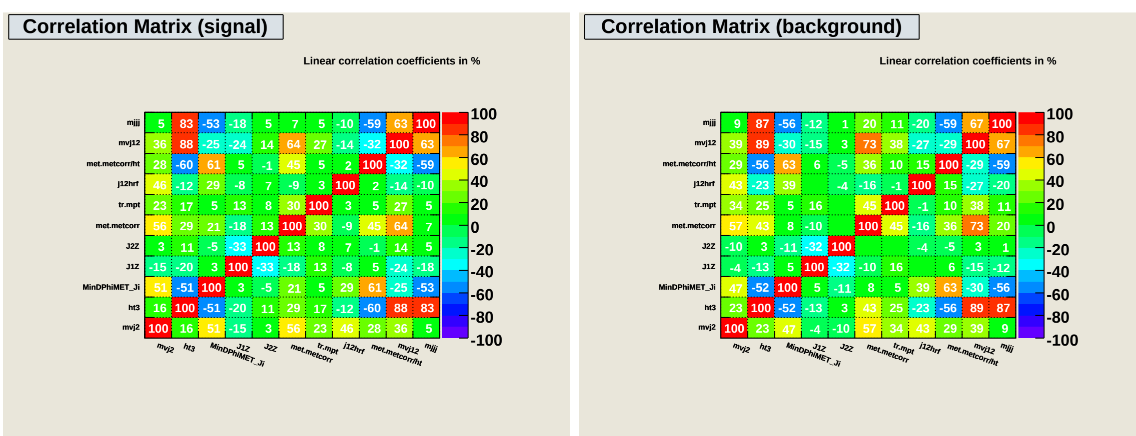

Figure 7: Correlations between the final MLP input variables, for signal and background mixtures

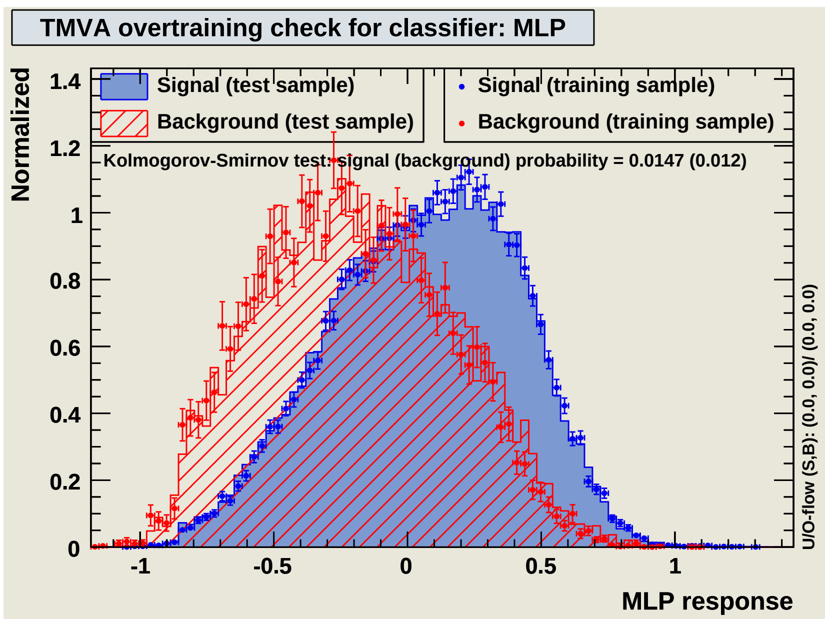

Figure 8: Final MLP output for the testing and training samples

6 Control regions

After the event preselection the data sample is mainly composed of multijet production (QCD+light flavour mistagged jets) processes. The high $\not\!\!E_T$ in these events comes both from severe mismeasurement of one of the jets, which causes the Missing Energy to point along one of the jets, and from real sources of $\not\!\!E_T$ such as neutrinos or muons from semi-leptonic b-decays. We use a subset of the $\not\!\!E_T$+JETS sample to derive a model for these types of events [14] which will be used in the final Signal Region defined in Sec. 5.1. We build three control regions, which we will use to test separately our data-driven and simulation-based background modeling.

6.1 Definitions

In order to test our ability to predict these type of backgrounds we check the performance of the method in two control regions. The first, Control Region 1 is a high statistics region where we check the data-based model and evaluate the systematic uncertainties on the shapes of various kinematic variables.

Since in the Signal Region we expect backgrounds originating from events with real high $\not\!\!E_T$, such as W/Z+jets, $t\bar{t}$, single top production and diboson production, we test our ability to predict this types of backgrounds in another Control Region. In order to remain unbiased to our final region, we test EWK/Top backgrounds in the kinematic region similar to Signal Region, with the exception of requiring at least one lepton in the event (all events with leptons are vetoed in the Signal Region definition). This region is sensitive to ElectroWeak/Top processes, and is used to check the overall shapes and normalizations of the Monte Carlo predictions. It also serves as an additional (but low statistics) check of the QCD model. The double-tagged events in this control region are dominated by the top processes, which yields an additional cross-check on top. In summary:

- Control Region 1 (QCD dominated)
  - All leptons are vetoed using the loose lepton identifications described in [9]
  - Azimuthal angular separation $\varphi(2^{nd}jet, \not\!\!E_T) \leq 0.4$
  - $\not\!\!E_T > 70$GeV (*50 GeV*$< \not\!\!E_T <$*70 GeV region is used to build the Tag-Rate-Matrix for the data-based model*)
- Control Region 2 (EWK processes)
  - Minimum 1 loose lepton is required
  - Azimuthal angular separation $\varphi(2^{nd}jet, \not\!\!E_T) > 0.4$
- Control Region 3 (QCD dominated, signal like)
  - All leptons are vetoed using the loose lepton identifications described in [9]

- Azimuthal angular separation $\varphi(1^{st} jet, \not\!\!E_T) \geq 1.5$, $\varphi(2^{nd} jet, \not\!\!E_T) \geq 0.4$, $\varphi(3^{rd} jet, \not\!\!E_T) \geq 0.4$
- $QCDNN < -0.1$ to have a high statistics sample where to check the data modeling as well as to extract the multijet normalization scale factor.

- Signal Region
  - $\not\!\!E_T > 50$
  - All leptons are vetoed using the loose lepton identifications described [9]
  - Azimuthal angular separation $\varphi(1^{st} jet, \not\!\!E_T) \geq 1.5$, $\varphi(2^{nd} jet, \not\!\!E_T) \geq 0.4$, $\varphi(3^{rd} jet, \not\!\!E_T) \geq 0.4$

Tables 4 to 6 list the expected and observed background yields in all Control Regions for all tagging categories. Comparisons of kinematic distributions in all Control Regions are shown in appendix A: fig. 20-28 for the CR1, in fig. 29-37 for CR2 and in fig. 38-46 for CR3. Additional CR plots can be found in [9]. The error line (in red) in the relative difference between observed and expected distributions takes only rate systematics into account, and does only so for the MC simulated backgrounds.

The QCD multijet scale factor is obtained by subtracting all MC processes (including the signal) from the data while weighting each event by the tag rate parameterization. We do so in each region but the signal region, where we apply the scale factor computed in CR3 (QCD dominated, signal like). However, for the validation plots, we did scale QCD to data in SR. This is the only place where we do not use SF from CR3 in SR.

Finally we show the comparisons of kinematic variables in the Signal Region in all tagging categories in Fig.56-65 (appendix A). Table 7 lists the expected and observed event yields in Signal Region. Also, we show in appendix B the shape comparison of all the input variables for each group of processes and each tagging category. We do so for the Signal Region and the Pre-selection region (SR + CR3).

Process	Excl. ST	ST+ST	ST+JP
Single Top S	0.6 ± 0.1	0.23 ± 0.04	0.27 ± 0.04
Single Top T	0.5 ± 0.1	0.02 ± 0.01	0.03 ± 0.01
Top Pair	7.0 ± 0.5	1.6 ± 0.2	1.9 ± 0.3
Di-Boson	0.9 ± 0.5	0 ± 0	0.1 ± 0.1
W + h.f.	20.5 ± 21.6	0.5 ± 0.3	1.8 ± 1.2
Z + h.f	26.8 ± 22.4	3.0 ± 1.4	3.9 ± 2.0
QCD Multijet	8751 ± 141	597 ± 32	1308 ± 55
Exp. Signal	1.1 ± 0.1	0.26 ± 0.04	0.31 ± 0.04
Exp. Background	8806 ± 148	602 ± 32	1316 ± 55
Total Expected	8807 ± 148	602 ± 32	1316 ± 55
DATA	8807	602	1316

Table 4: Number of expected and observed events in the CR1 (QCD) in all tagging categories.

Process	Excl. ST	ST+ST	ST+JP
Single Top S	15.8 ± 0.3	7.6 ± 0.2	6.4 ± 0.2
Single Top T	31.9 ± 4.6	1.7 ± 0.1	1.4 ± 0.1
Top Pair	204.9 ± 25.7	61.8 ± 12.2	56 ± 12.1
Di-Boson	24.7 ± 6.4	2.4 ± 0.4	2.4 ± 0.5
W + h.f.	148.0 ± 57.9	10.1 ± 2.7	11.6 ± 3.1
Z + h.f	27.7 ± 13.8	1.7 ± 0.9	2.8 ± 1.3
QCD Multijet	455 ± 32	21.6 ± 9.5	44.5 ± 13.6
Exp. Signal	47.7 ± 4.6	9.3 ± 0.2	7.9 ± 0.2
Exp. Background	860 ± 83	98 ± 16	117 ± 19
Total Expected	908 ± 83	107 ± 16	125 ± 19
DATA	908	107	125

Table 5: Number of expected and observed events in the CR2 (EWK) in all tagging categories.

Process	Excl. ST	ST+ST	ST+JP
Single Top S	2.1 ± 0.1	0.36 ± 0.04	0.48 ± 0.05
Single Top T	3.8 ± 0.2	0.09 ± 0.02	0.17 ± 0.03
Top Pair	21.7 ± 0.8	2.0 ± 0.2	2.7 ± 0.3
Di-Boson	6.7 ± 1.1	0.3 ± 0.2	0.4 ± 0.2
W + h.f.	119.0 ± 52.2	0.7 ± 0.6	2.8 ± 1.3
Z + h.f	40.6 ± 13.8	1.3 ± 0.6	2.1 ± 0.8
QCD Multijet	2149 ± 97	68.2 ± 8.9	157.4 ± 15.7
Exp. Signal	5.9 ± 0.2	0.46 ± 0.05	0.65 ± 0.06
Exp. Background	2337 ± 117	72.5 ± 9.0	165.4 ± 15.8
Total Expected	2343 ± 117	73 ± 9	166 ± 16
DATA	2343	73	166

Table 6: Number of expected and observed events in the CR3 (QCD, signal like) in all tagging categories.

CDF Run II Preliminary, 2.1 fb^{-1}

Process	Excl. ST	ST+ST	ST+JP
Single Top S	15.7±2.0	7.6±0.9	6.3±0.8
Single Top T	31.2±4.9	1.7±0.2	1.6±0.2
Top Pair	125±23	30.3±5.8	29.2±5.7
Di-Boson	33.0±6.5	4.9±0.6	4.2±0.6
W + h.f.	269±113	12.7±7.5	22.7±13.7
Z + h.f	105±53	11.8±5.8	11.8±6.0
QCD Multijet	592±27	28.9±3.8	58.5±5.8
Exp. Signal	46.8±5.2	9.3±1.0	7.9±0.8
Exp. Background	1125±169	89±15	126±21
Total Expected	1172±169	98±15	134±21
DATA	1167	113	131

Table 7: Number of expected and observed events in the Signal Region in all tagging categories.

7 The single top cross section measurement

7.1 Systematics

The systematic uncertainties are:

- Luminosity Uncertainty. The procedure for determining the uncertainty on the luminosity for Run 2 until August 2004 is described in CDF Note 7446. This uncertainty amounts to 6% and applies to those simulations that are normalized to luminosity. This uncertainty does not apply on the QCD, which is data-driven.

- PDF Uncertainty. The PDF uncertainty has been determined using the method that is described in CDF Note 7051. In earlier analyses (see CDF Note [21]), it has been determined that a 2% uncertainty on the acceptance due to the choice of the PDF is sufficient.

- Jet Energy Scale Uncertainty. The Jet Energy Scale uncertainty was determined by varying the jet energy correction factor by plus and minus one sigma while correcting the transverse energy of the jets. This variation then propagates to the $\not\!\!E_T$ reconstruction, the calculation of the azimuthal direction of $\not\!\!E_T$ and thus to the expected number of events after applying the selection cuts. The influence of this variation is different for each background component; therefore, it needs to be determined separately by running the entire analysis code twice on all the simulated backgrounds.

  Since in this analysis we use H1 algorithm to correct jets, additional systematic uncertainties need to be assigned. This is done by varying p_T of the tracks used in H1 algorithm by $\pm 3\%$. The procedure is described in [11]

  The JES uncertainty can also modify the shape of the distributions. It is taken into account in the cross section calculation for each background channels separatelly and is also is propagated into the errors displayed in the data-MC comparison plots.

  In some cases, the JES can be very asymmetric. In the cross section calculation the $\pm 1\sigma$ shapes and rates are provided for each backgrounds and signal, thus taking the asymmetric nature of the uncertainty into account.

  The JES uncertainties are shown for each process and each tagging category in table 8.

- Multijet background. The systematic error on the normalization is obtained from the scale factor in CR3 and is 4.5% (from 1.079 ± 0.048) in the single tag, 13.1% (from 0.785 ± 0.103) in the ST + ST & 10% (from 0.762 ± 0.076) in the ST + JP tagging categories. Those numbers are obtained from CR3, propagating the errors:

$$\text{SF} = \frac{\text{DATA - Exp. (MC) Signal - Exp. MC Background}}{\text{QCD (before SF)}} \tag{6}$$

$$\frac{\Delta\text{SF}}{\text{SF}} = \sqrt{\left(\frac{\text{MC}_{Err}}{\text{DATA - MC}}\right)^2 + \left(\frac{\text{QCD}_{Err}}{\text{QCD}}\right)^2}, \tag{7}$$

Process	ST	ST+ST	ST+JP
Single Top S	-5.7% / +5.4%	-4.7% / +4.2%	-5.3% / +4.9%
Single Top T	-6% / +5.7%	-5.8% / +4.3%	-6.6% / +7.2%
TTBAR	-2.2% / +2%	-1.9% / +1.9%	-1.8% / +1.8%
WW	-6.9% / +8.4%	-0.5% / +0.4%	-11.3% / +35.4%
WZ	-7.6% / +10.4%	-4.3% / +9.3%	-8% / +8.8%
ZZ	-6.1% / +8.7%	-8.7% / +7%	-6.9% / +4.2%
$W \to e\nu$	-9.3% / +10.3%	-8.2% / +8.2%	-7.5% / +6.2%
$W \to \mu\nu$	-7.9% / +12.9%	-11.3% / +-2.3%	-6% / +2.7%
$W \to \tau\nu$	-16.2% / +19.9%	-13.1% / +11.2%	-6.9% / +11.5%
$Z \to ee$	-1.7% / +1.1%	-0.5% / +0.3%	0% / +0%
$Z \to \mu\mu$	-0.8% / +10.3%	-0.9% / +0.7%	-0.4% / +20.1%
$Z \to \tau\tau$	-22.5% / +13.5%	0% / +0%	-22% / +1.2%
$Z \to \nu\nu$	-8% / +9.2%	-8.3% / +7.7%	-4.9% / +7.7%
$Z \to bb$	-20.9% / +23%	-41.9% / +12.3%	-1.6% / +12.2%

Table 8: Uncertainties due to jet energy scale

where MC is the number of expected MC events (including signal), QCD is the QCD prediction before applying the scale factor, QCD_{Err} is the statistical error on the QCD prediction (before SF) and MC_{Err} is is computed adding the errors (stat. + syst.) on its components in quadrature. The values fo these for each tagging category are shown in table 9.

Process	Excl. ST	ST+ST	ST+JP
DATA	2343	73	166
QCD before SF	1992 +/- 65	86.9 +/- 11.3	207 +/- 20
Exp. (MC) Signal	5.9 +/- 0.2	0.46 +/- 0.05	0.65 +/- 0.06
Exp. MC Background	188 +/- 66	4.4 +/- 1.2	8.0 +/- 2.1

Table 9: Number of expected and observed events in the CR3 (QCD, signal like) in all tagging categories used to derive the QCD normalization scale factor. See table 6 for details.

We also take into account the normalization uncertainty on the processes which are part of the background in the region from which we get the QCD normalization. Those uncertainties are anti-correlated with respect to the normalization on these processes, and weighted appropriately. Table 10 shows the proportion of the MC processes in the CR3.

Additionaly, the variations in Tag Rate Matrix are taken into account (see TRF systematic).

- B-tagging scale factor. The efficiency of tagging a taggable jet in the simulation is different than that in real events. This difference has to be taken into account when calculating the predicted number of events in the simulation after requiring a tag. For the tight SecVTX tagger in 6.1.4 the correct scale factor is 0.95±0.01(stat)±0.04(syst) as it is described in CDF Note 8666, therefore we use a 4.3% error for all the simulated background components in the single and 8.6% in the ST+ST. For JetProbability tagger ($< 5\%$ operating point) the Data-MC scale

Process	ST	ST+ST	ST+JP
Top Pair	0.9%	2.7%	1.63%
W + h.f.	5.1%	1%	1.66%
Di-boson	0.3%	0.5%	0.25%
Z + h.f.	1.7%	1.8%	1.26%

Table 10: Contribution of MC processes in CR3.

factor is 0.846±0.017(stat)±0.066(syst), so we use 12.3% uncertainty for ST+JP category.

- W/Z+h.f. and Diboson Monte Carlo NLO corrections. We use a 40% uncertainty on the W and Z background prediction and 11.5% on the diboson as described in Section 4.2.3.
- Top pair production cross-setion. We use a ±12.4% uncertainty, from *Cacciari et al.* [6] (see 4.2.2).
- Trigger Efficiency. The trigger efficiency study is described in [20]. Since we are now using data below the full efficient region, we assign a systematic uncertainty to both MC based backgrounds and signal acceptances, by varying the trigger efficiency by $\pm$ 1σ. Table 11 summarizes the uncertainties assigned for each channel in all tagging categories.

Process	ST	ST+ST	ST+JP
Single Top S	±1.3%	±1.4%	±1.3%
Single Top T	±1.4%	±1.5%	±1.6%
TTBAR	±0.9%	±0.9%	±0.9%
WW	±1.3%	±1.4%	±1.2%
WZ	±1.2%	±1.7%	±1.4%
ZZ	±1.1%	±1.3%	±1%
$W \to e\nu$	±1.7%	±1.3%	±1.2%
$W \to \mu\nu$	±1.5%	±1.2%	±1.6%
$W \to \tau\nu$	±2.1%	±2.1%	±2%
$Z \to ee$	±2%	±1.3%	±0%
$Z \to \mu\mu$	±1.4%	±1.7%	±1.1%
$Z \to \tau\tau$	±2.4%	±0%	±2.5%
$Z \to \nu\nu$	±1.3%	±1.4%	±1.3%
$Z \to bb$	±2.4%	±2.6%	±2.4%

Table 11: Uncertainties due to trigger efficiency

- Lepton Veto. The uncertainty in the efficiency of these cuts were determined to be less than 2% [9].
- ISR/FSR. The uncertainty associated with the initial and final state radiation was evaluated for the signal by generating samples with more/less ISR/FSR according to the Joint Physics recommendation (see table 12). This uncertainty is applied to all top processes.

- Top mass dependence. The uncertainty associated with the variation of the top mass. We consider top masses of 170 & 180 GeV as $\pm 2\sigma$ variations (see table 13). This uncertainty is applied to all top processes.

Systematic	Single Tag		ST+ST		ST+JP	
Single Top S	More	Less	More	Less	More	Less
ISR	0.3%	3.8%	1.9%	6.8%	3%	7.7%
FSR	0.6%	5%	1.3%	5%	1.2%	8.8%
ISR/FSR	0.9%	8.8%	3.2%	11.8%	4.2%	16.5%
Single Top T	More	Less	More	Less	More	Less
ISR	-0.1%	1.4%	-3.3%	-0.1%	4.7%	7.3%
FSR	-2%	2.2%	-8.2%	-0.1%	-0.7%	9.1%
ISR/FSR	-2.1%	3.6%	-11.5%	-0.2%	4%	16.4%
Top pair	More	Less	More	Less	More	Less
ISR/FSR	-4.5%	2.4%	-0.5%	6.1%	-4.4%	-2.2%

Table 12: ISR/FSR variation uncertainties for single top and top pair

Process	Single Tag		ST+ST		ST+JP	
	More	Less	More	Less	More	Less
Single Top S	4.1%	-4.9%	4.9%	-4%	5%	-4%
Single Top T	3.5%	-5%	-3.2%	-16.4%	8.4%	-9.9%
Top pair	2.9%	2.7%	7.5%	3.7%	5.7%	-0.4%

Table 13: Top mass dependence for single top and top pair

- TRF. The uncertainty due to varying the tag rate function parameters. This is only applied to the QCD multijet background. The variations in TagRateMatrix, which is used to estimate the multijet background, can also modify the distrivutions. It is taken into account by varying the tagrate probability in each bin of the matrix by $\pm 1\sigma$, and the alternative shapes are used in the limit calculation.

- Signal contamination. The uncertainty associated with the removal of single top MC from data (applying the tag rate parameterization to both) to estimate the QCD multijet background. We vary the amount of single top we subtract by 50%.

- Background scaling. Because of the overlap we have with the other analyses, we have scaled down the background by 2% and assigned a systematic uncertainty of 2%.

The shape systematics for signal and background are shown in appendix C (fig. 80 -85) for each tagging category, with the binning used for the final fit, together with the ratio to the central value.

In summary, table 14 shows all the systematics, with their effects. More aspects of the treatment of systematics have been addressed in the Q&A page[3].

Systematic	Rate	Shape	Comment
Luminosity	6%	-	Not for QCD multijet
PDF	+0.7% / -0.4% (s-chan)	X	
	+2.3% / -2.1% (t-chan)	X	
	+0.8% / -1.4% (top pair)	-	
	2% (MC backgrounds)	-	
JES	-13.9% ... 23%	X	
QCD multijet normalization	4.5% (ST)	-	Only QCD multijet
	13.1% (ST + ST)	-	
	10.0% (ST + JP)	-	
B tagging	4.3% (ST)	-	
	8.6% (ST + ST)	-	
	12.3% (ST + JP)	-	
W & Z + h.f. cross-section	40%	-	
Di-bonson cross-section	11.5%	-	
Top pair cross-section	±12.4%	-	
Trigger Efficiency	±0% ... ± 2.6%	X	Not for QCD multijet
Lepton Veto	2%	-	
ISR/FSR	-4.5% ... 16.5%	X	Only top-processes
Top mass dependence	-16.4% ... 7.5%	X	Top mass only for V_{tb} and p-value
TRF	-	X	Only QCD multijet
Signal contamination	-	X	Only QCD multijet
Background scaling	2%	-	
Signal cross-section	± 12.4% (s-chan)	-	Only for p-value and V_{tb}
	± 12.6% (t-chan)	-	

Table 14: Summary of systematics

[3] http://www-cdf.fnal.gov/~karolos/internal/SingleTop_in_METbb_QandA.html

7.2 Results

Figs. 9-11 show the final discriminant in the various control regions, for our three tagging categories. Fig. 12 does so in the signal region. Fig. 13 shows the final discriminant in the signal region as used for the binned likelihood fit. We use MC_LIMIT [23] to estimate the cross-section of single top production. We propagate all systematic uncertainties.

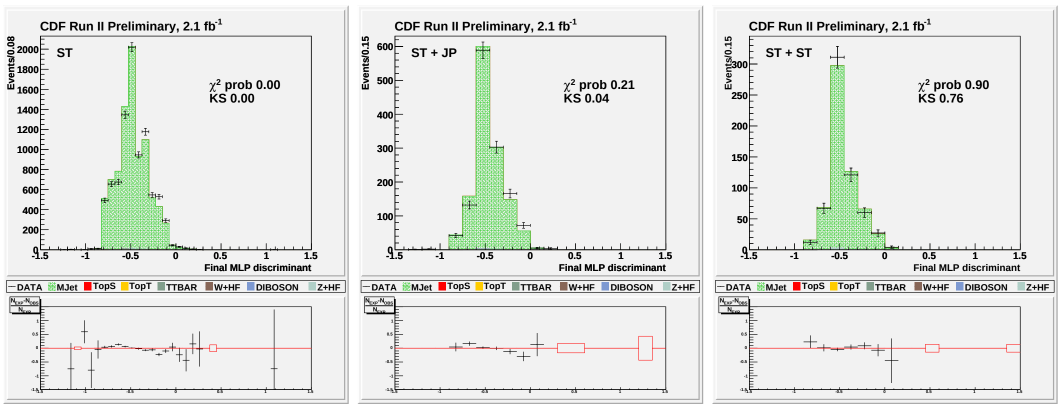

(a) Excl. ST (b) ST+JP (c) ST+ST

Figure 9: Final MLP discriminant output distribution in QCD Control Region

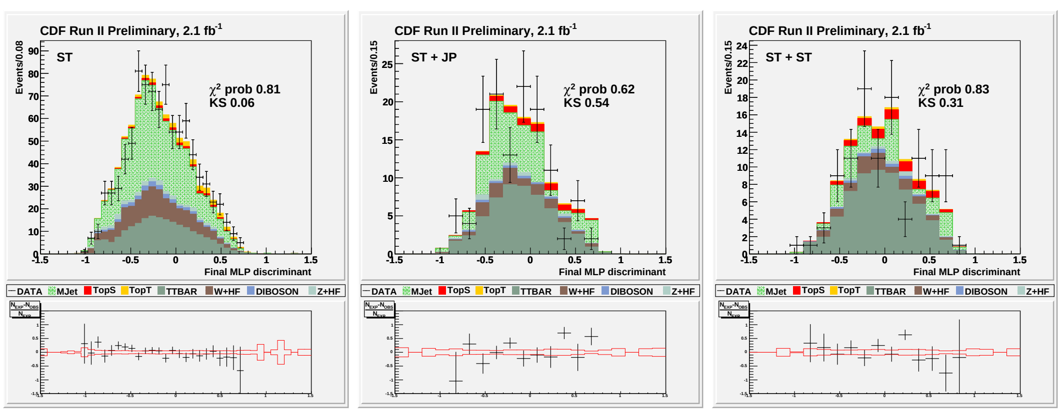

(a) Excl. ST (b) ST+JP (c) ST+ST

Figure 10: Final MLP discriminant output distribution in Electroweak Control Region

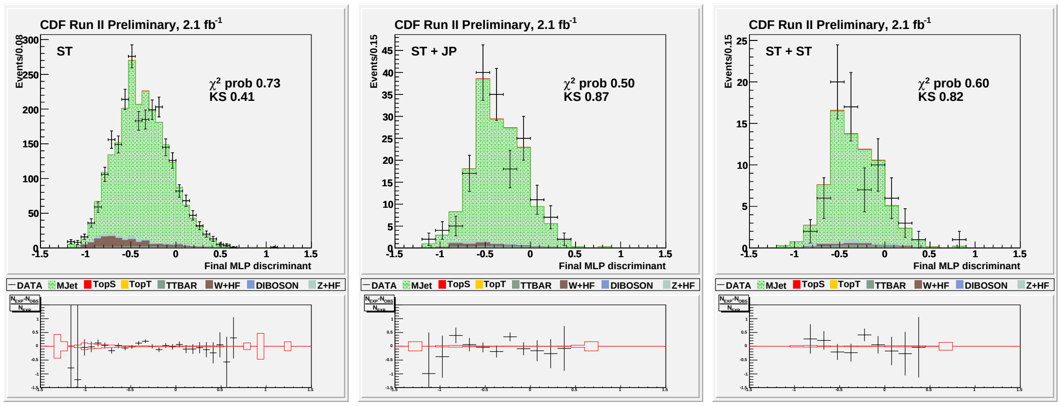

(a) Excl. ST (b) ST+JP (c) ST+ST

Figure 11: Final MLP discriminant output distribution in CR3 (QCD, signal like)

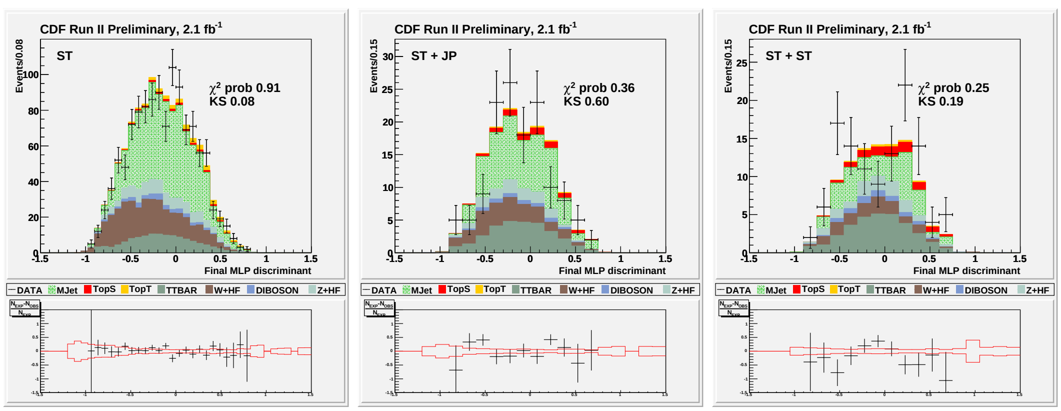

(a) Excl. ST (b) ST+JP (c) ST+ST

Figure 12: Final MLP discriminant output distribution in Signal Region

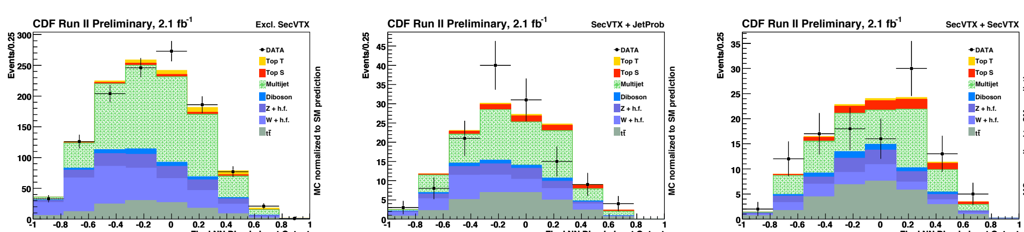

(a) Excl. ST (b) ST+JP (c) ST+ST

Figure 13: Final MLP discriminant output distribution in Signal Region, with the binning used for the likelihood fit.

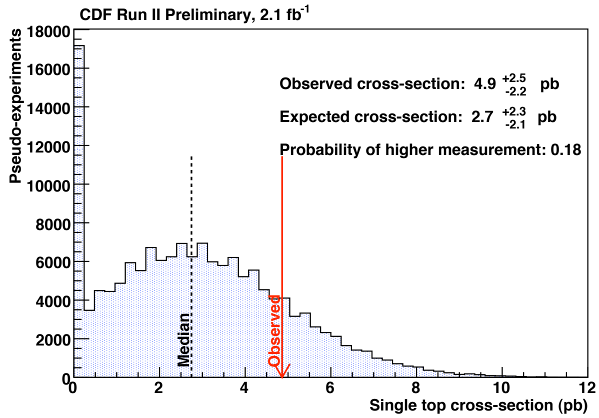

Figure 14: Distribution of the outcomes of the 150000 pseudo-experiments used to get the expected cross-section (all systematics turned on).

Using a test statistic, we compute the probablility that the background model (B) fluctuated equal or up to the observed value in the data (observed p-value) or to the median of signal plus background (S+B) pseudo-experiments (expected p-value). We also perform a linearity test, shown in figure 17.

Table 15 shows the expected cross-section measurement performing 150000 pseudo-experiments with all systematics turned on (we also performed 10000 samplings of the systematics space during the MC integration of the systematics in MC_LIMIT). Figure 14 shows the distribution of the outcomes of those pseudo-experiments.

We expect a cross-section of

$$\sigma_{s+t}^{exp} = 2.7^{+2.3}_{-2.1} \text{ pb}$$

Once this analysis is applied to 2.1 fb^{-1} of CDF Run II data, the observed cross-section is

$$\sigma_{s+t}^{obs} = 4.9^{+2.5}_{-2.2} \text{ pb.}$$

According to figure 14, there is a 0.21 probability that the outcome would have been higher that what observed. Figure 16 shows our measurement of V_{tb}. Using an unconstrained flat prior, we measure the latter to be

$$|V_{tb}| = 1.24^{+0.34}_{-0.29} \pm 0.07(\text{theory}).$$

Using a Bayesian technique with a flat prior on $|V_{tb}|^2$ between zero and one, we extract a lower limit at 95% confidence level of $|V_{tb}| > 0.36$.

Fig. 15 shows the distribution of the test statistics for one million pseudo-experiments performed for the null (B) and test (S+B) hypothesis with all the systematics turned on. We expect a p-value of 0.0785 (1.4 σ). The observed p-value is 0.0160 (2.1 σ).

We also have computed the observed cross-section for each individual tagging category. Figure 18 shows these results. Table 16 shows the χ^2 probability between these measurements. We see that

Expected cross-section	-2σ	$-\sigma$	Median	$+\sigma$	$+2\sigma$
x SM	0	0.22	0.96	1.75	2.63
pb	0	0.6	2.7	5.0	7.5

Table 15: Expected cross-section measurement, using our three tagging categories (all systematics turned on).

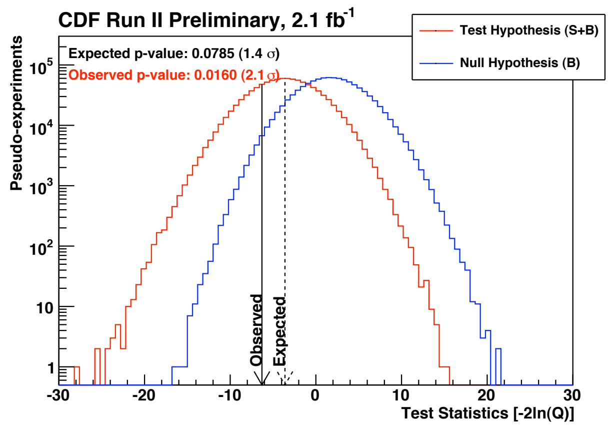

Figure 15: Test statistics for expected cross-section measurement (all systematics turned on).

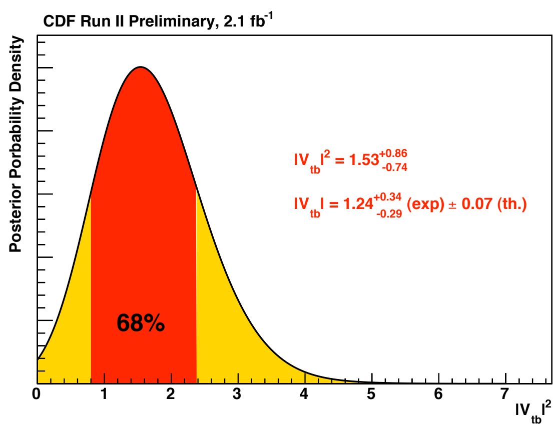

Figure 16: V_{tb} measurement (all systematics turned on).

most of the excess is measured in the ST + ST category, but the results are compatible with each other.

Finally, we have measured the cross-section limit (95% CL for the SM cross-section times branching ratio) for the single top production. Table 17 and figure 19 show our results. We observe a limit of 8.6 pb (3 xSM).

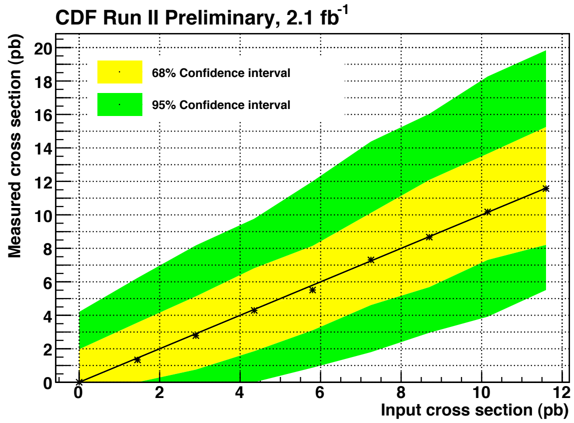

Figure 17: Linearity test for expected cross-section measurement (all systematics turned on).

	Combination (3 ch)	Excl. SecVTX	SecVTX + JetProb	SecVTX + SecVTX
SM	0.73	0.85	1	0.77
Combination (3 ch)	1	0.99	0.92	0.98
Excl. SecVTX		1	0.95	0.95
SecVTX + JetProb			1	0.88
SecVTX + SecVTX				1

Table 16: χ^2 probability between the measurements shown in fig. 18. The first row is comparing each measurement to the SM prediction.

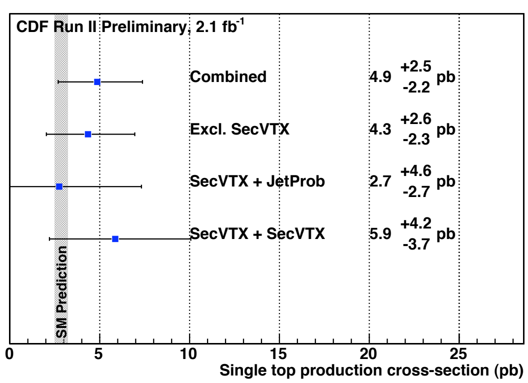

Figure 18: Observed cross-section in each channel (all systematics turned on).

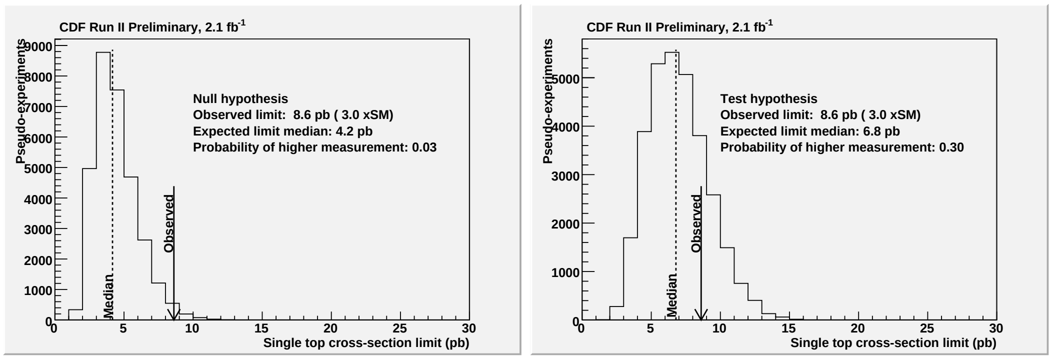

(a) Null Hypothesis (B)

(b) Test Hypothesis (S+B)

Figure 19: Expected and observed limits for the test and null hypotheses, using our three tagging categories (all systematics turned on).

Exp. cross-section limit (pb)	-2σ	$-\sigma$	Median	$+\sigma$	$+2\sigma$
Test Hypothesis (S+B)	3.40	4.80	6.79	9.15	11.84
Null Hypothesis (B)	2.16	2.96	4.17	5.92	8.18

Table 17: Expected limits for the test and null hypotheses, using our three tagging categories (all systematics turned on).

8 Summary

We have presented a search for s and t channel electroweak single top production in the $\not{E}_T$+jets channel. We have analyzed 2.1 fb^{-1} of CDF Run II data and measured the single top production cross-section for the first time in this channel (events where the lepton from the W decay is either not identified or reconstructed as a jet):

$$\sigma_{s+t}^{obs} = 4.9^{+2.5}_{-2.2}\text{pb} \; (\sigma_{s+t}^{exp} = 2.7^{+2.3}_{-2.1}\text{ pb});$$

assuming a top quark mass of 175 GeV/c^2. The expected p-value is 0.0785 (1.4 σ). The observed p-value is 0.0160 (2.1 σ).

Finally we have measured the V_{tb} element of the CKM matrix

$$|V_{tb}| = 1.24^{+0.34}_{-0.29} \pm 0.07(\text{theory}).$$

We also extract a 95% CL lower limit of $|V_{tb}| > 0.36$.

References

[1] D.Abe *et al.* The CDF collaboration, Phys.Rev.Lett.74, 2626 (1995);

[2] S.Abachi *et al.* The D0 collaboration, Phys.Rev.Lett.74,2632 (1995);

[3] Harris, B. W. and Laenen, E. and Phaf, L. and Sullivan, Z. and Weinzierl, S., "Fully differential single-top-quark cross section in next-to-leading order QCD", Phys. Rev. D, 66, 054024, 2002

[4] Sullivan, Zack, "Understanding single-top-quark production and jets at hadron colliders", Phys. Rev. D, 70, 114012, 2004

[5] Nikolaos Kidonakis, "Single top quark production at the Fermilab Tevatron: Threshold resummation and finite-order soft gluon corrections", Phys. Rev. D, 74, 114012, 2006

[6] Cacciari, Matteo et al., "Updated predictions for the total production cross sections of top and of heavier quark pairs at the Tevatron and at the LHC", JHEP, 09 (127), 2008, arXiv:0804.2800 [hep-ex].

[7] T. Aaltonen *et al.* [CDF Collaboration], "Measurement of the Single Top Quark Production Cross Section at CDF," arXiv:0809.2581 [hep-ex].

[8] V. M. Abazov *et al.* [D0 Collaboration], "Evidence for production of single top quarks," Phys. Rev. D **78** (2008) 012005, arXiv:0803.0739 [hep-ex].

[9] A. Apresyan, D. Bortoletto, F. Margaroli, K. Potamianos, Oscar González, M.Vidal, Song Ming Wang *"Event selection for Higgs search in the $\not{E}_T$ plus jets sample"*, CDF 9358, 2008;

[10] M.Grunewald: http://lepewwg.web.cern.ch/LEPEWWG/

[11] A.Mehta: *"Calibration of H1 Algorithm Improved Jets"*, CDF/DOC/CDF/GROUP/8564, 2006

[12] V. Veszpremi, D. Bortoletto, O. Gonzalez, A. Garfinkel, S.M. Wang : *"Search for the Standard Model Higgs boson in the $\not\!\!E_T$ and b-jet signature"*, CDF/ANAL/EXOTIC/CDFR/8362, 2007

[13] A.Apresyan,V.Veszpremi, D.Bortoletto, F.Margaroli, O.Gonzalez, S.M.Wang: *"Search for the Standard Model Higgs boson in the Missing Et and b-jet Signature"*, CDF/ANAL/EXOTIC/PUBLIC/8973, 2007

[14] A.Apresyan, D.Bortoletto, F.Margaroli, O.Gonzalez, S.M.Wang: *"Tag Rate Matrix method to estimate QCD background fromdata in VH search in MET + b-jets signature"*, CDF/ANAL/EXOTIC/CDFR/9275, 2008

[15] The D0 collaboration: *"Search for the standard model Higgs boson in the $HZ \rightarrow bb\nu\nu$ channel in 2.1 fb^{-1} of $p\bar{p}$ collisions at $\sqrt{(s)} = 1.96\ TeV$"*, Conference Note 5586, 2008

[16] The D0 collaboration: *"A search for the standard model Higgs boson in the missing energy and acoplanar b-jet topology at ps = 1.96 TeV"*, Fermilab-Pub-08/294-E, arXiv:0808.1266v1;

[17] B.Kilminster, B.Parks, R.Hughes, B.Winer: *"Neural Network Search for Standard Model Higgs Boson in Met Plus Jets Channel with 1.7 fb-1"*, CDF/PUB/EXOTIC/PUBLIC/9166, 2008

[18] A. Apresyan,D.Bortoletto, F. Margaroli, K. Potamianos, O. Gonzalez, M. Vidal, S. M. Wang, B. Parks, R.Hughes, B.Kilminster, B.Winer *"Search for the Standard Model Higgs boson in the MET plus jets sample"* CDF/PUB/EXOTIC/PUBLIC/9483;

[19] O.Gonzalez, M.Vidal: *"Report for the official dataset to recover events in the Missing-ET sample"*, CDF/ANAL/EXOTIC/CDFR/9231, 2008

[20] O.Gonzalez, M.Vidal: *"Trigger efficiency of the MET+JETS sample for the 2 fb-1 dataset"*, CDF/PHYS/MISSING_ET/CDFR/9355, 2008

[21] C. Rott, at al. CDF Note 7136; "Search for Scalar Bottom Quarks from Gluino Decays in Proton-Antiproton Collisions at 1.96TeV", PhD Thesis, CDF/THESIS/EXOTIC/PUBLIC/7526, 2005.

[22] Y. Freund and R.E. Schapire, J. of Computer and System Science 55, 119 (1997).

[23] T. Junk, "Sensitivity, Exclusion and Discovery with Small Signals, Large Backgrounds, and Large Systematics", CDF/DOC/STATISTICS/PUBLIC/8128, 2007.

A Validation Plots

A.1 QCD Control Region Plots

A.1.1 Excl. Single Tag

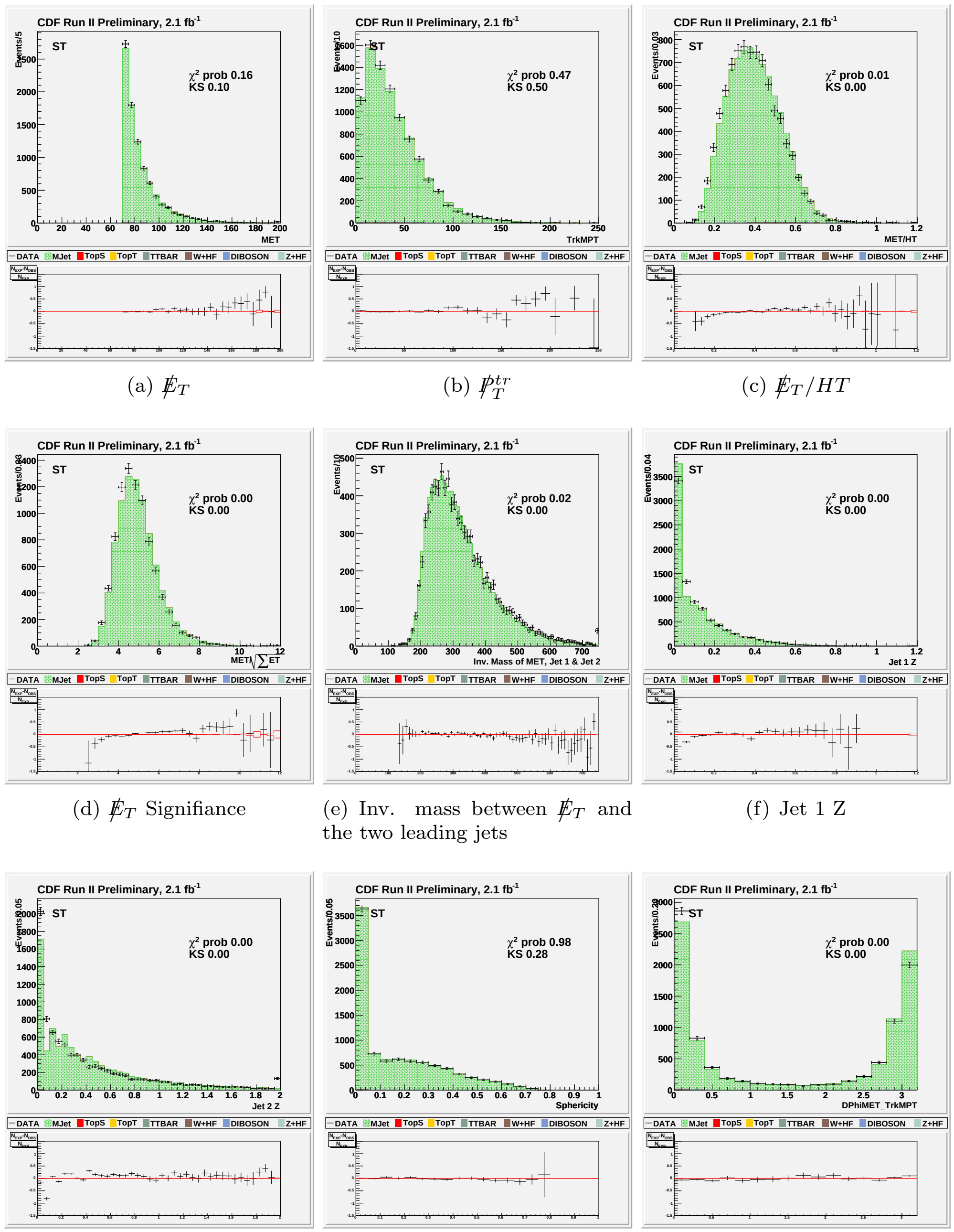

(a) $\not\!\!E_T$

(b) $\not\!p_T^{tr}$

(c) $\not\!\!E_T/HT$

(d) $\not\!\!E_T$ Significance

(e) Inv. mass between $\not\!\!E_T$ and the two leading jets

(f) Jet 1 Z

(g) Jet 2 Z

(h) Sphericity

(i) $\Delta\phi(\not\!p_T^{tr}, \not\!\!E_T)$

Figure 20: QCD Control Region, Excl. Single Tag

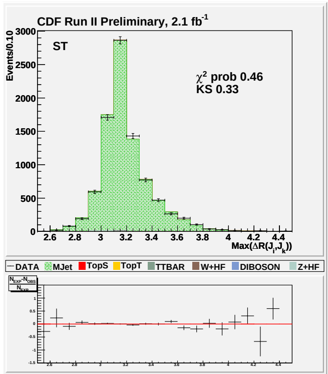

(a) Max($\Delta R(J_i, J_k)$)

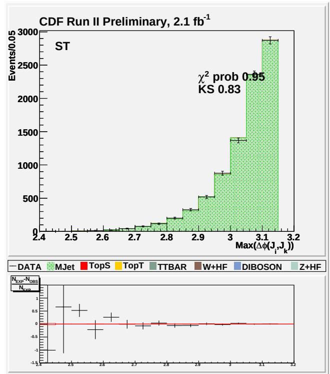

(b) Max($\Delta\phi(J_i, J_k)$)

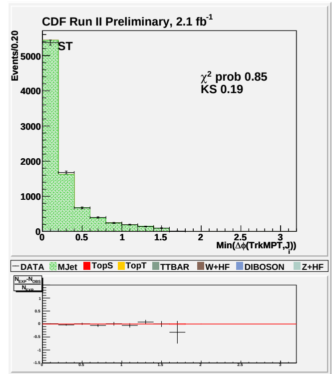

(c) Min($\Delta\phi(\not{p}_T^{tr}, J_i)$)

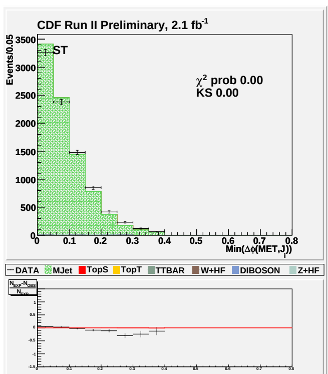

(d) Min($\Delta\phi(\not{E}_T, J_i)$)

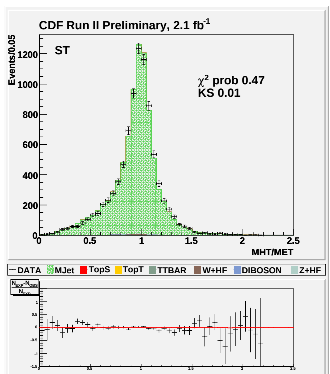

(e) $\not{H}_T/\not{E}_T$

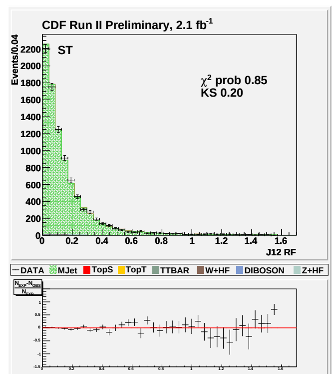

(f) $\Delta\phi$(J1/2 in RF, boost)

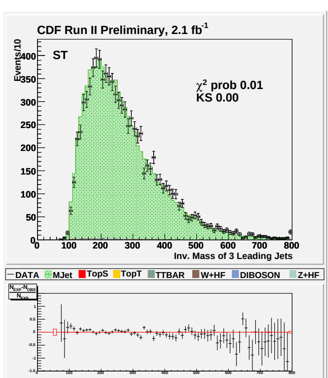

(g) Inv. mass between the two (or three) leading jets

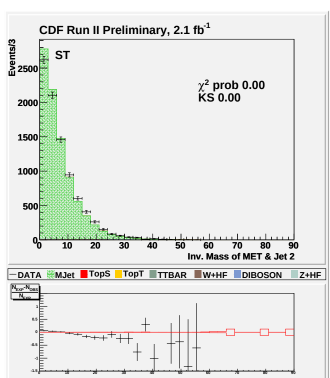

(h) Inv. mass between $\not{E}_T$ and the second leading jet

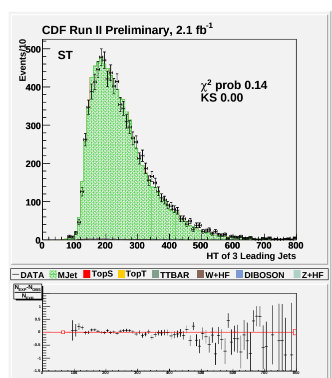

(i) H_T^3

Figure 21: QCD Control Region, Excl. Single Tag

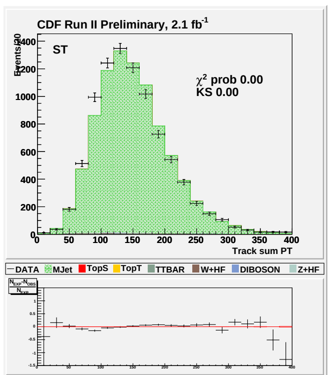

(a) $\sum P_T^{tr}$

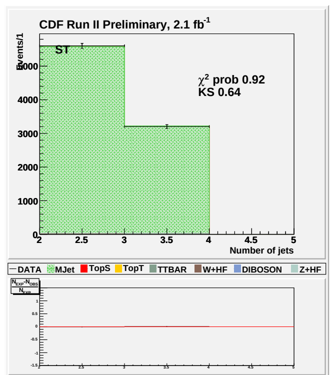

(b) Number of jets

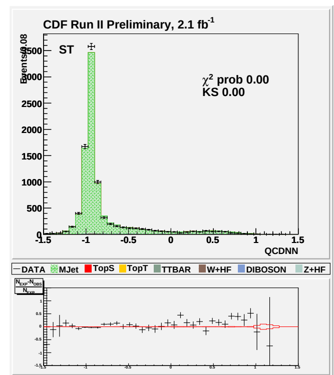

(c) QCDNN

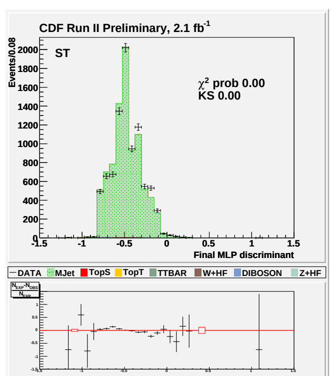

(d) Final MLP Discriminant

Figure 22: QCD Control Region, Excl. Single Tag

A.1.2 ST + ST

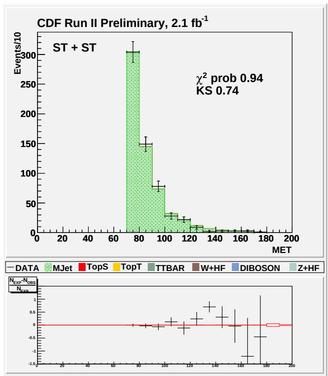

(a) $\not\!\!E_T$

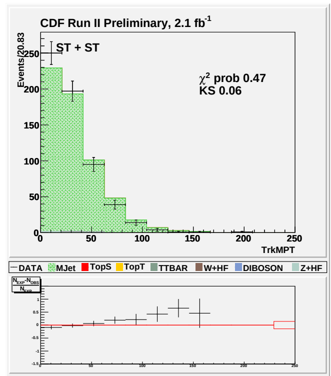

(b) $\not\!\!P_T^{tr}$

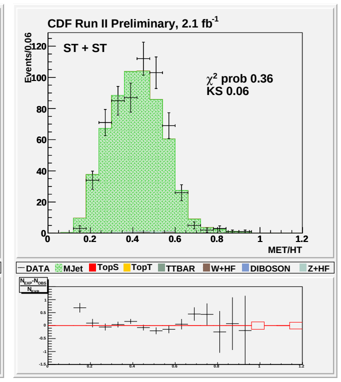

(c) $\not\!\!E_T/HT$

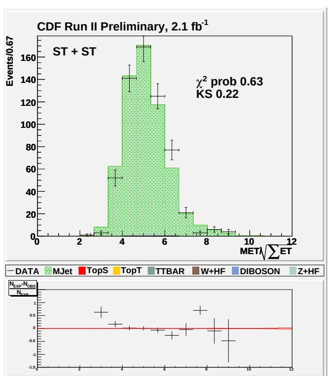

(d) $\not\!\!E_T$ Significance

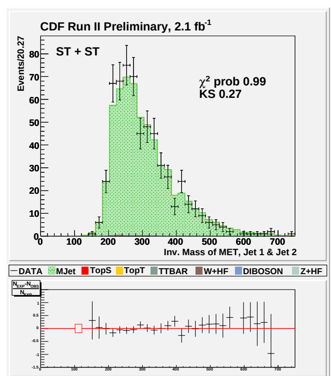

(e) Inv. mass between $\not\!\!E_T$ and the two leading jets

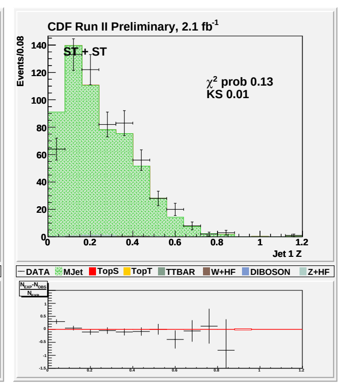

(f) Jet 1 Z

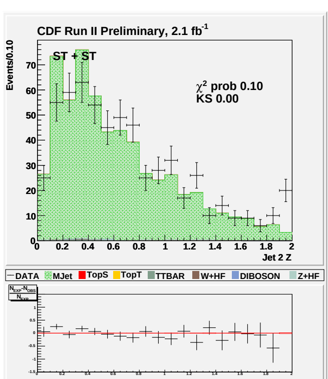

(g) Jet 2 Z

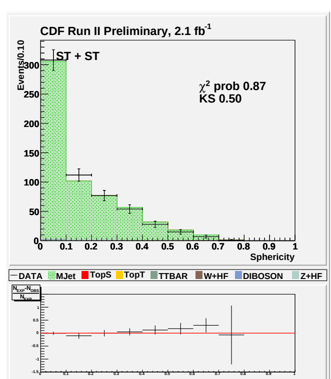

(h) Sphericity

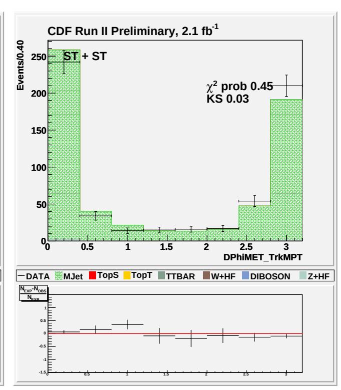

(i) $\Delta\phi(\not\!\!P_T^{tr}, \not\!\!E_T)$

Figure 23: QCD Control Region, ST + ST

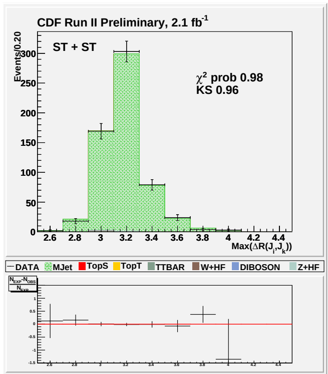

(a) Max($\Delta R(J_i, J_k)$)

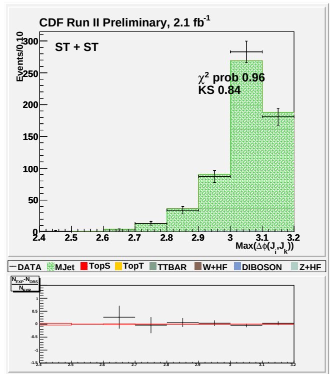

(b) Max($\Delta\phi(J_i, J_k)$)

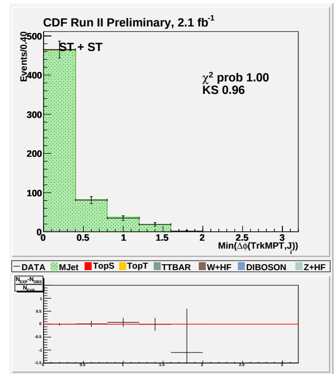

(c) Min($\Delta\phi(\not{p}_T^{tr}, J_i)$)

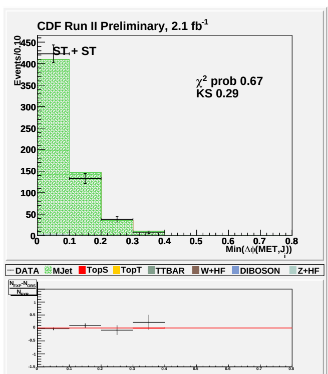

(d) Min($\Delta\phi(\not{E}_T, J_i)$)

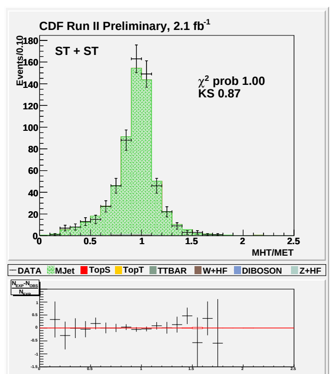

(e) $\not{H}_T/\not{E}_T$

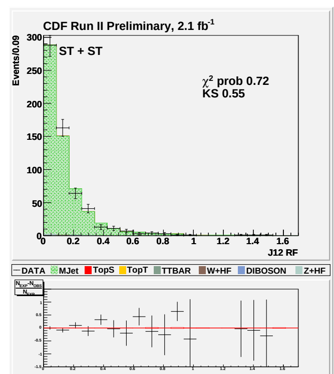

(f) $\Delta\phi$(J1/2 in RF, boost)

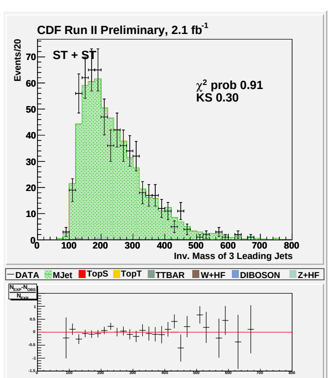

(g) Inv. mass between the two (or three) leading jets

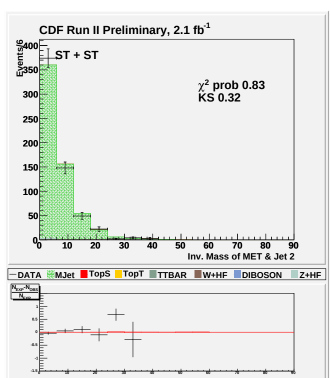

(h) Inv. mass between $\not{E}_T$ and the second leading jet

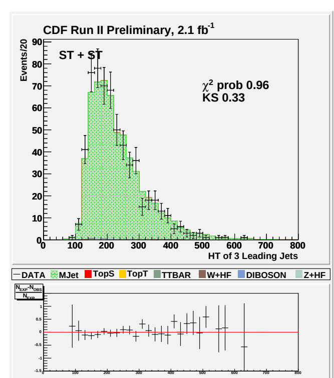

(i) H_T^3

Figure 24: QCD Control Region, ST + ST

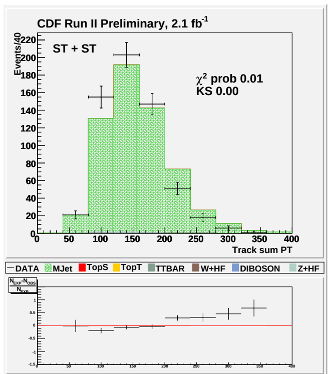

(a) $\sum P_T^{tr}$

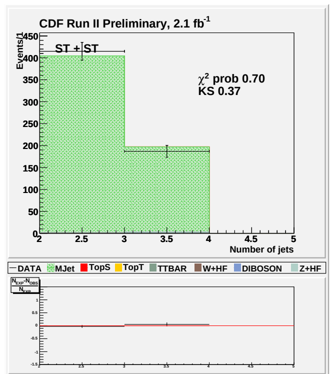

(b) Number of jets

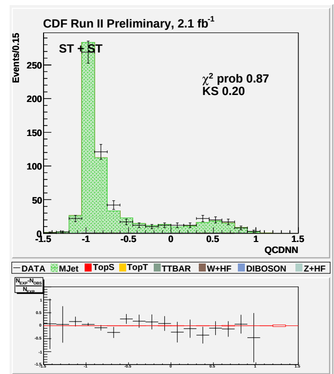

(c) QCDNN

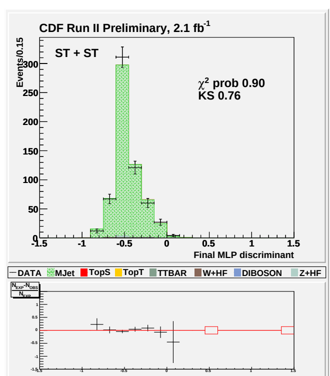

(d) Final MLP Discriminant

Figure 25: QCD Control Region, ST + ST

A.1.3 ST + JP

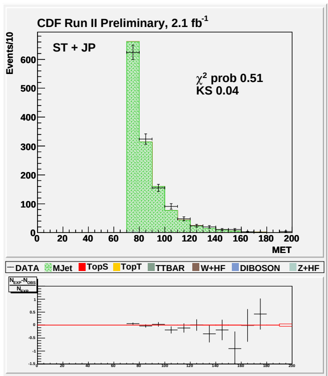

(a) $\not\!\!E_T$

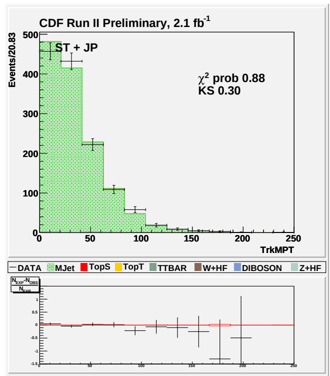

(b) $\not\!\!P_T^{tr}$

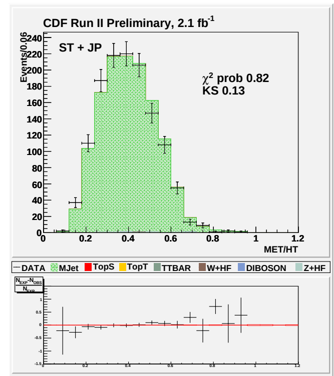

(c) $\not\!\!E_T/HT$

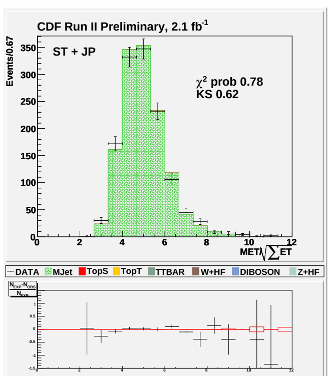

(d) $\not\!\!E_T$ Significance

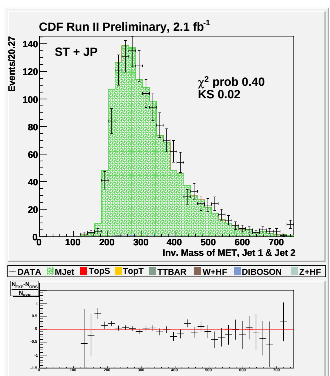

(e) Inv. mass between $\not\!\!E_T$ and the two leading jets

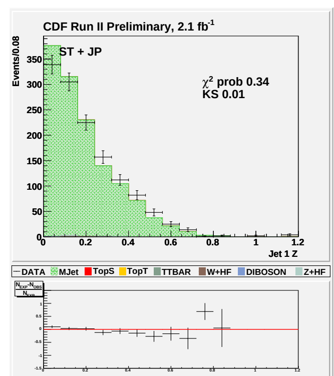

(f) Jet 1 Z

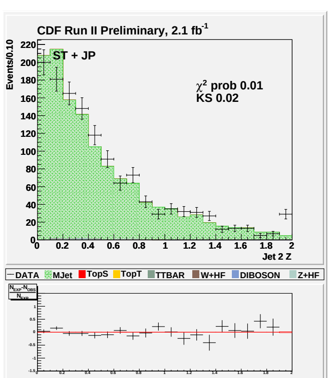

(g) Jet 2 Z

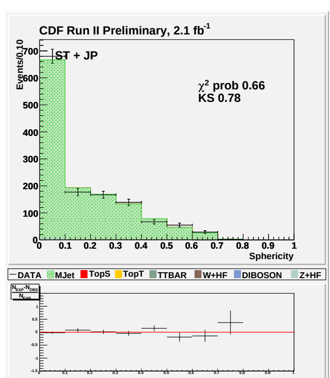

(h) Sphericity

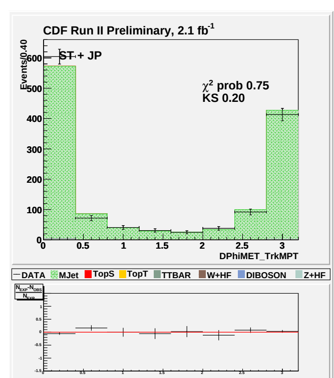

(i) $\Delta\phi(\not\!\!P_T^{tr}, \not\!\!E_T)$

Figure 26: QCD Control Region, ST + JP

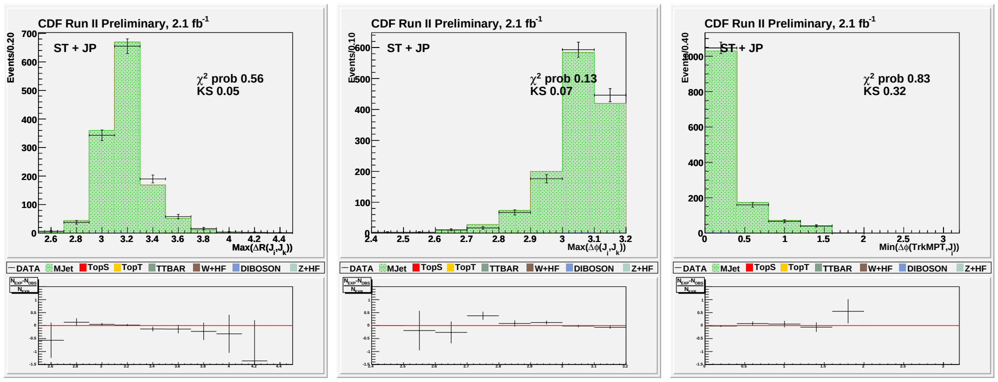

(a) $\text{Max}(\Delta R(J_i, J_k))$ (b) $\text{Max}(\Delta\phi(J_i, J_k))$ (c) $\text{Min}(\Delta\phi(\not{p}_T^{tr}, J_i))$

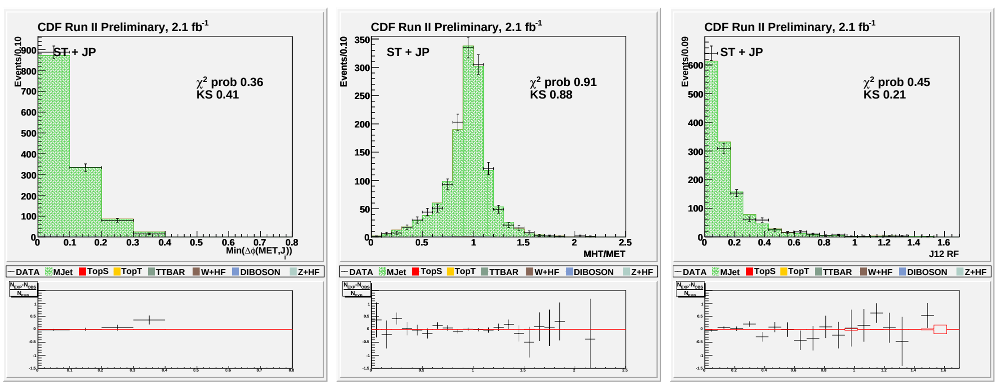

(d) $\text{Min}(\Delta\phi(\not{E}_T, J_i))$ (e) $\not{H}_T/\not{E}_T$ (f) $\Delta\phi(\text{J1/2 in RF, boost})$

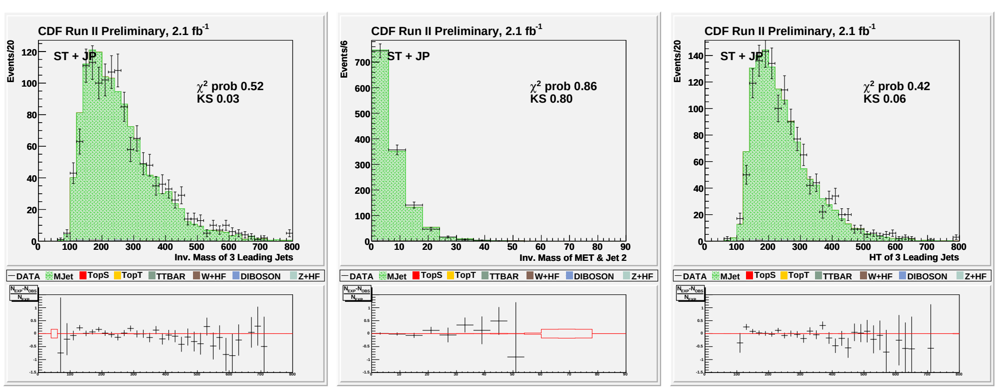

(g) Inv. mass between the two (or three) leading jets (h) Inv. mass between $\not{E}_T$ and the second leading jet (i) H_T^3

Figure 27: QCD Control Region, ST + JP

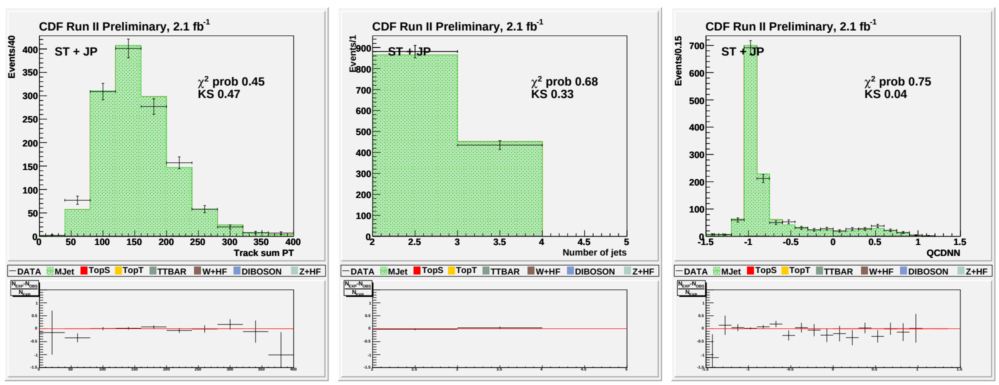

(a) $\sum P_T^{tr}$ (b) Number of jets (c) QCDNN

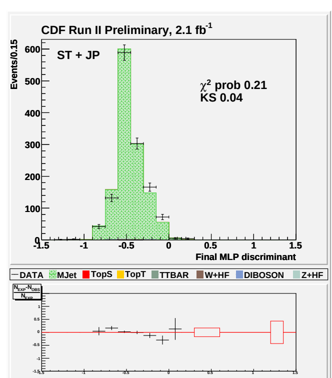

(d) Final MLP Discriminant

Figure 28: QCD Control Region, ST + JP

A.2 Electroweak Control Region Plots

A.2.1 Excl. Single Tag

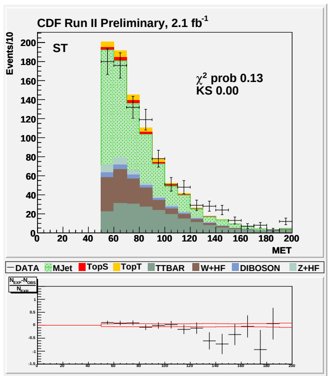

(a) $\not\!\!E_T$

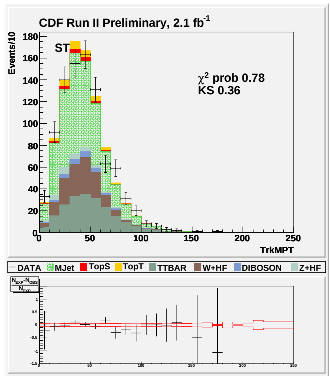

(b) $\not\!p_T^{tr}$

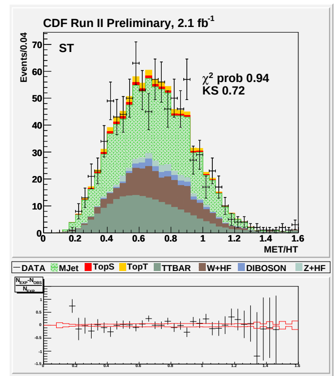

(c) $\not\!\!E_T/HT$

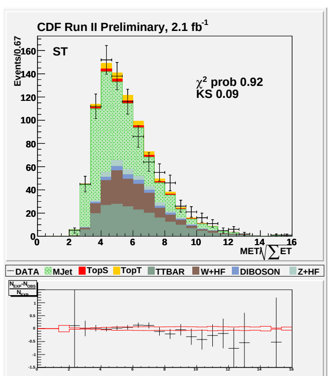

(d) $\not\!\!E_T$ Signifiance

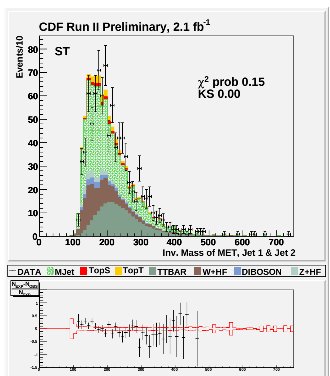

(e) Inv. mass between $\not\!\!E_T$ and the two leading jets

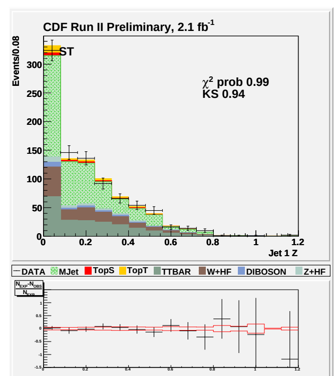

(f) Jet 1 Z

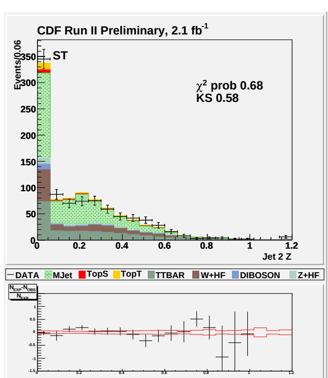

(g) Jet 2 Z

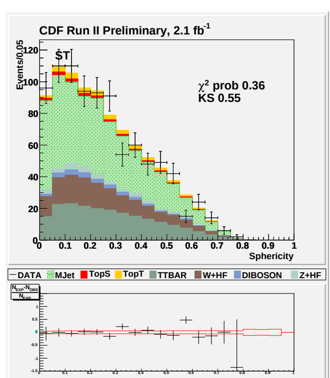

(h) Sphericity

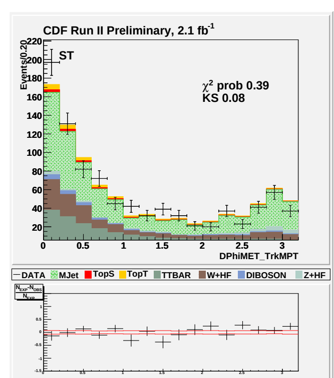

(i) $\Delta\phi(\not\!p_T^{tr}, \not\!\!E_T)$

Figure 29: Electroweak Control Region, Excl. Single Tag

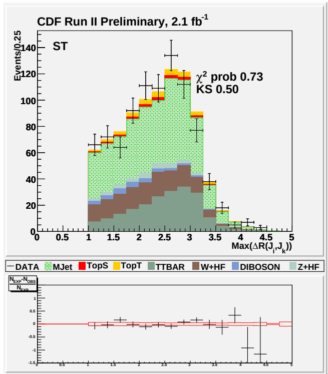

(a) $\mathrm{Max}(\Delta R(J_i, J_k))$

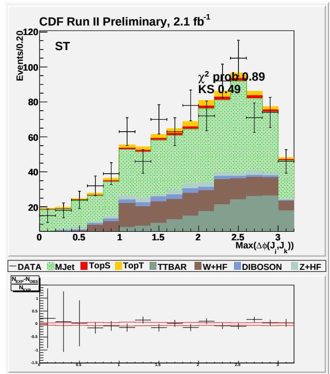

(b) $\mathrm{Max}(\Delta\phi(J_i, J_k))$

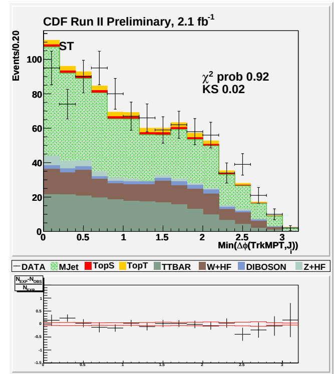

(c) $\mathrm{Min}(\Delta\phi(\not{p}_T^{tr}, J_i))$

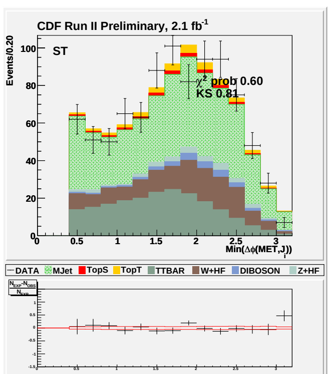

(d) $\mathrm{Min}(\Delta\phi(\not{E}_T, J_i))$

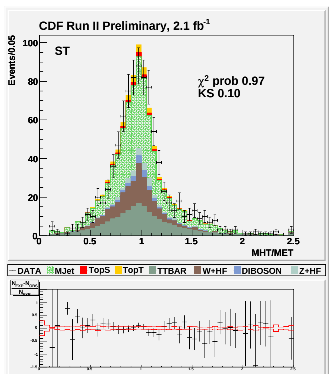

(e) $\not{H}_T/\not{E}_T$

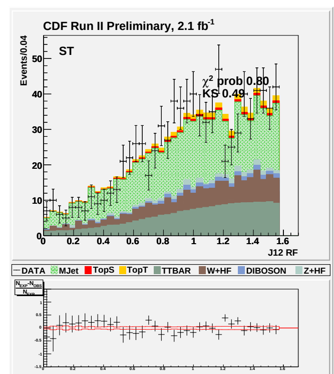

(f) $\Delta\phi(\mathrm{J1/2\ in\ RF, boost})$

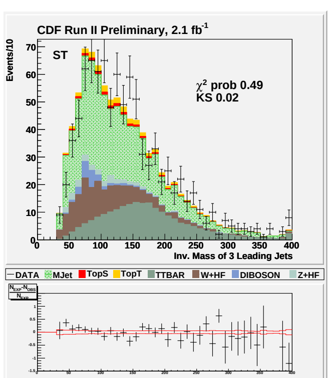

(g) Inv. mass between the two (or three) leading jets

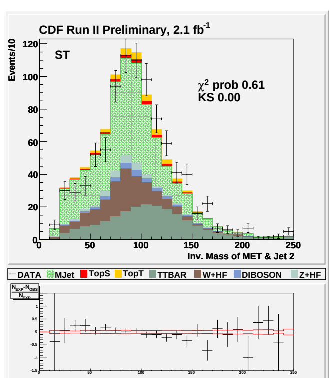

(h) Inv. mass between $\not{E}_T$ and the second leading jet

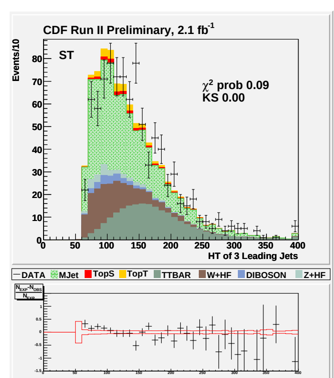

(i) H_T^3

Figure 30: Electroweak Control Region, Excl. Single Tag

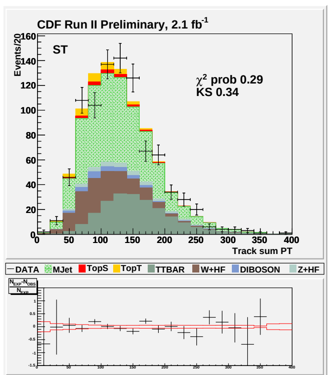

(a) $\sum P_T^{tr}$

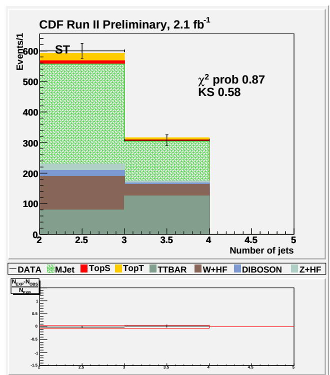

(b) Number of jets

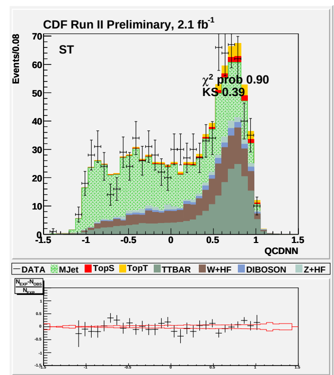

(c) QCDNN

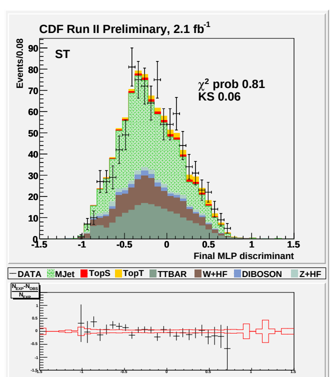

(d) Final MLP Discriminant

Figure 31: Electroweak Control Region, Excl. Single Tag

A.2.2 ST + ST

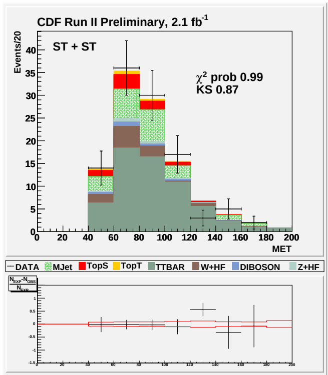

(a) $\not\!\!E_T$

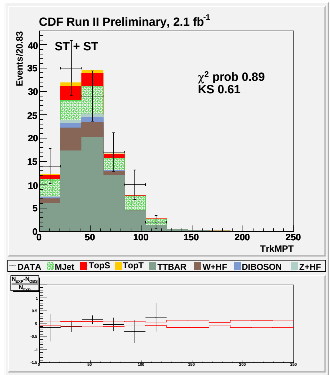

(b) $\not\!\!P_T^{tr}$

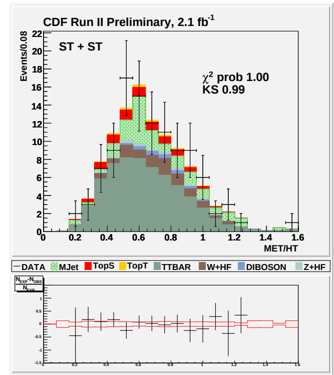

(c) $\not\!\!E_T/HT$

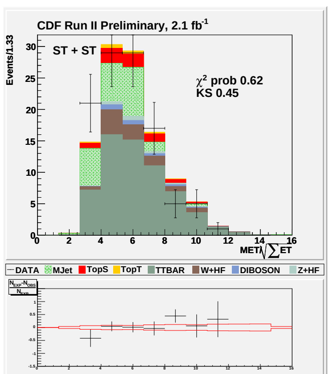

(d) $\not\!\!E_T$ Signifiance

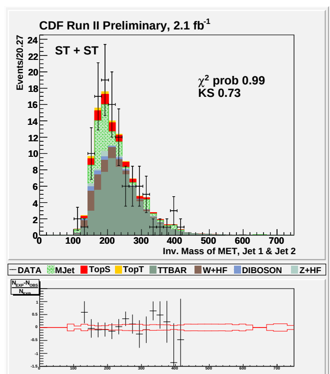

(e) Inv. mass between $\not\!\!E_T$ and the two leading jets

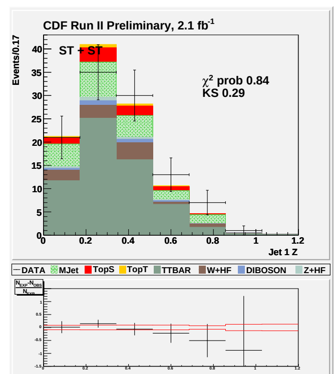

(f) Jet 1 Z

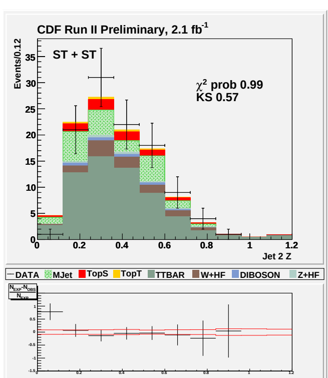

(g) Jet 2 Z

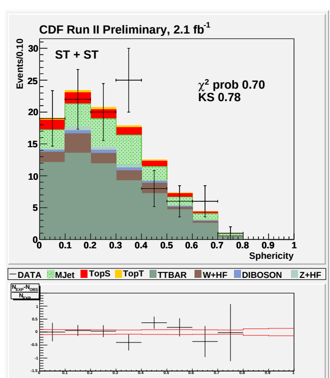

(h) Sphericity

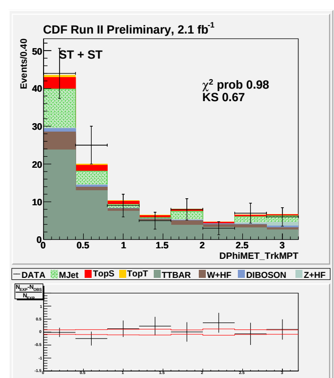

(i) $\Delta\phi(\not\!\!P_T^{tr}, \not\!\!E_T)$

Figure 32: Electroweak Control Region, ST + ST

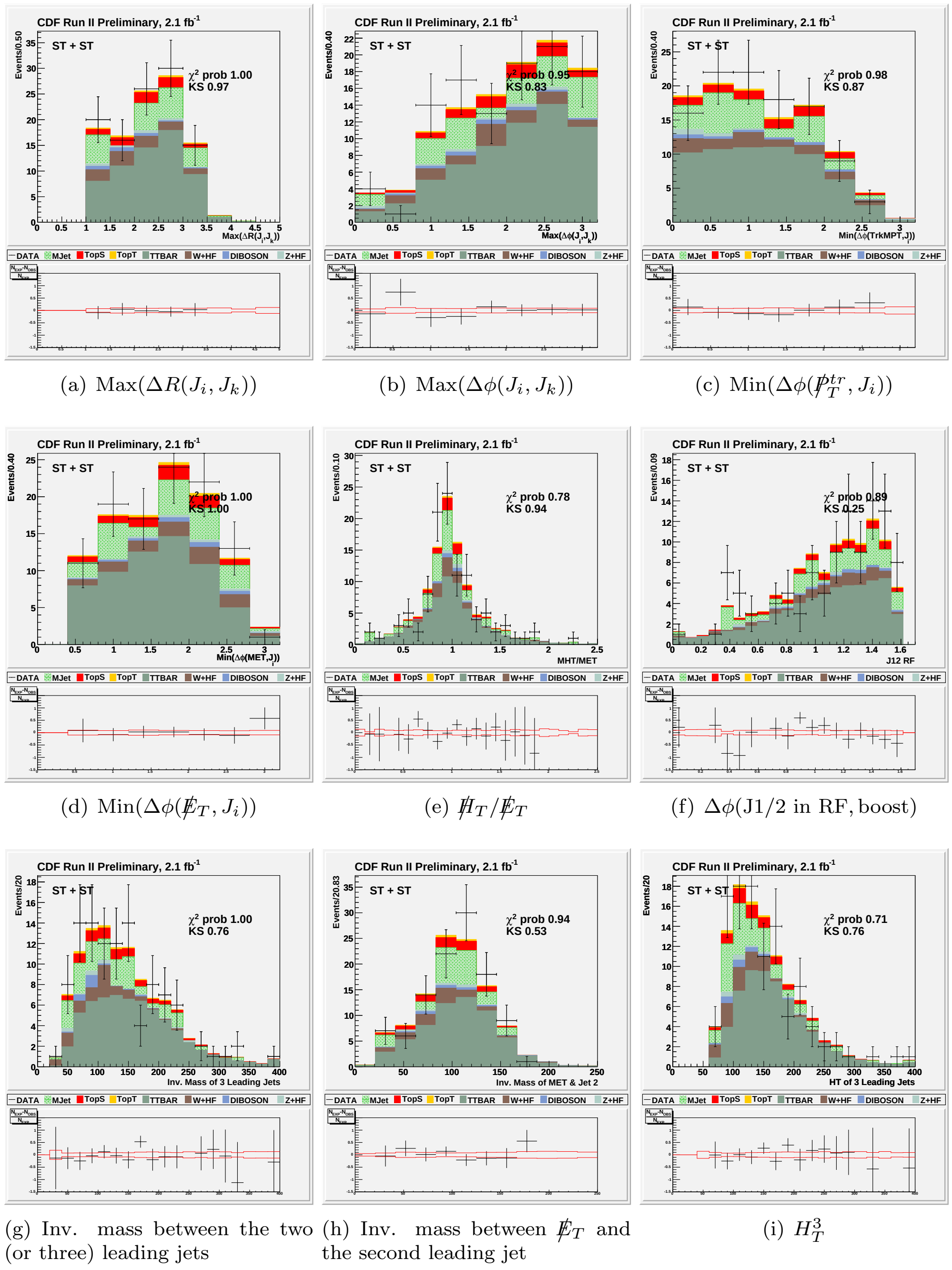

(a) Max$(\Delta R(J_i, J_k))$

(b) Max$(\Delta\phi(J_i, J_k))$

(c) Min$(\Delta\phi(\not{P}_T^{tr}, J_i))$

(d) Min$(\Delta\phi(\not{E}_T, J_i))$

(e) $\not{H}_T/\not{E}_T$

(f) $\Delta\phi$(J1/2 in RF, boost)

(g) Inv. mass between the two (or three) leading jets

(h) Inv. mass between $\not{E}_T$ and the second leading jet

(i) H_T^3

Figure 33: Electroweak Control Region, ST + ST

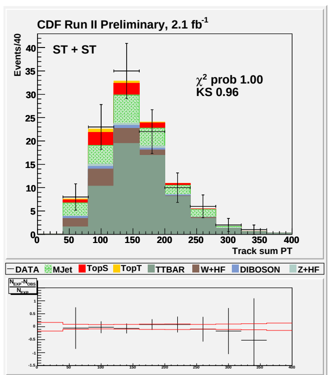

(a) $\sum P_T^{tr}$

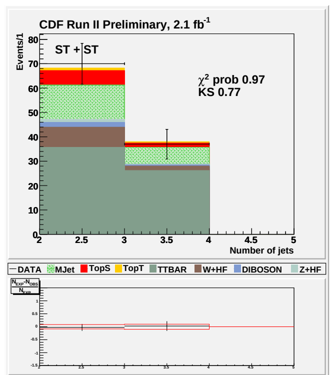

(b) Number of jets

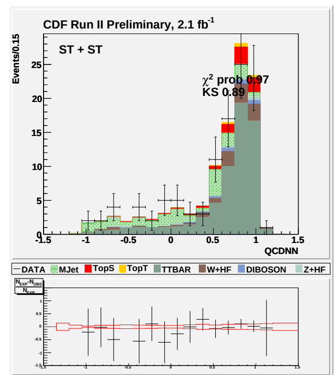

(c) QCDNN

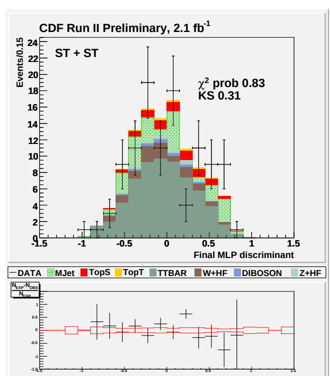

(d) Final MLP Discriminant

Figure 34: Electroweak Control Region, ST + ST

A.2.3 ST + JP

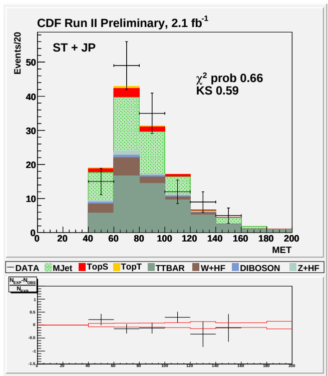

(a) $\not\!\!E_T$

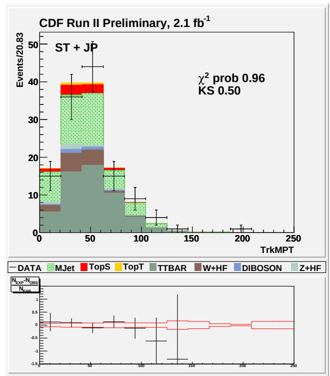

(b) $\not\!\!P_T^{tr}$

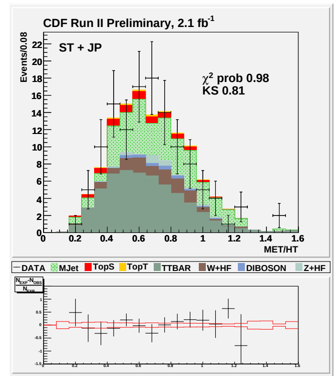

(c) $\not\!\!E_T/HT$

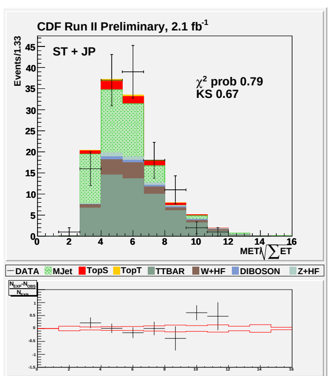

(d) $\not\!\!E_T$ Signifiance

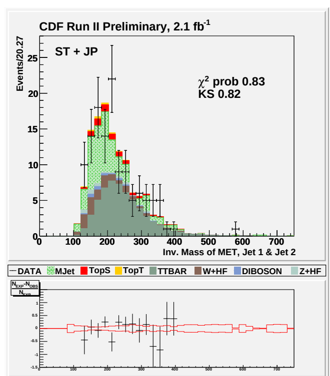

(e) Inv. mass between $\not\!\!E_T$ and the two leading jets

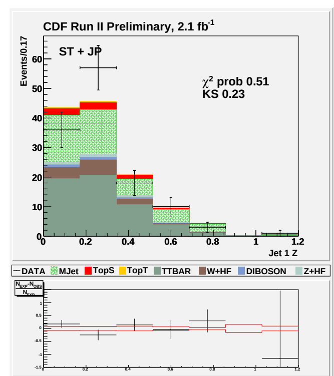

(f) Jet 1 Z

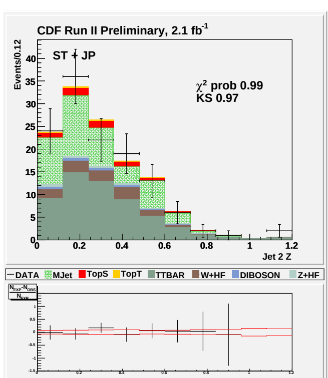

(g) Jet 2 Z

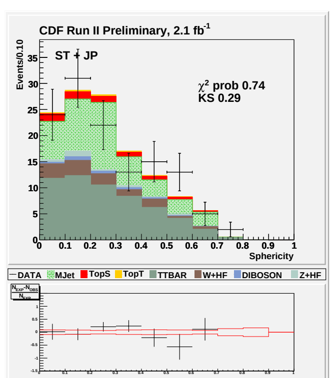

(h) Sphericity

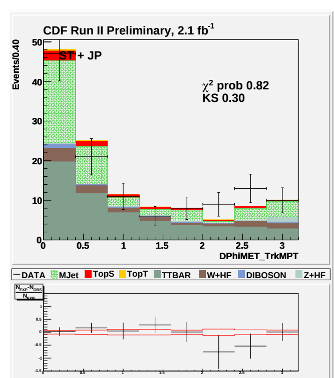

(i) $\Delta\phi(\not\!\!P_T^{tr}, \not\!\!E_T)$

Figure 35: Electroweak Control Region, ST + JP

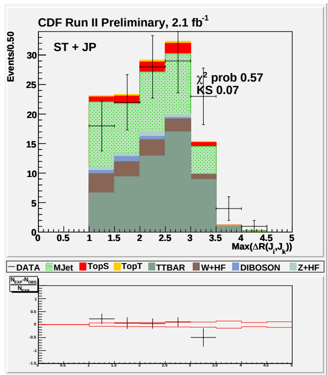

(a) Max($\Delta R(J_i, J_k)$)

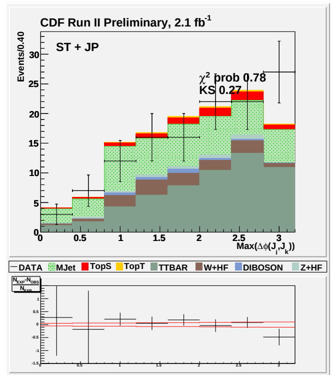

(b) Max($\Delta\phi(J_i, J_k)$)

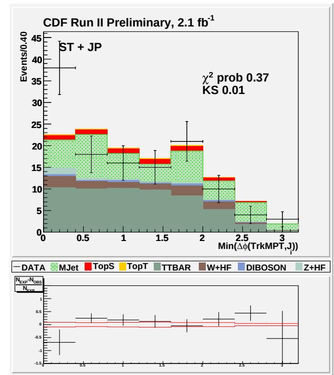

(c) Min($\Delta\phi(\not{P}_T^{tr}, J_i)$)

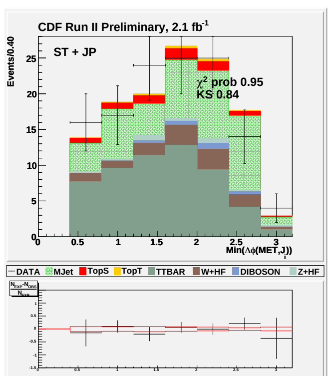

(d) Min($\Delta\phi(\not{E}_T, J_i)$)

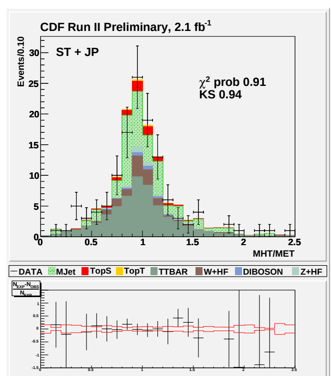

(e) $\not{H}_T/\not{E}_T$

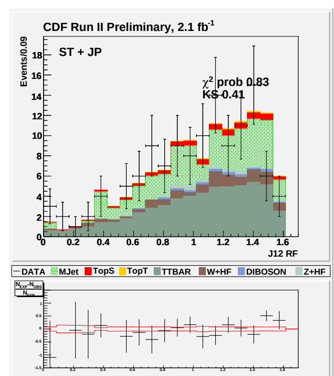

(f) $\Delta\phi$(J1/2 in RF, boost)

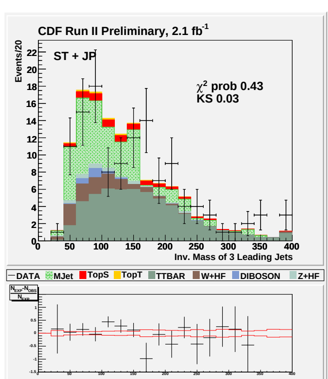

(g) Inv. mass between the two (or three) leading jets

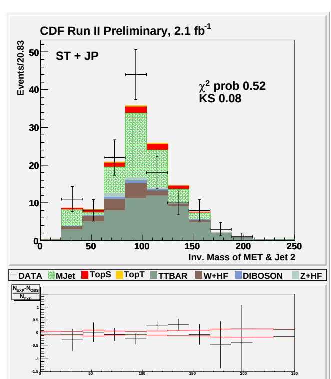

(h) Inv. mass between $\not{E}_T$ and the second leading jet

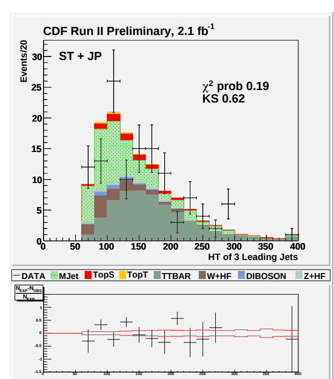

(i) H_T^3

Figure 36: Electroweak Control Region, ST + JP

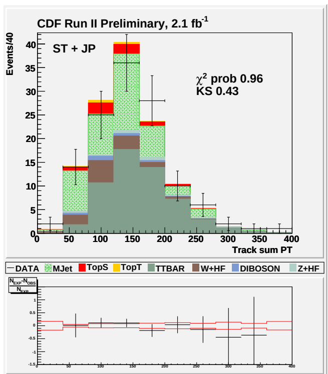

(a) $\sum P_T^{tr}$

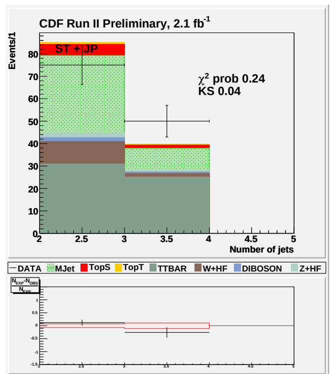

(b) Number of jets

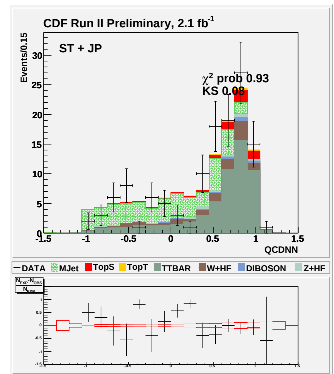

(c) QCDNN

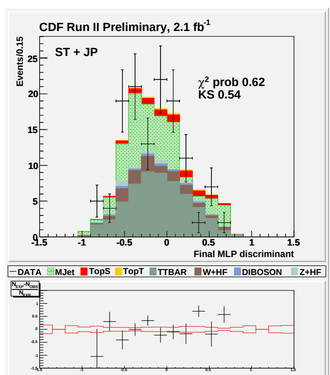

(d) Final MLP Discriminant

Figure 37: Electroweak Control Region, ST + JP

A.3 Control Region 3 (QCD) Plots

A.3.1 Excl. Single Tag

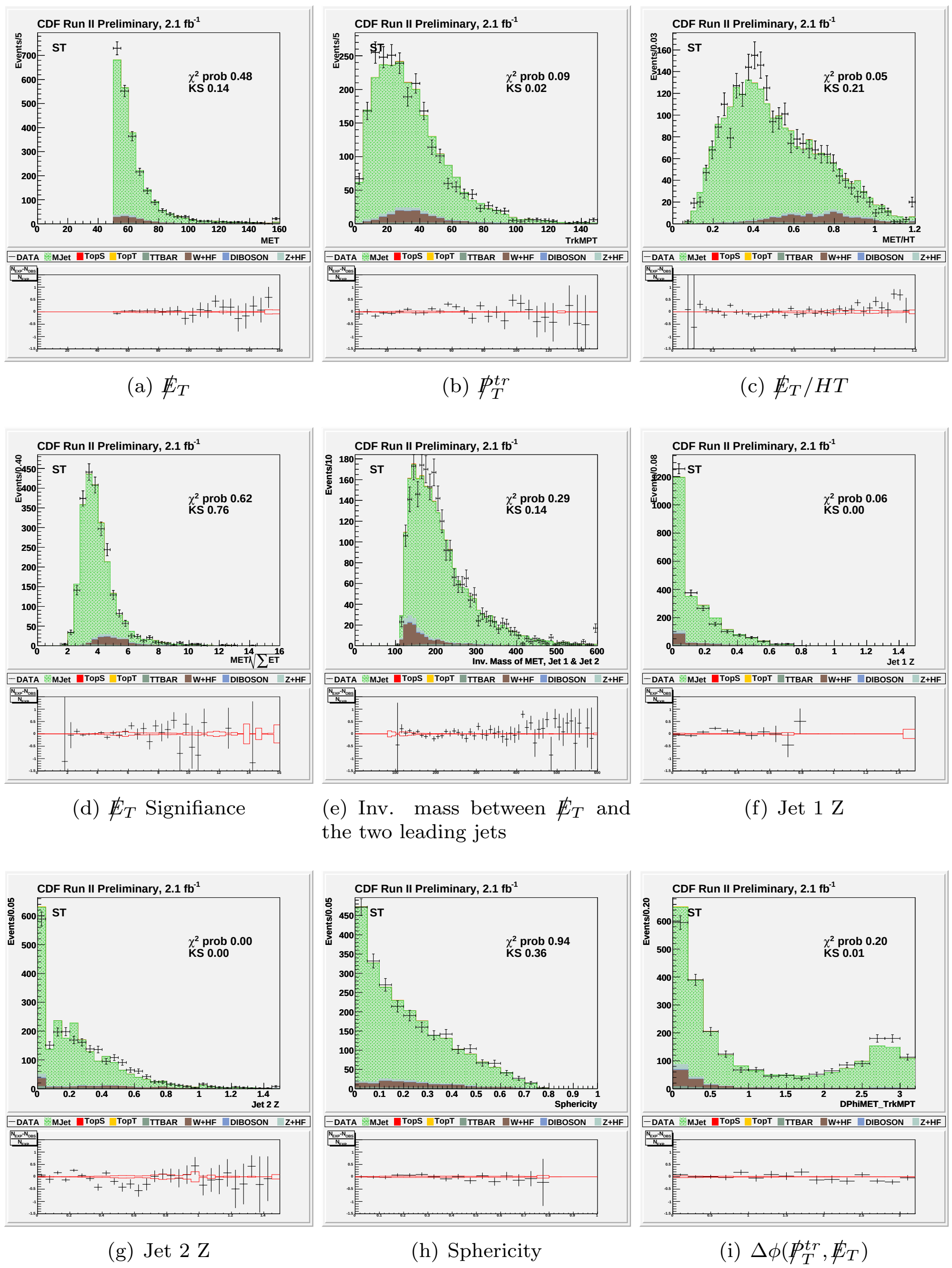

(a) $\not\!\!E_T$ (b) $\not\!\!P_T^{tr}$ (c) $\not\!\!E_T/HT$

(d) $\not\!\!E_T$ Signifiance (e) Inv. mass between $\not\!\!E_T$ and the two leading jets (f) Jet 1 Z

(g) Jet 2 Z (h) Sphericity (i) $\Delta\phi(\not\!\!P_T^{tr}, \not\!\!E_T)$

Figure 38: Control Region 3 (QCD), Excl. Single Tag

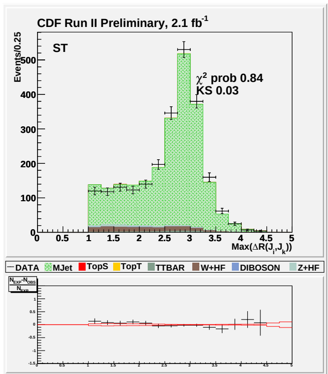

(a) Max($\Delta R(J_i, J_k)$)

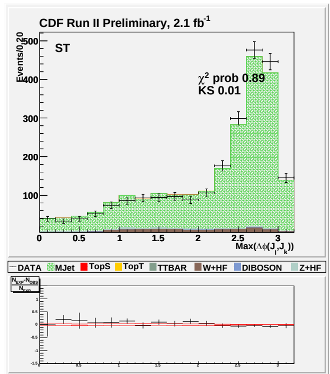

(b) Max($\Delta\phi(J_i, J_k)$)

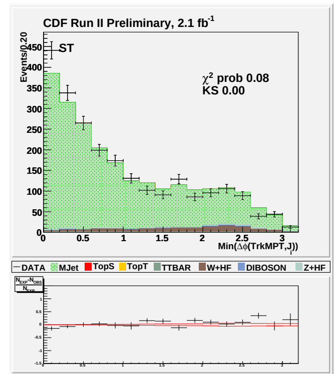

(c) Min($\Delta\phi(\not{p}_T^{tr}, J_i)$)

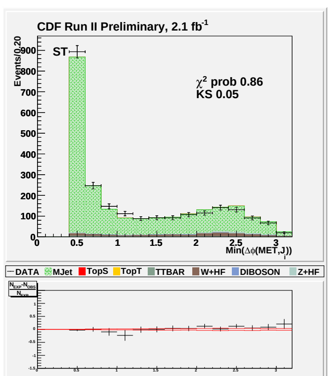

(d) Min($\Delta\phi(\not{E}_T, J_i)$)

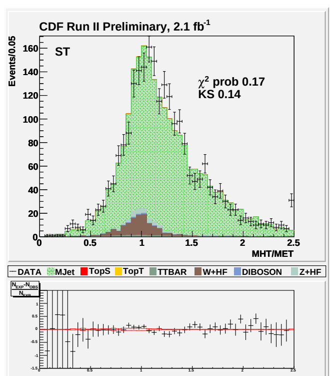

(e) $\not{H}_T/\not{E}_T$

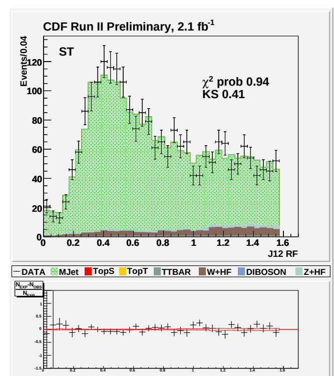

(f) $\Delta\phi$(J1/2 in RF, boost)

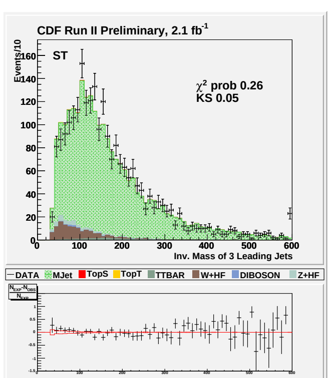

(g) Inv. mass between the two (or three) leading jets

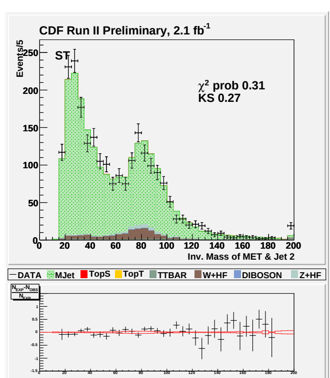

(h) Inv. mass between $\not{E}_T$ and the second leading jet

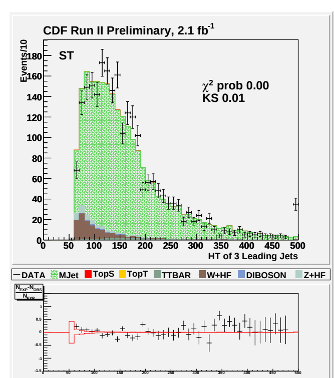

(i) H_T^3

Figure 39: Control Region 3 (QCD), Excl. Single Tag

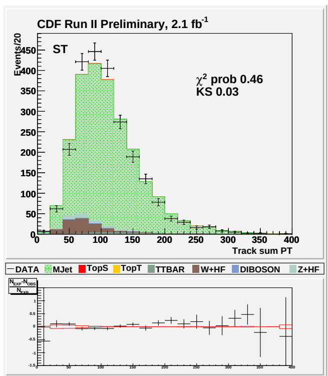

(a) $\sum P_T^{tr}$

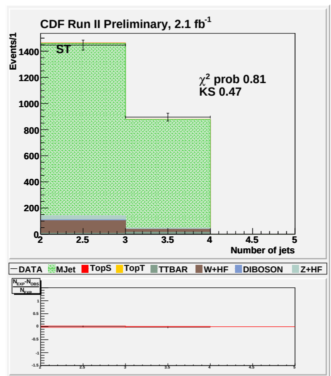

(b) Number of jets

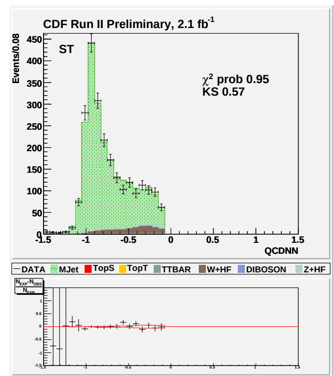

(c) QCDNN

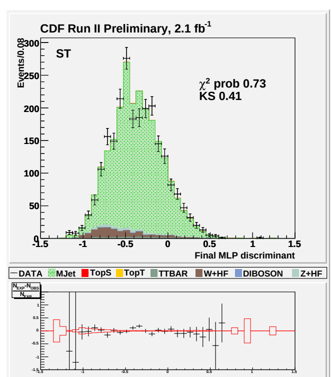

(d) Final MLP Discriminant

Figure 40: Control Region 3 (QCD), Excl. Single Tag

A.3.2 ST + ST

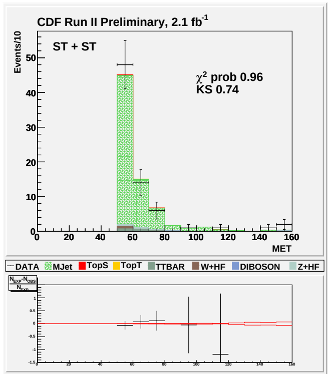

(a) $\not\!\!E_T$

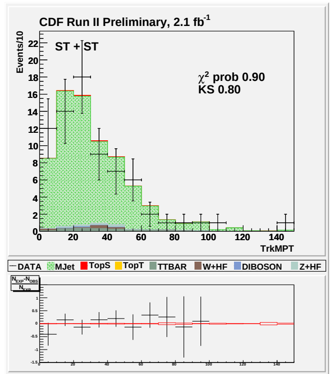

(b) $\not\!\!P_T^{tr}$

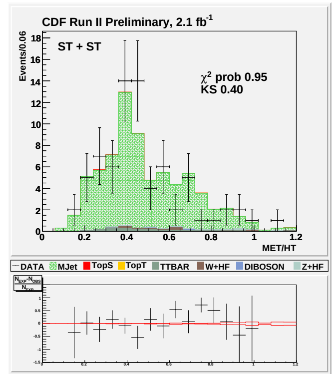

(c) $\not\!\!E_T/HT$

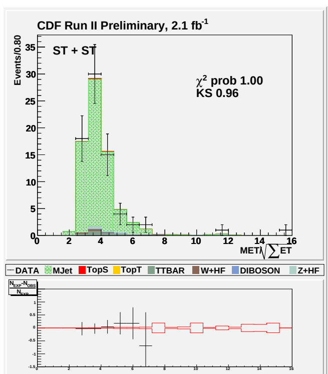

(d) $\not\!\!E_T$ Signifiance

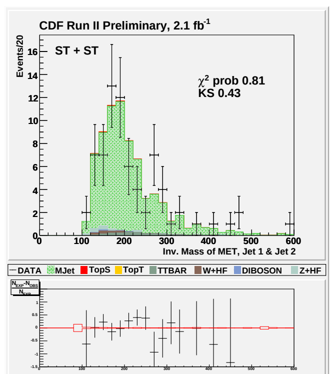

(e) Inv. mass between $\not\!\!E_T$ and the two leading jets

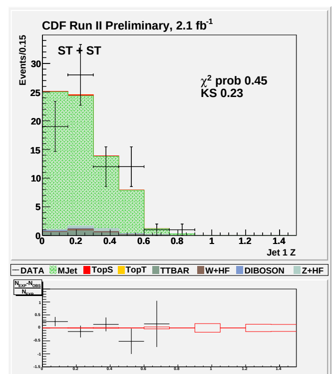

(f) Jet 1 Z

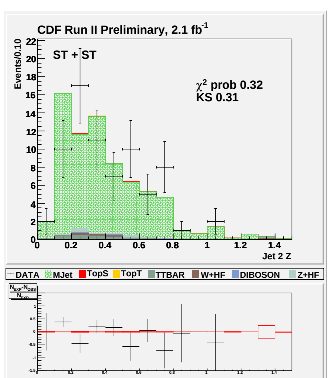

(g) Jet 2 Z

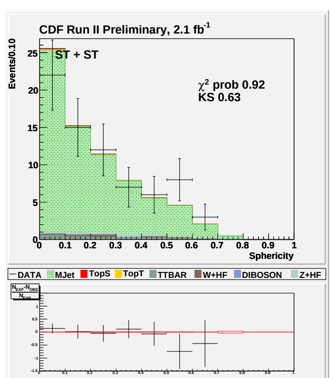

(h) Sphericity

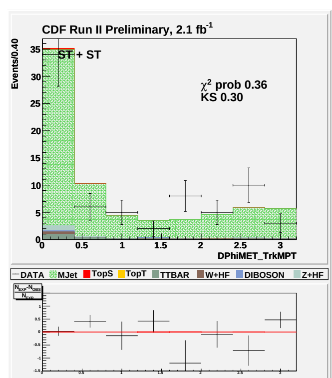

(i) $\Delta\phi(\not\!\!P_T^{tr}, \not\!\!E_T)$

Figure 41: Control Region 3 (QCD), ST + ST

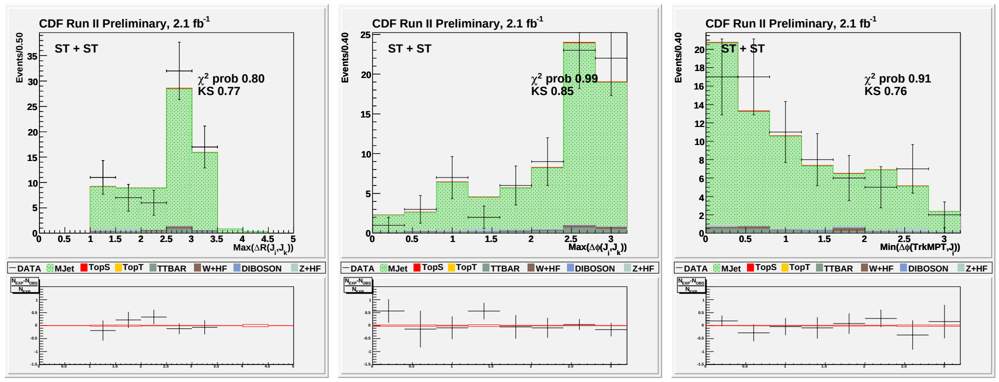

(a) Max$(\Delta R(J_i, J_k))$ (b) Max$(\Delta\phi(J_i, J_k))$ (c) Min$(\Delta\phi(\not{P}_T^{tr}, J_i))$

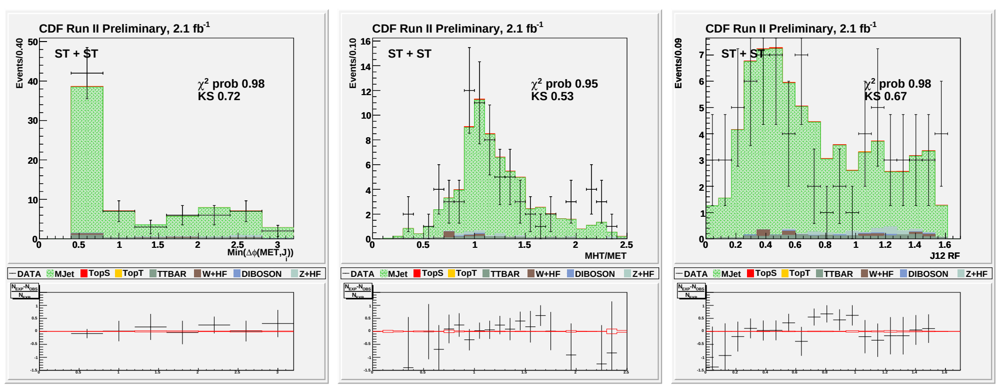

(d) Min$(\Delta\phi(\not{E}_T, J_i))$ (e) $\not{H}_T/\not{E}_T$ (f) $\Delta\phi$(J1/2 in RF, boost)

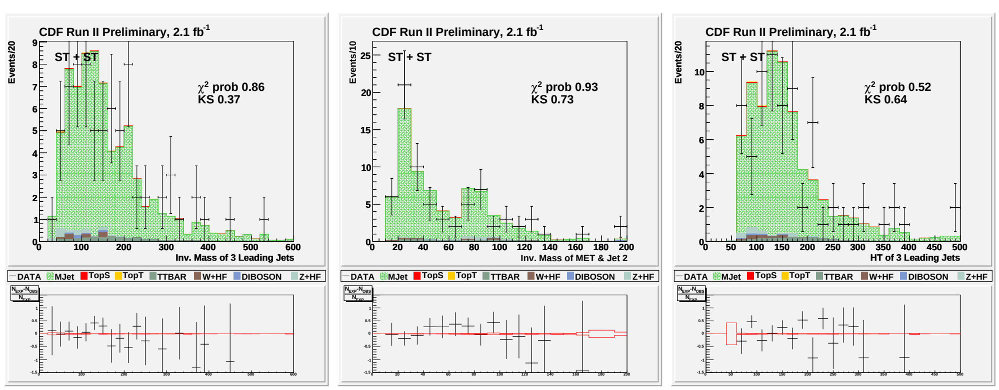

(g) Inv. mass between the two (or three) leading jets (h) Inv. mass between $\not{E}_T$ and the second leading jet (i) H_T^3

Figure 42: Control Region 3 (QCD), ST + ST

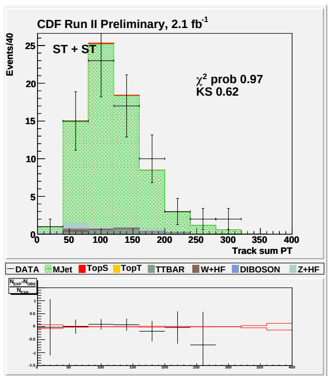

(a) $\sum P_T^{tr}$

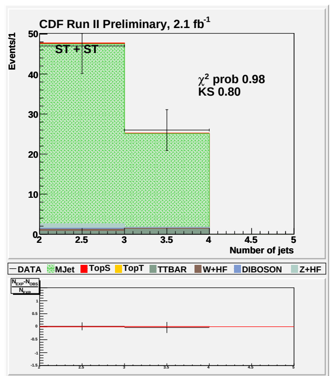

(b) Number of jets

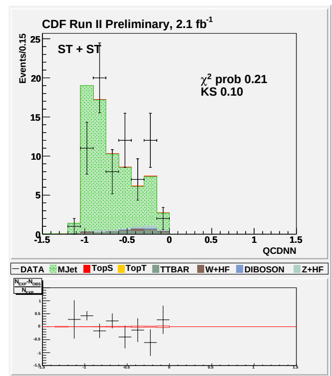

(c) QCDNN

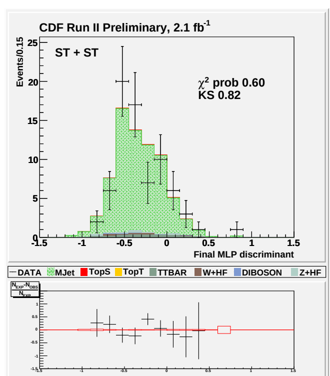

(d) Final MLP Discriminant

Figure 43: Control Region 3 (QCD), ST + ST

A.3.3 ST + JP

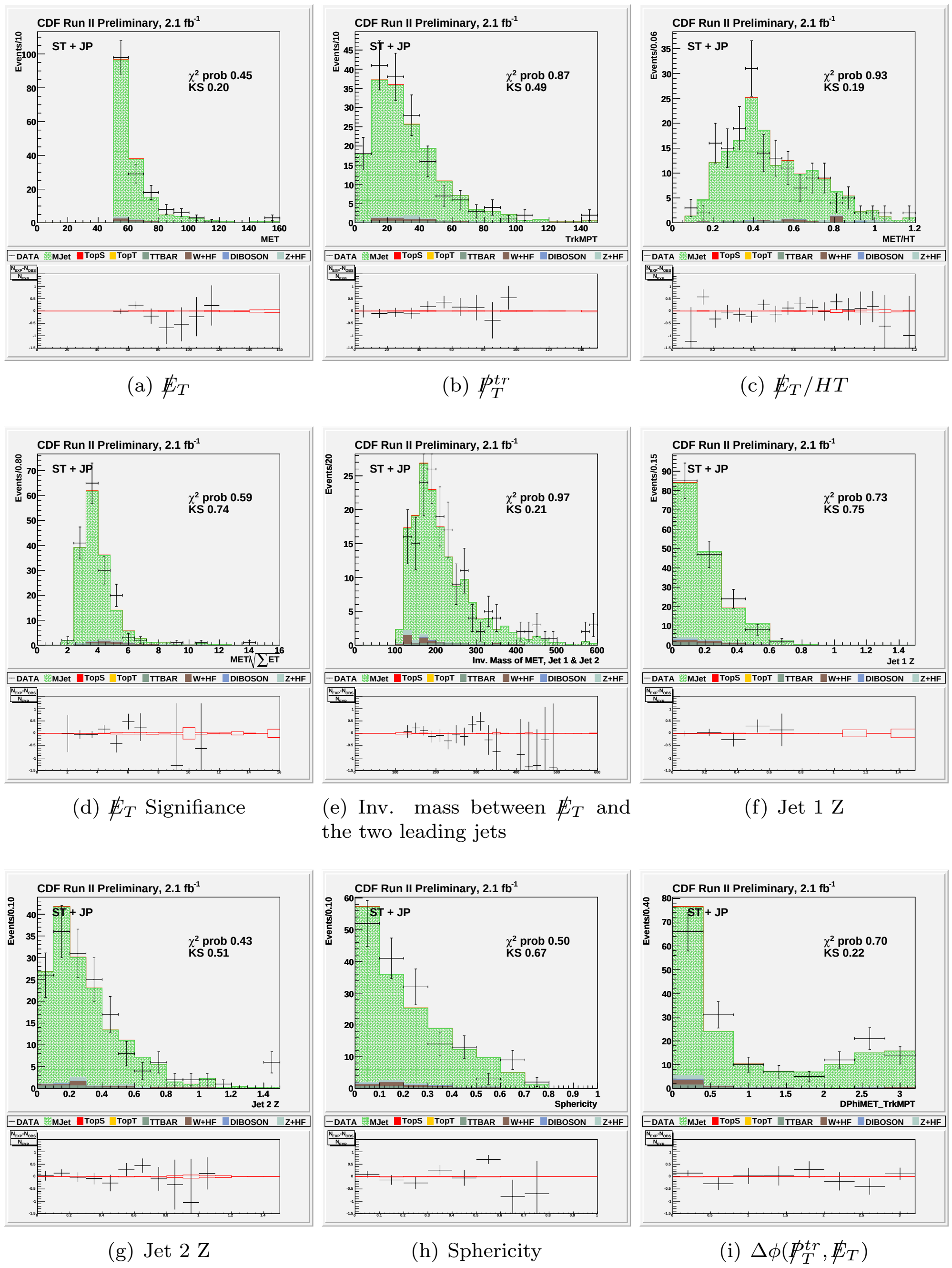

(a) $\not\!\!E_T$ (b) $\not\!\!P_T^{tr}$ (c) $\not\!\!E_T/HT$

(d) $\not\!\!E_T$ Significance (e) Inv. mass between $\not\!\!E_T$ and the two leading jets (f) Jet 1 Z

(g) Jet 2 Z (h) Sphericity (i) $\Delta\phi(\not\!\!P_T^{tr}, \not\!\!E_T)$

Figure 44: Control Region 3 (QCD), ST + JP

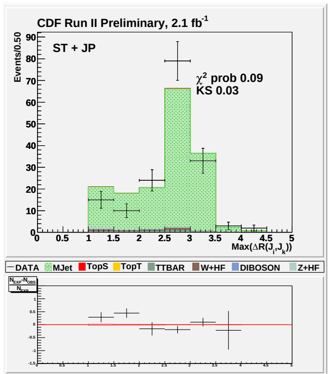

(a) Max$(\Delta R(J_i, J_k))$

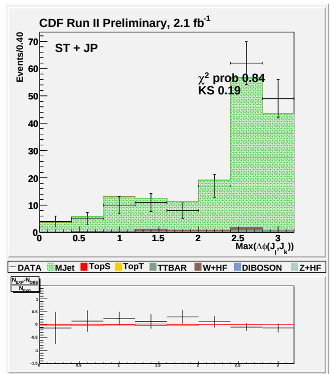

(b) Max$(\Delta\phi(J_i, J_k))$

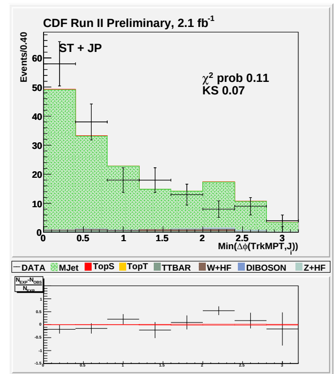

(c) Min$(\Delta\phi(\not{p}_T^{tr}, J_i))$

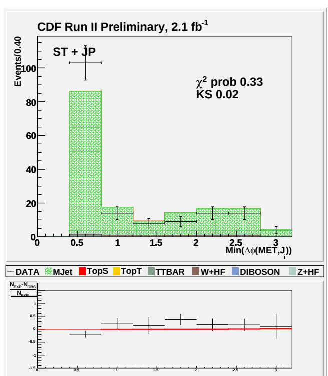

(d) Min$(\Delta\phi(\not{E}_T, J_i))$

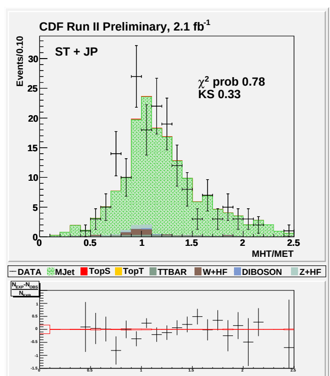

(e) $\not{H}_T/\not{E}_T$

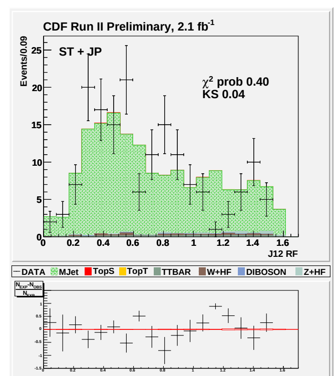

(f) $\Delta\phi$(J1/2 in RF, boost)

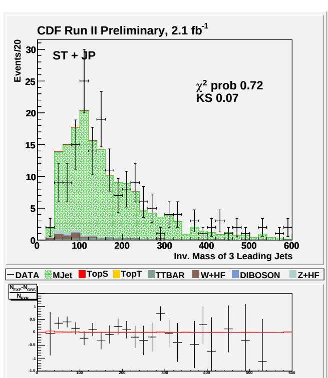

(g) Inv. mass between the two (or three) leading jets

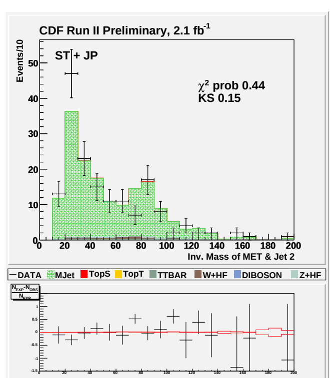

(h) Inv. mass between $\not{E}_T$ and the second leading jet

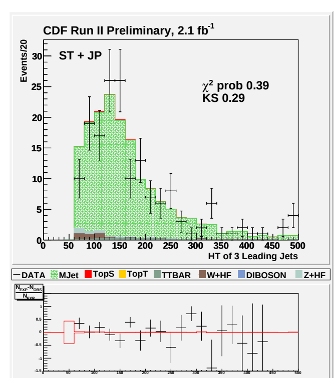

(i) H_T^3

Figure 45: Control Region 3 (QCD), ST + JP

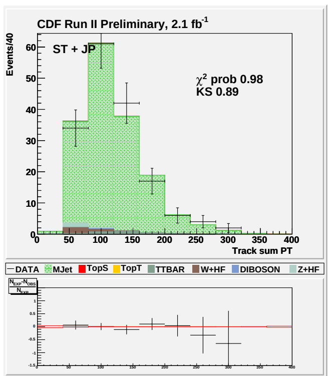

(a) $\sum P_T^{tr}$

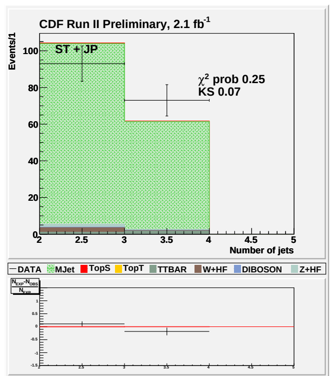

(b) Number of jets

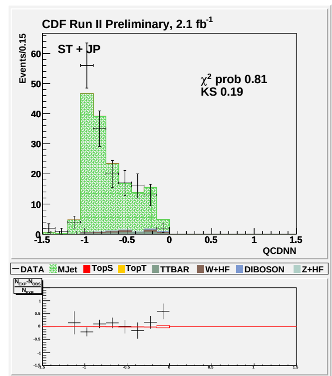

(c) QCDNN

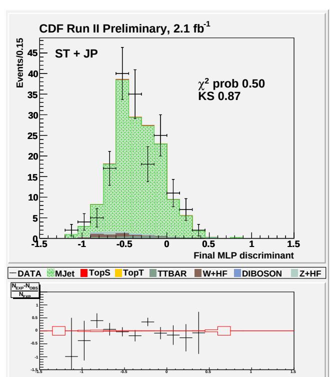

(d) Final MLP Discriminant

Figure 46: Control Region 3 (QCD), ST + JP

A.4 Signal Region Plots

A.4.1 Excl. Single Tag

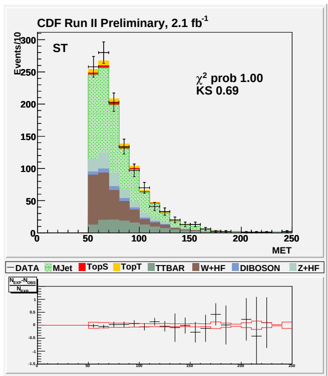

(a) $\not{E}_T$

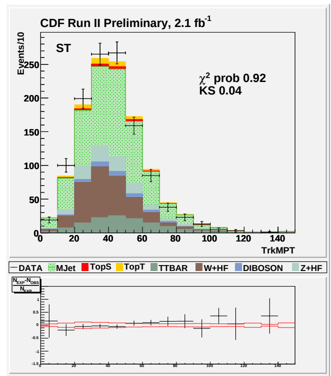

(b) $\not{P}_T^{tr}$

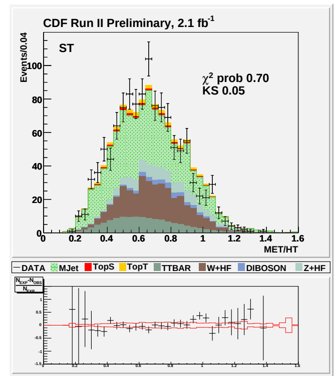

(c) $\not{E}_T/HT$

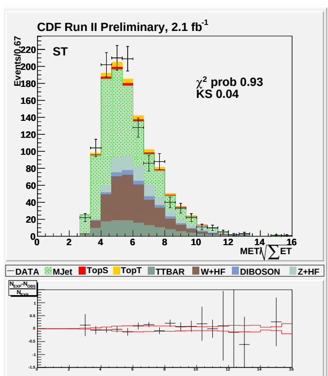

(d) $\not{E}_T$ Signifiance

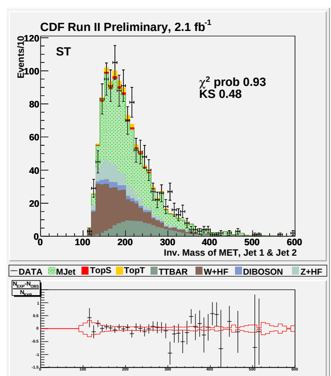

(e) Inv. mass between $\not{E}_T$ and the two leading jets

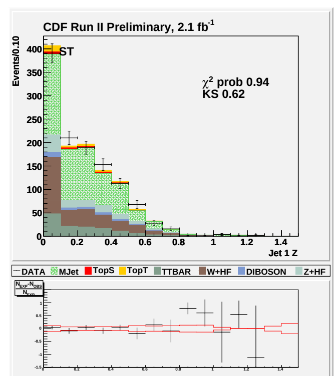

(f) Jet 1 Z

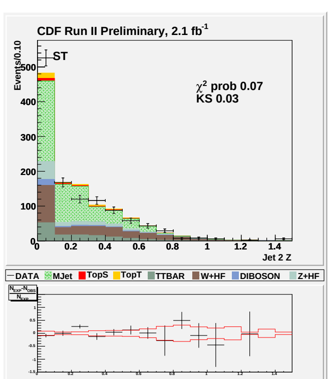

(g) Jet 2 Z

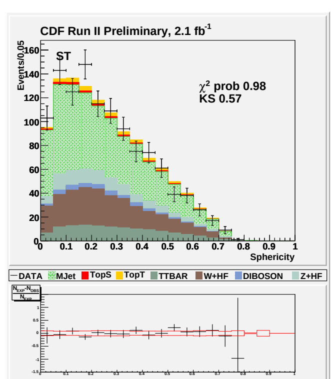

(h) Sphericity

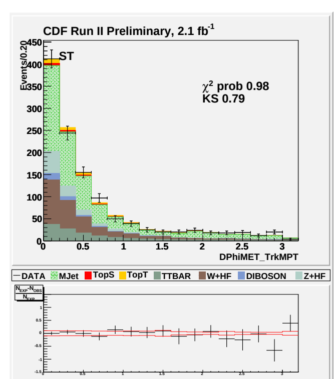

(i) $\Delta\phi(\not{P}_T^{tr}, \not{E}_T)$

Figure 47: Signal Region, Excl. Single Tag

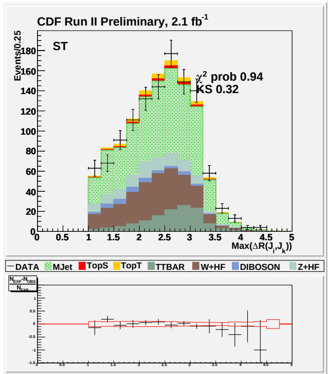

(a) Max$(\Delta R(J_i, J_k))$

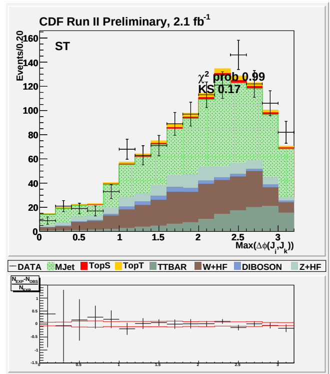

(b) Max$(\Delta\phi(J_i, J_k))$

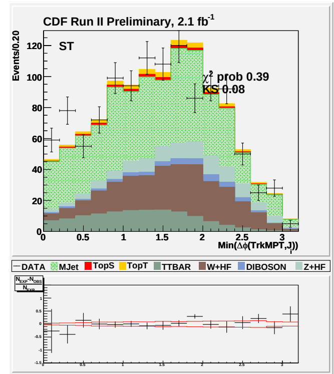

(c) Min$(\Delta\phi(\not{p}_T^{tr}, J_i))$

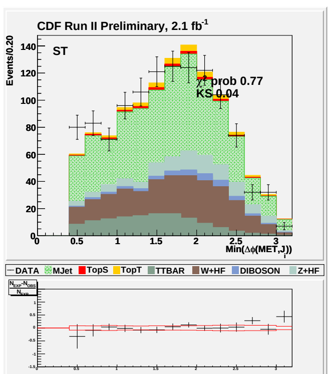

(d) Min$(\Delta\phi(\not{E}_T, J_i))$

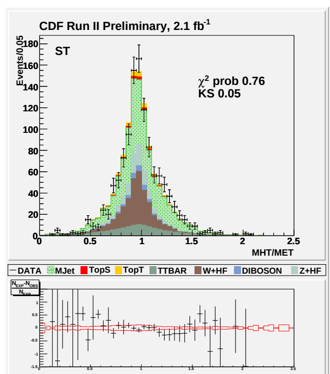

(e) $\not{H}_T/\not{E}_T$

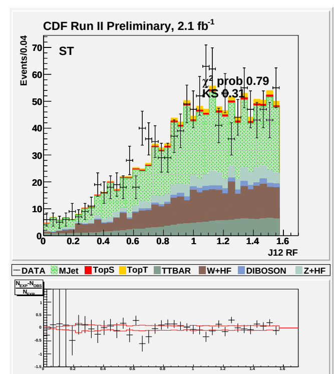

(f) $\Delta\phi$(J1/2 in RF, boost)

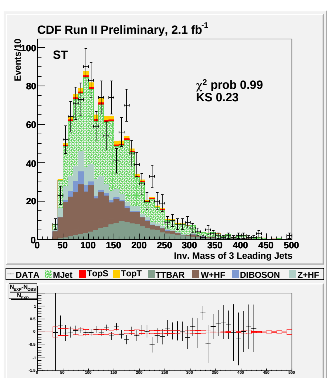

(g) Inv. mass between the two (or three) leading jets

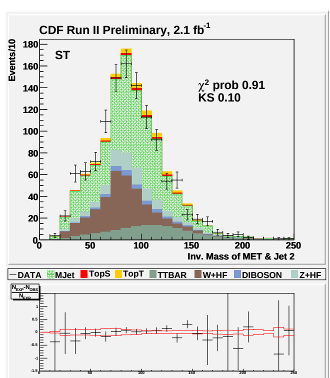

(h) Inv. mass between $\not{E}_T$ and the second leading jet

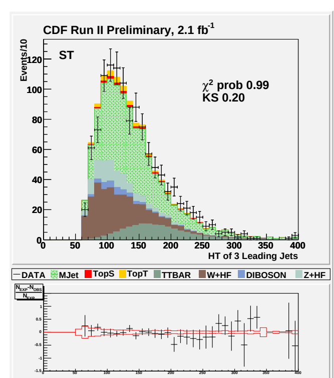

(i) H_T^3

Figure 48: Signal Region, Excl. Single Tag

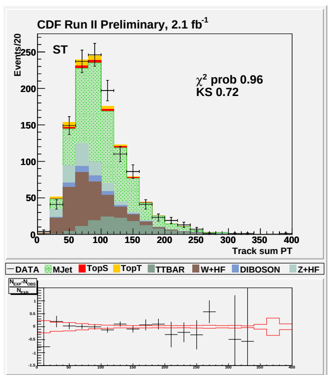

(a) $\sum P_T^{tr}$

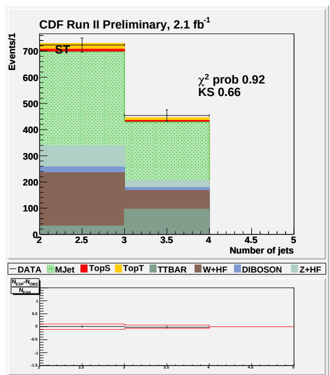

(b) Number of jets

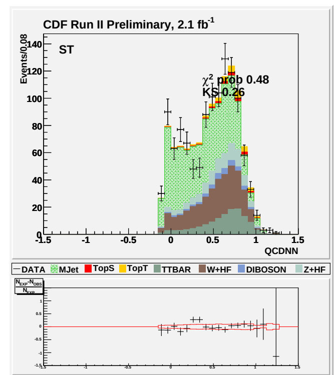

(c) QCDNN

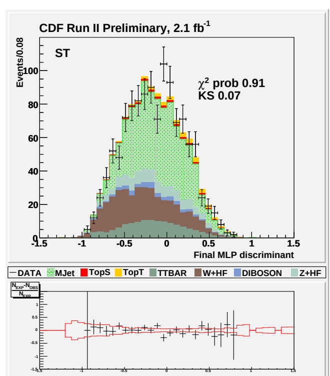

(d) Final MLP Discriminant

Figure 49: Signal Region, Excl. Single Tag

A.4.2 ST + ST

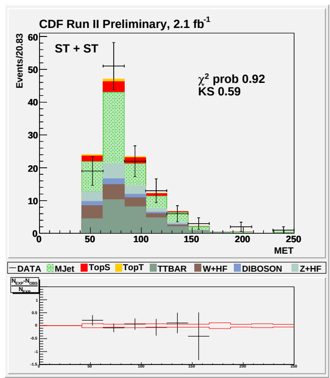

(a) $\not{E}_T$

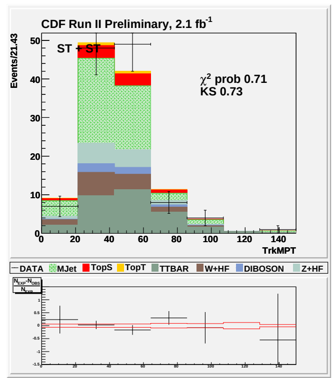

(b) $\not{P}_T^{tr}$

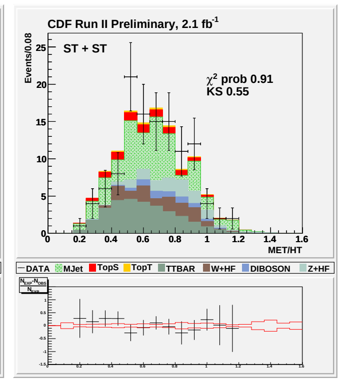

(c) $\not{E}_T/HT$

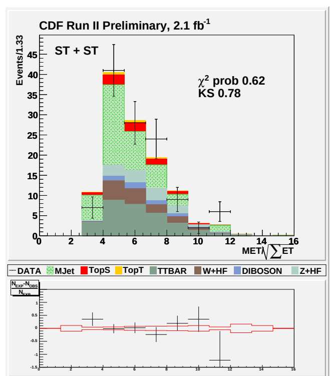

(d) $\not{E}_T$ Signifiance

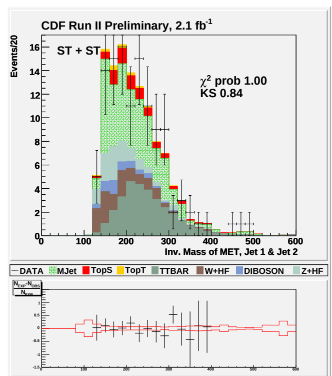

(e) Inv. mass between $\not{E}_T$ and the two leading jets

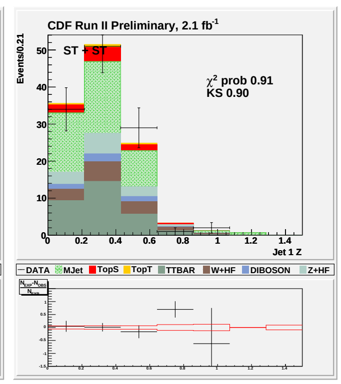

(f) Jet 1 Z

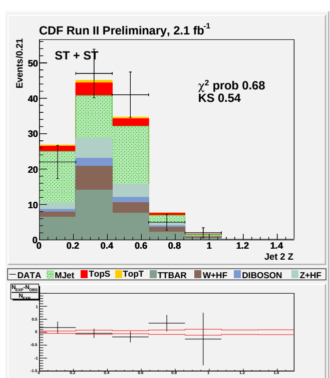

(g) Jet 2 Z

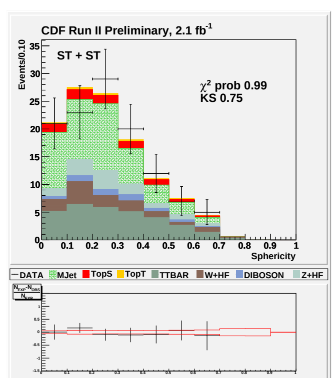

(h) Sphericity

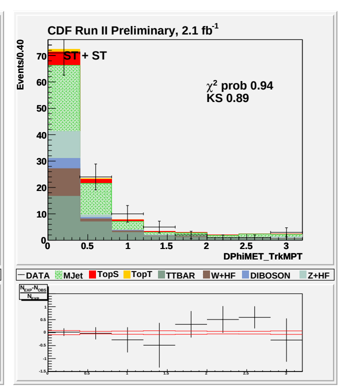

(i) $\Delta\phi(\not{P}_T^{tr}, \not{E}_T)$

Figure 50: Signal Region, ST + ST

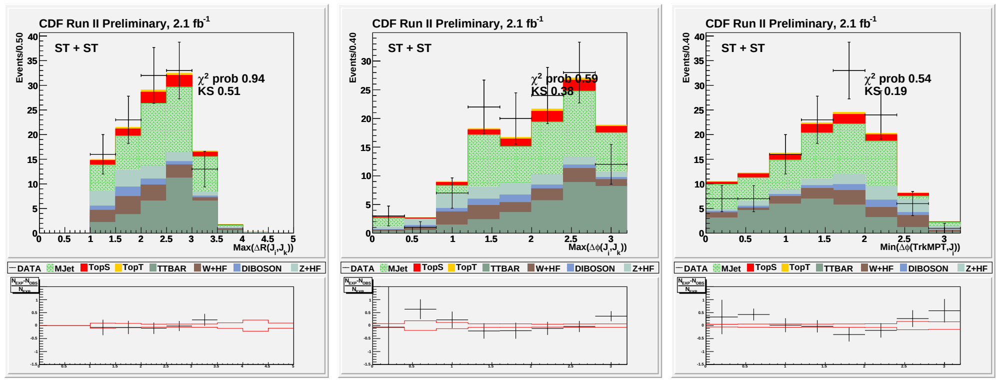

(a) Max($\Delta R(J_i, J_k)$) (b) Max($\Delta\phi(J_i, J_k)$) (c) Min($\Delta\phi(\not\!p_T^{tr}, J_i)$)

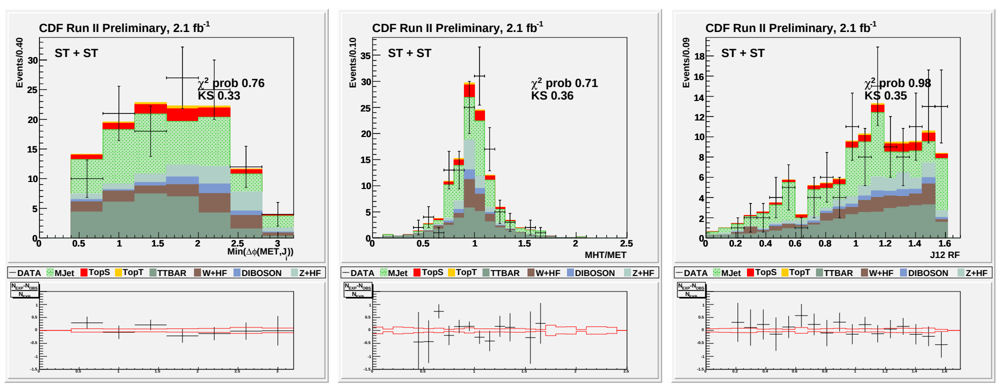

(d) Min($\Delta\phi(\not\!\!E_T, J_i)$) (e) $\not\!\!H_T/\not\!\!E_T$ (f) $\Delta\phi$(J1/2 in RF, boost)

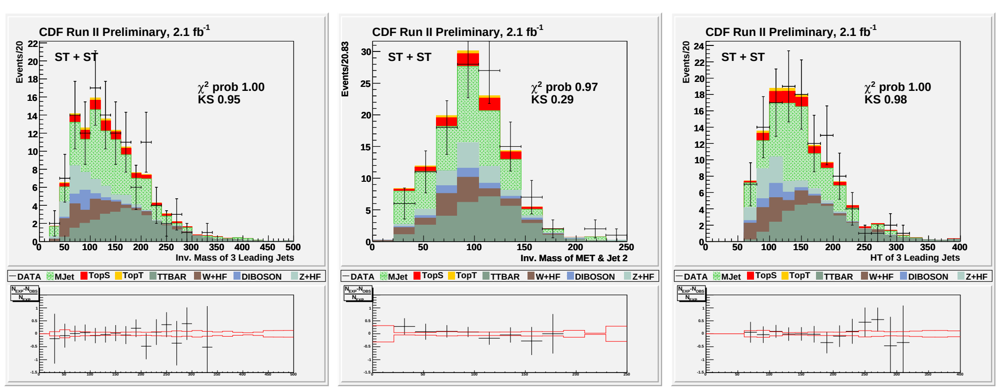

(g) Inv. mass between the two (or three) leading jets (h) Inv. mass between $\not\!\!E_T$ and the second leading jet (i) H_T^3

Figure 51: Signal Region, ST + ST

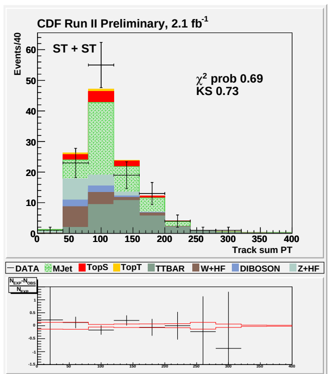

(a) $\sum P_T^{tr}$

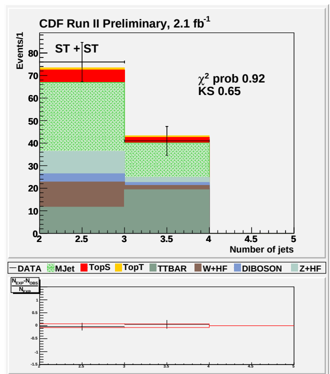

(b) Number of jets

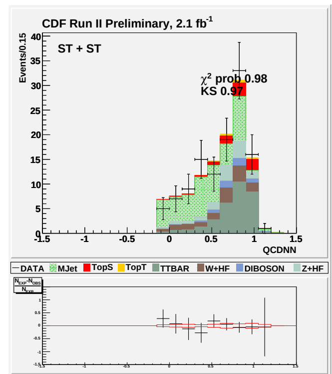

(c) QCDNN

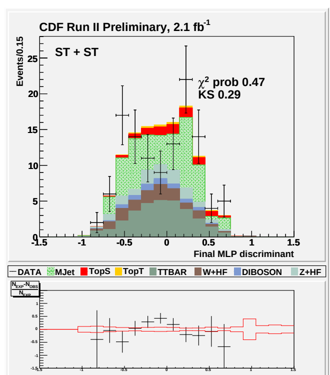

(d) Final MLP Discriminant

Figure 52: Signal Region, ST + ST

A.4.3 ST + JP

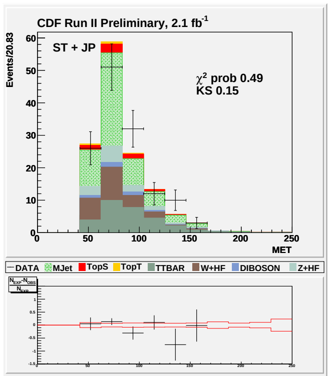

(a) $\not\!\!E_T$

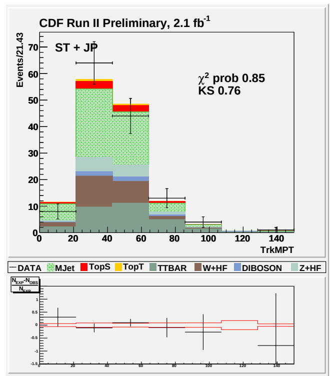

(b) $\not\!\!P_T^{tr}$

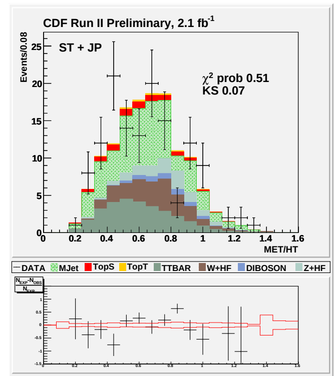

(c) $\not\!\!E_T/HT$

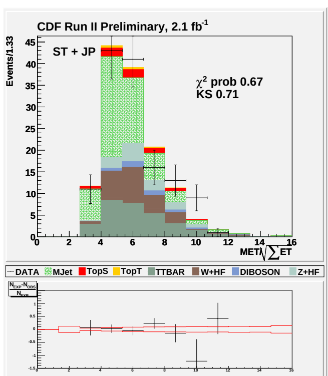

(d) $\not\!\!E_T$ Signifiance

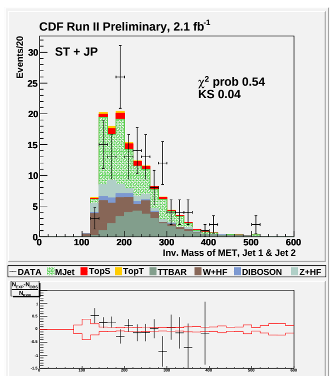

(e) Inv. mass between $\not\!\!E_T$ and the two leading jets

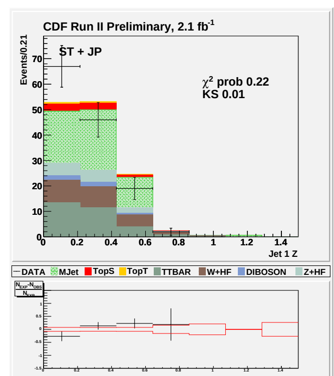

(f) Jet 1 Z

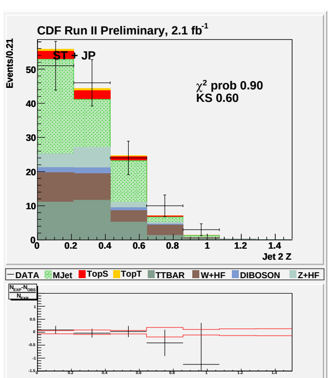

(g) Jet 2 Z

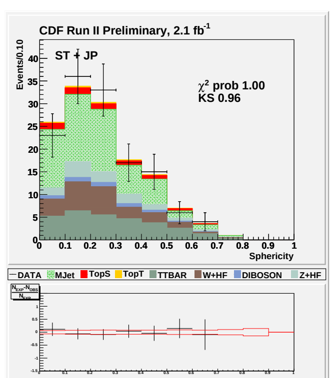

(h) Sphericity

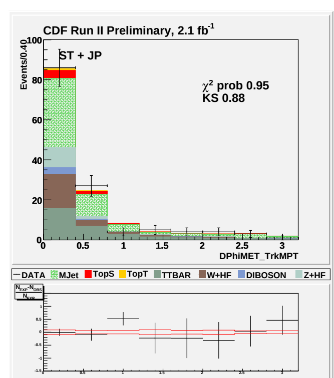

(i) $\Delta\phi(\not\!\!P_T^{tr}, \not\!\!E_T)$

Figure 53: Signal Region, ST + JP

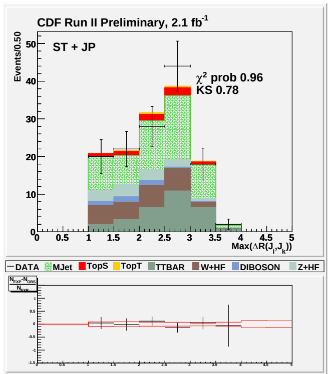

(a) Max($\Delta R(J_i, J_k)$)

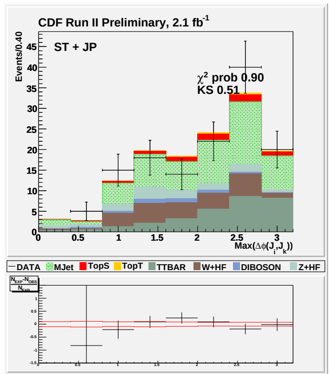

(b) Max($\Delta\phi(J_i, J_k)$)

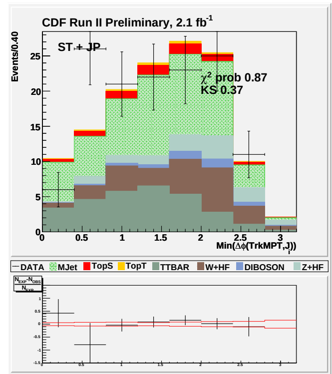

(c) Min($\Delta\phi(\not{p}_T^{tr}, J_i)$)

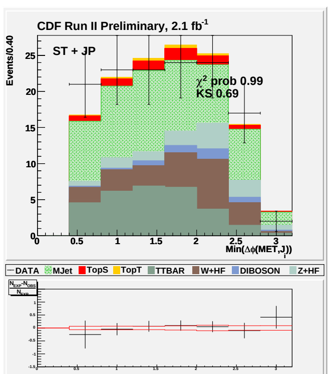

(d) Min($\Delta\phi(\not{E}_T, J_i)$)

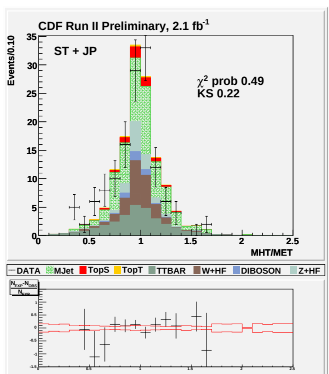

(e) $\not{H}_T/\not{E}_T$

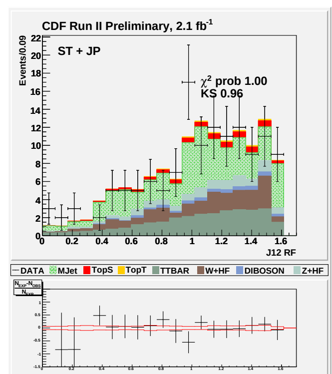

(f) $\Delta\phi$(J1/2 in RF, boost)

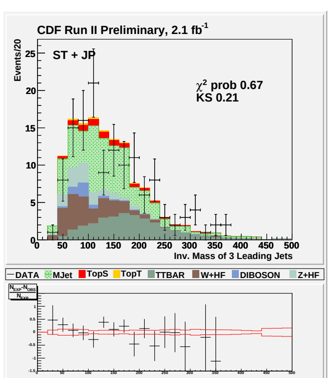

(g) Inv. mass between the two (or three) leading jets

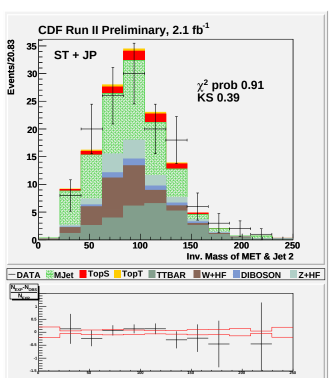

(h) Inv. mass between $\not{E}_T$ and the second leading jet

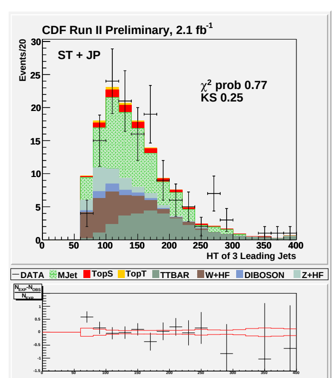

(i) H_T^3

Figure 54: Signal Region, ST + JP

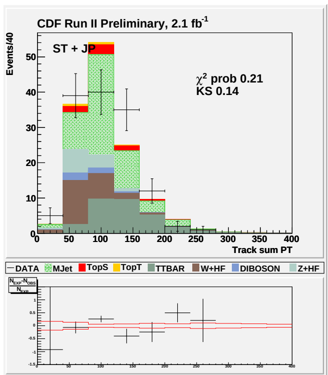

(a) $\sum P_T^{tr}$

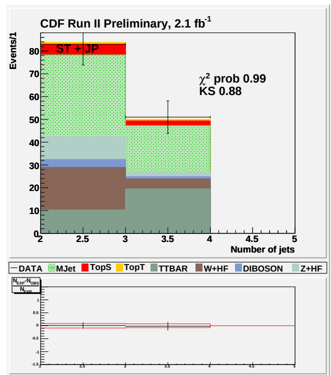

(b) Number of jets

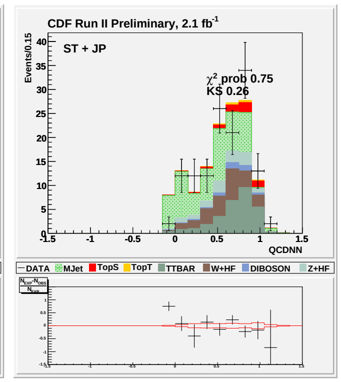

(c) QCDNN

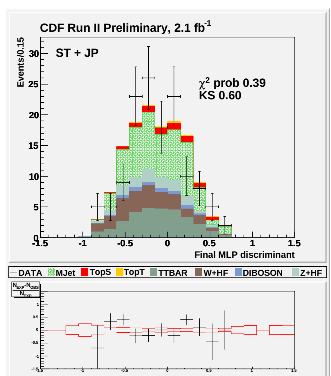

(d) Final MLP Discriminant

Figure 55: Signal Region, ST + JP

B Shape Comparison Plots

B.1 Signal Region Plots

B.1.1 Excl. Single Tag

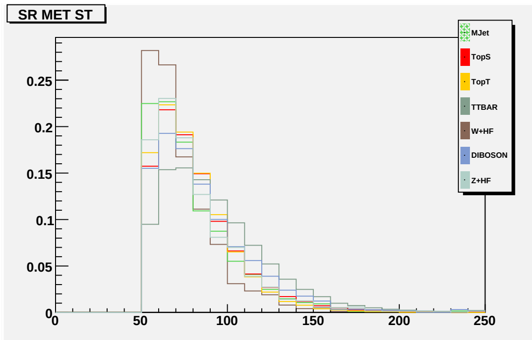

(a) $\not{E}_T$

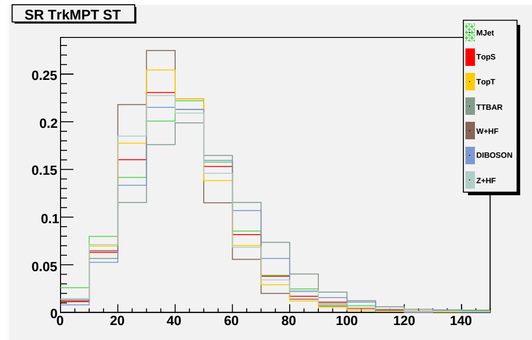

(b) $\not{p}_T^{tr}$

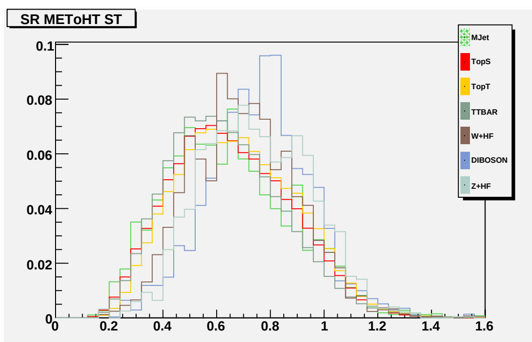

(c) $\not{E}_T/HT$

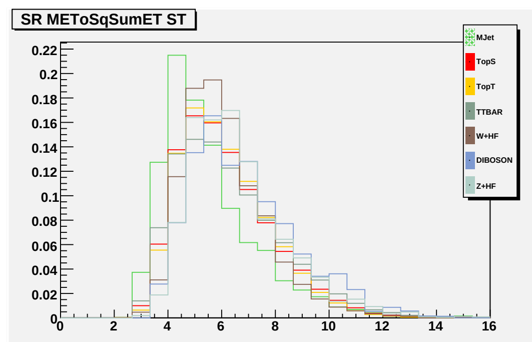

(d) $\not{E}_T$ Signifiance

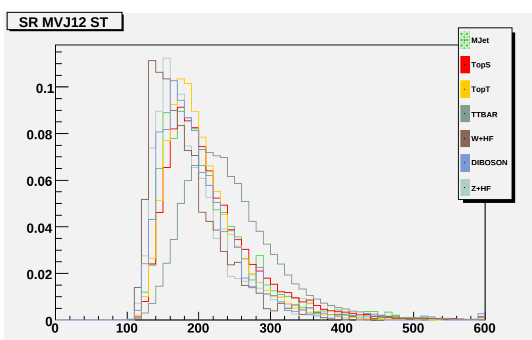

(e) Inv. mass between $\not{E}_T$ and the two leading jets

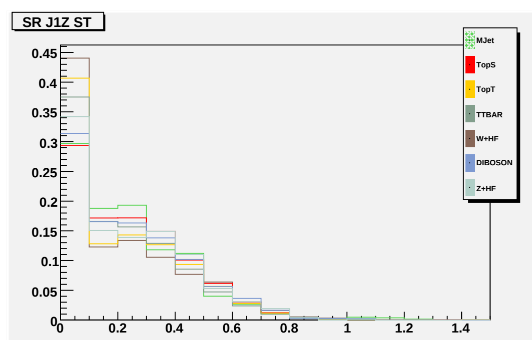

(f) Jet 1 Z

Figure 56: Signal Region, Excl. Single Tag

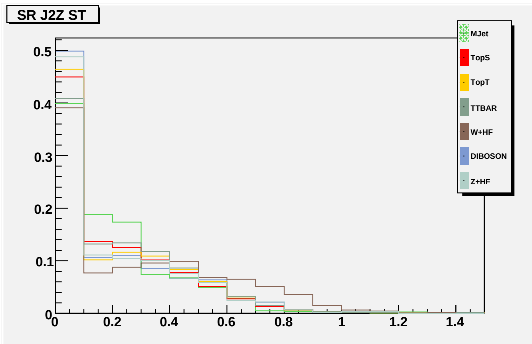

(a) Jet 2 Z

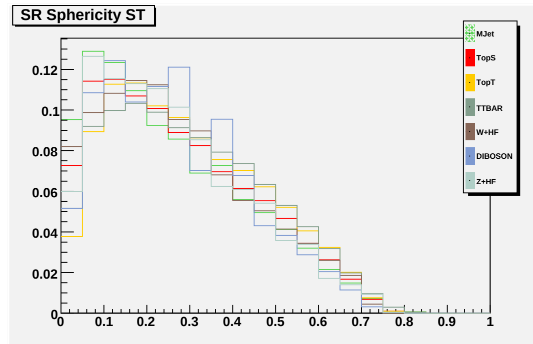

(b) Sphericity

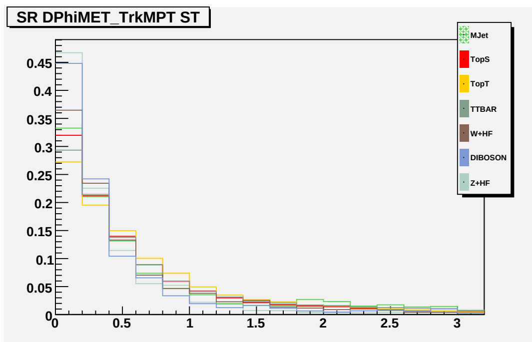

(c) $\Delta\phi(\not{p}_T^{tr}, \not{E}_T)$

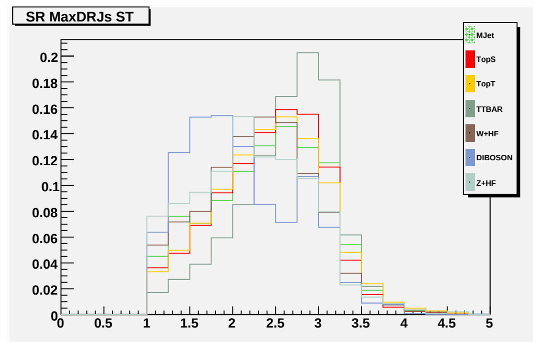

(d) Max($\Delta R(J_i, J_k)$)

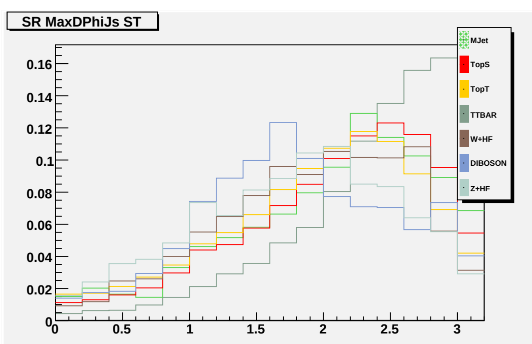

(e) Max($\Delta\phi(J_i, J_k)$)

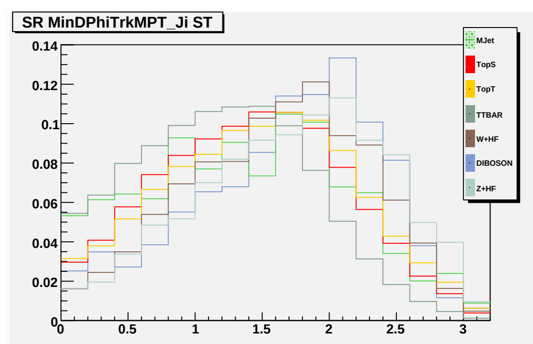

(f) Min($\Delta\phi(\not{p}_T^{tr}, J_i)$)

Figure 57: Signal Region, Excl. Single Tag

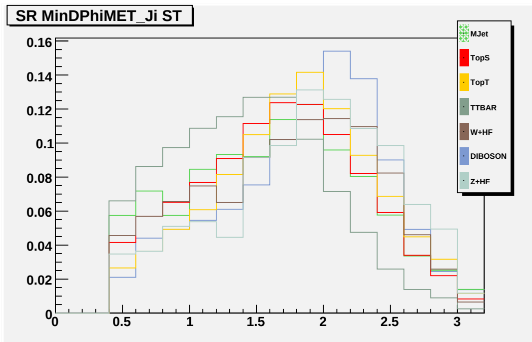

(a) Min($\Delta\phi(\not{E}_T, J_i)$)

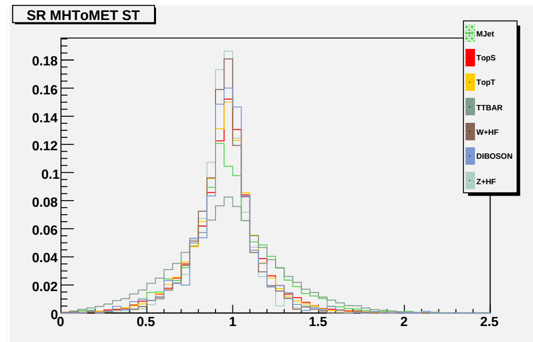

(b) $\not{H}_T/\not{E}_T$

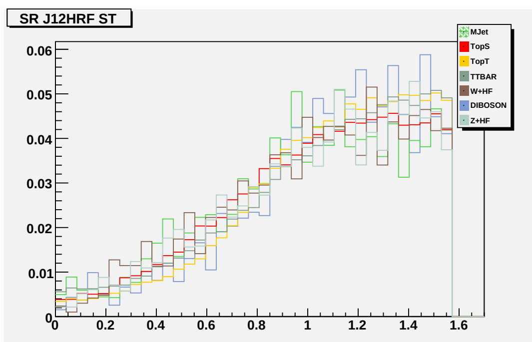

(c) $\Delta\phi(\mathrm{J1/2\ in\ RF, boost})$

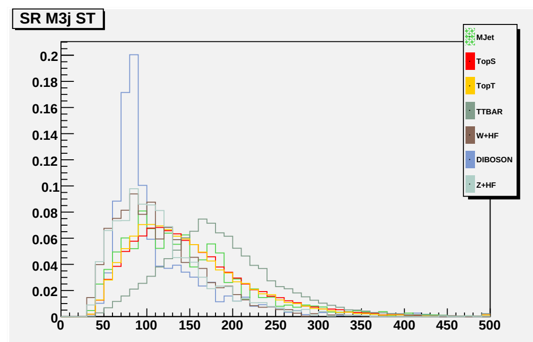

(d) Inv. mass between the two (or three) leading jets

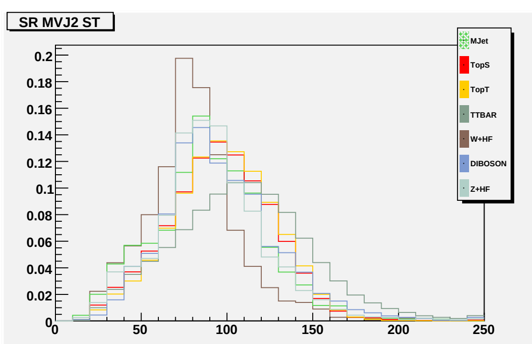

(e) Inv. mass between $\not{E}_T$ and the second leading jet

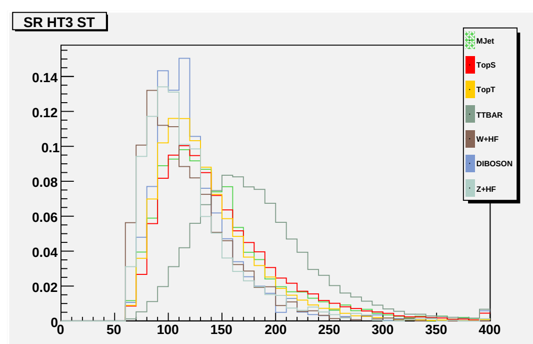

(f) H_T^3

Figure 58: Signal Region, Excl. Single Tag

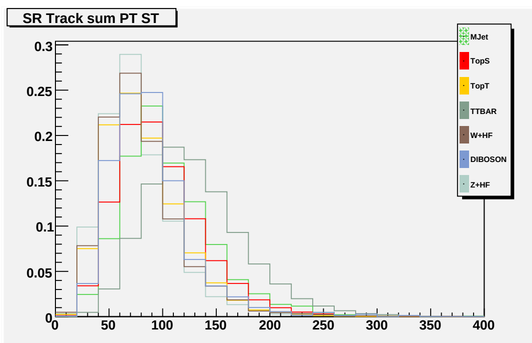

(a) $\sum P_T^{tr}$

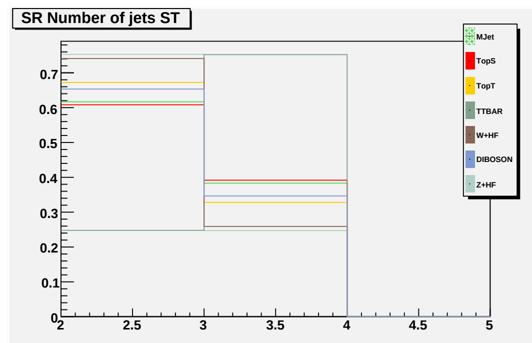

(b) Number of jets

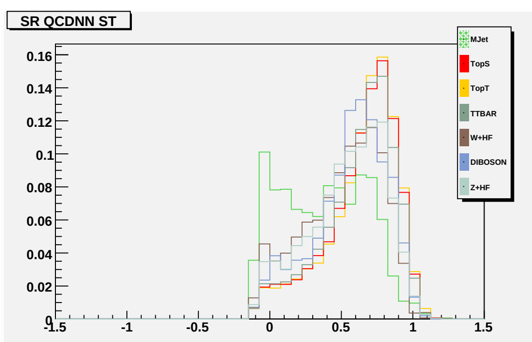

(c) QCDNN

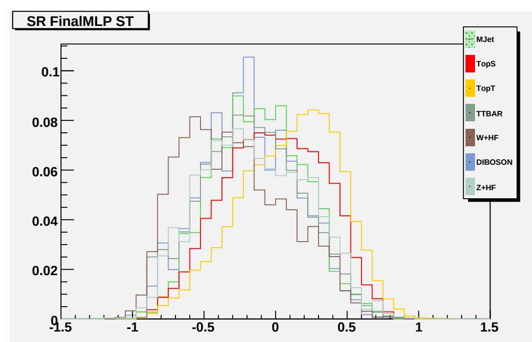

(d) Final MLP Discriminant

Figure 59: Signal Region, Excl. Single Tag

B.1.2 ST + ST

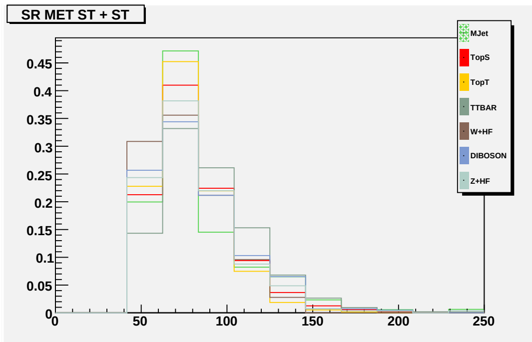

(a) $\not{E}_T$

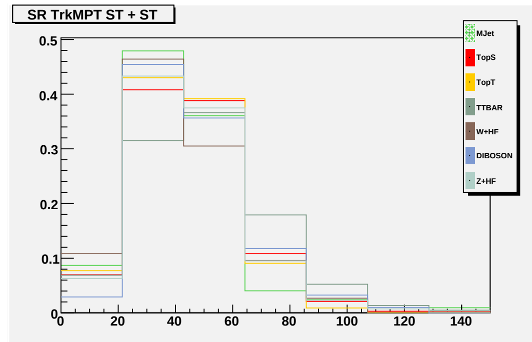

(b) $\not{p}_T^{tr}$

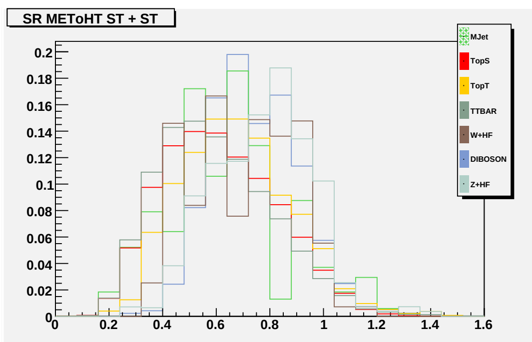

(c) $\not{E}_T/HT$

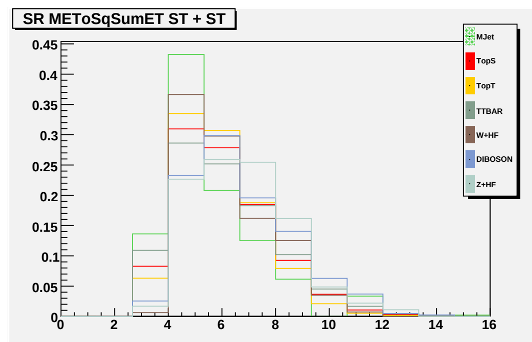

(d) $\not{E}_T$ Signifiance

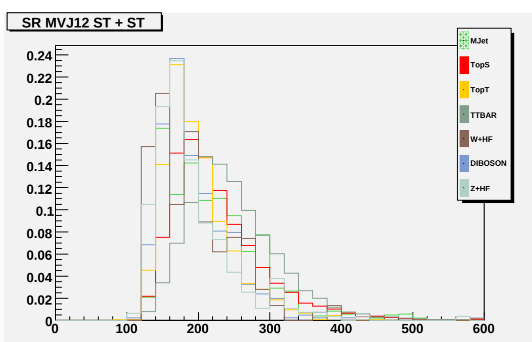

(e) Inv. mass between $\not{E}_T$ and the two leading jets

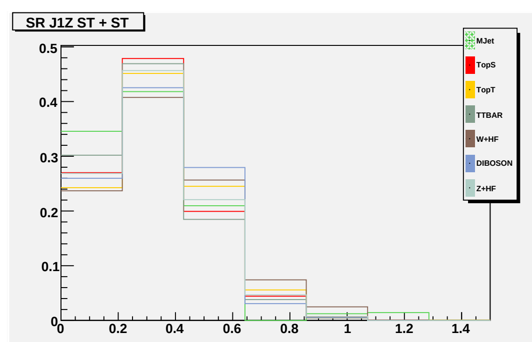

(f) Jet 1 Z

Figure 60: Signal Region, ST + ST

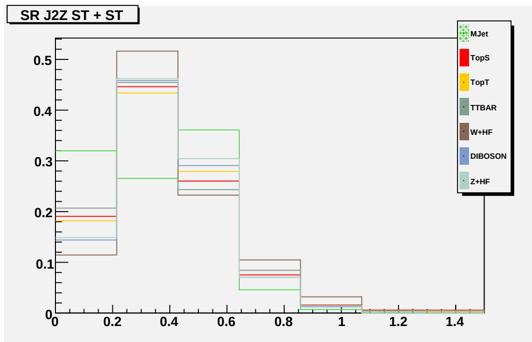

(a) Jet 2 Z

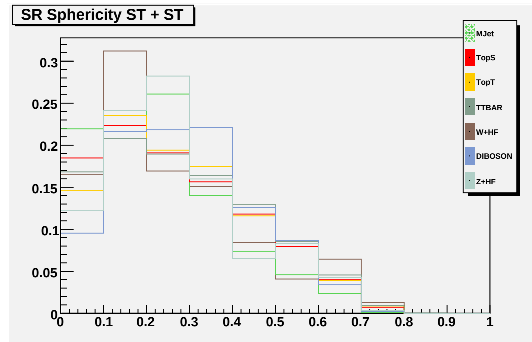

(b) Sphericity

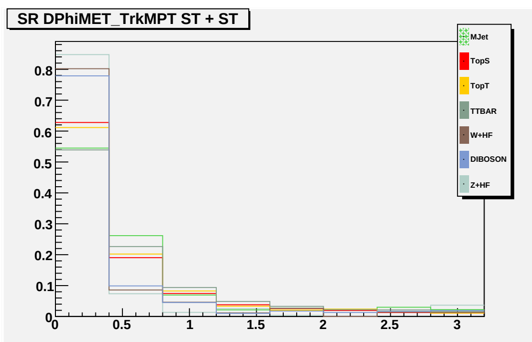

(c) $\Delta\phi(\not{p}_T^{tr}, \not{E}_T)$

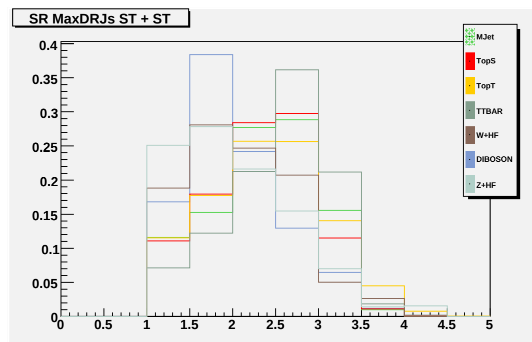

(d) $\mathrm{Max}(\Delta R(J_i, J_k))$

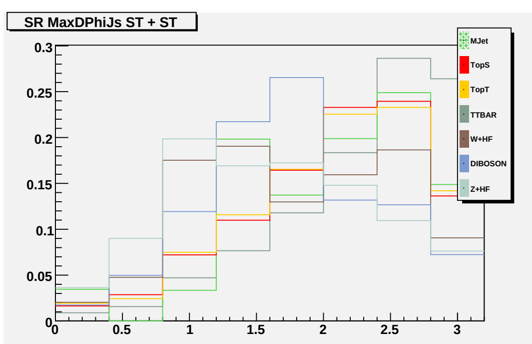

(e) $\mathrm{Max}(\Delta\phi(J_i, J_k))$

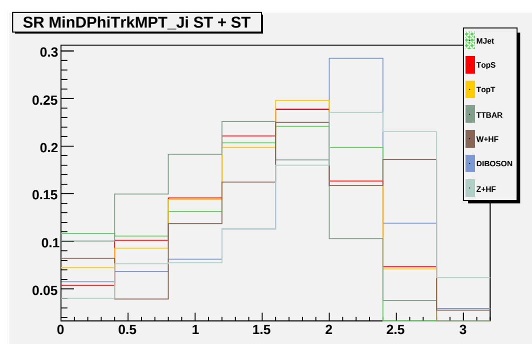

(f) $\mathrm{Min}(\Delta\phi(\not{p}_T^{tr}, J_i))$

Figure 61: Signal Region, ST + ST

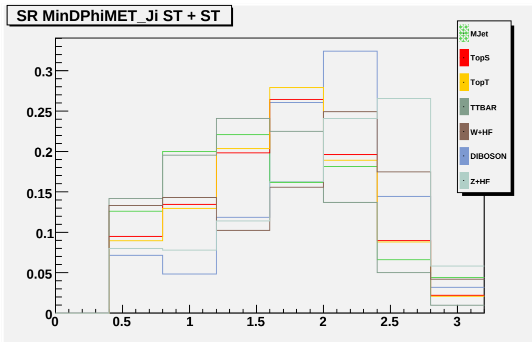

(a) Min($\Delta\phi(\not{E}_T, J_i)$)

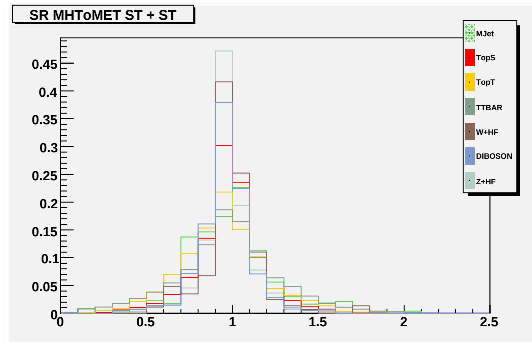

(b) $\not{H}_T/\not{E}_T$

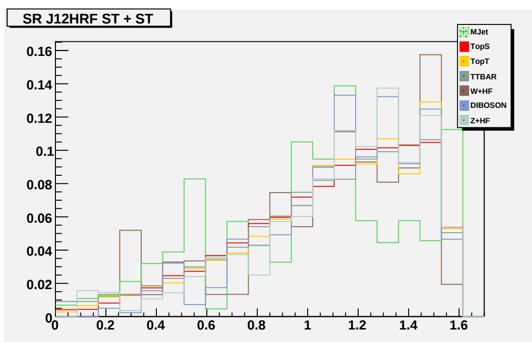

(c) $\Delta\phi$(J1/2 in RF, boost)

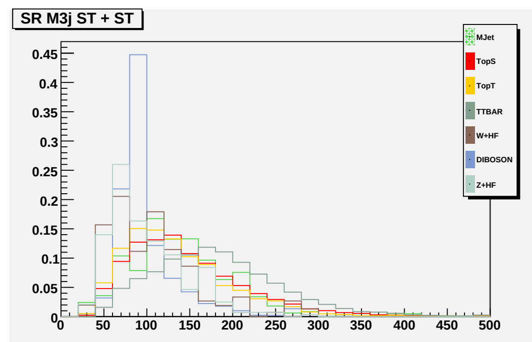

(d) Inv. mass between the two (or three) leading jets

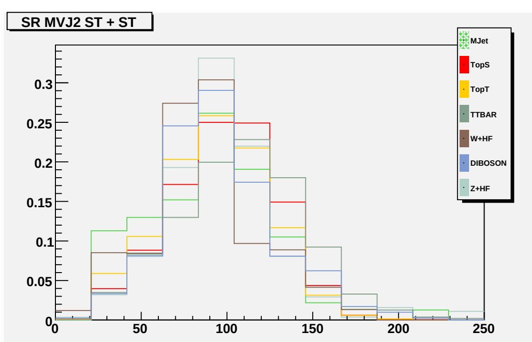

(e) Inv. mass between $\not{E}_T$ and the second leading jet

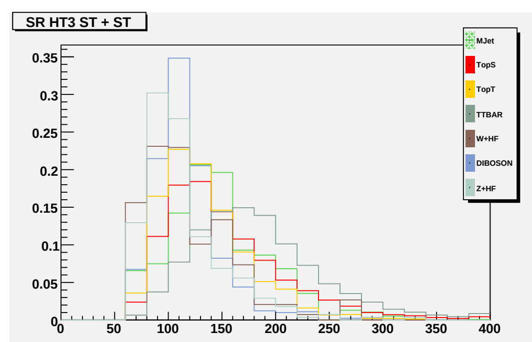

(f) H_T^3

Figure 62: Signal Region, ST + ST

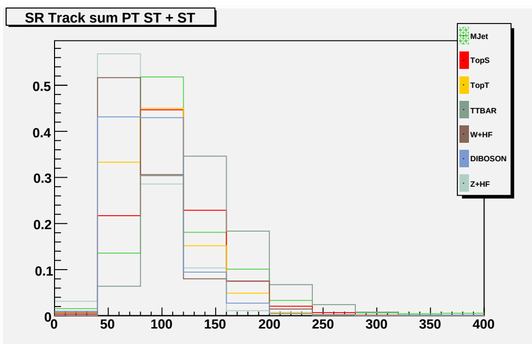

(a) $\sum P_T^{tr}$

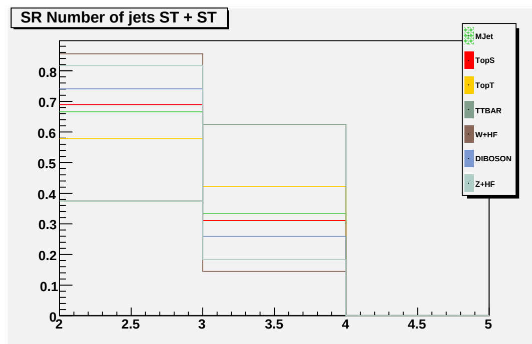

(b) Number of jets

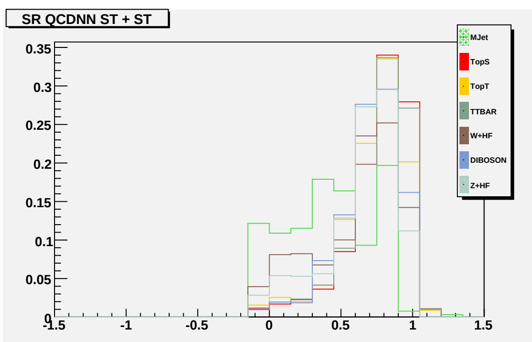

(c) QCDNN

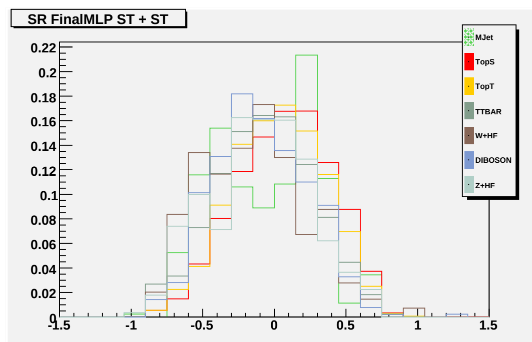

(d) Final MLP Discriminant

Figure 63: Signal Region, ST + ST

B.1.3 ST + JP

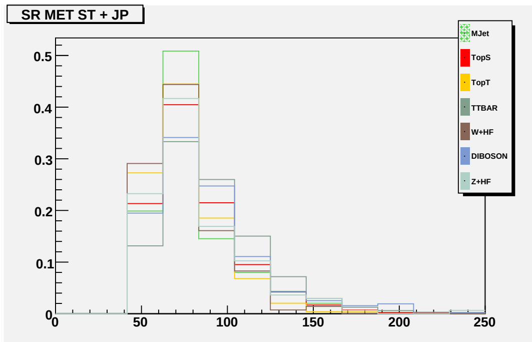

(a) $\not\!\!E_T$

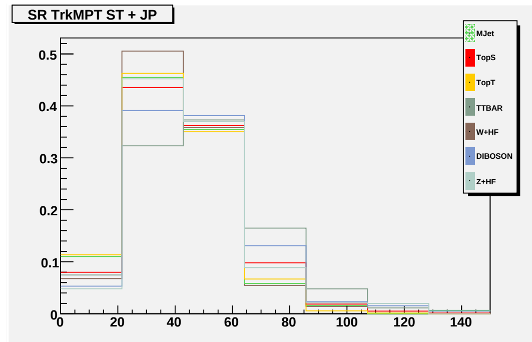

(b) $\not\!p_T^{tr}$

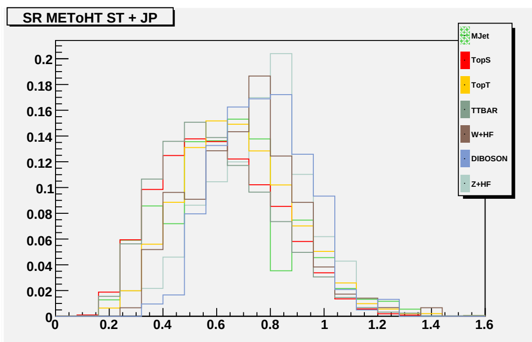

(c) $\not\!\!E_T/HT$

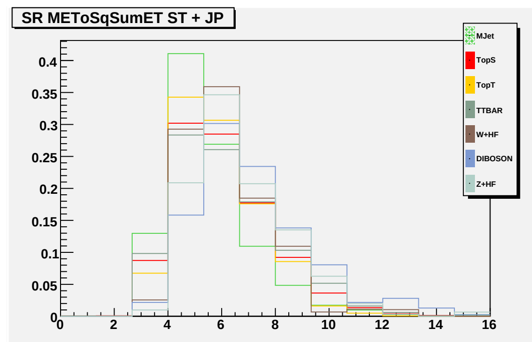

(d) $\not\!\!E_T$ Signifiance

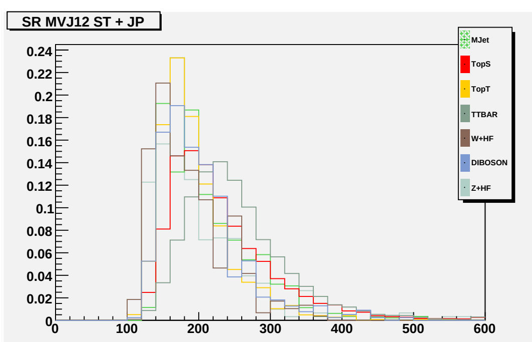

(e) Inv. mass between $\not\!\!E_T$ and the two leading jets

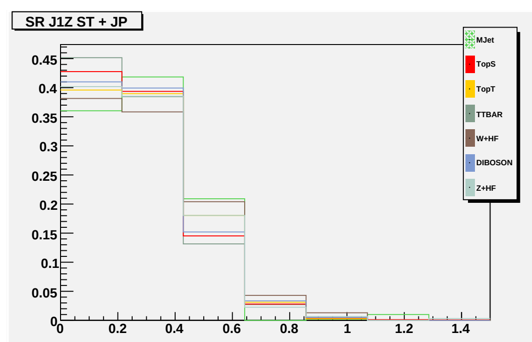

(f) Jet 1 Z

Figure 64: Signal Region, ST + JP

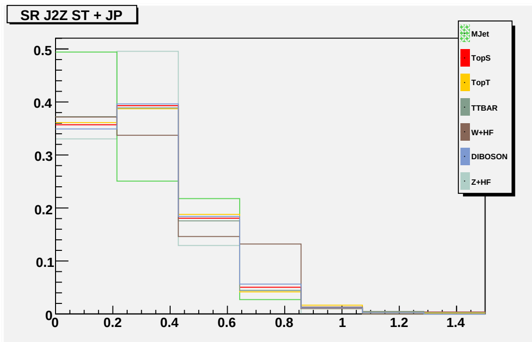

(a) Jet 2 Z

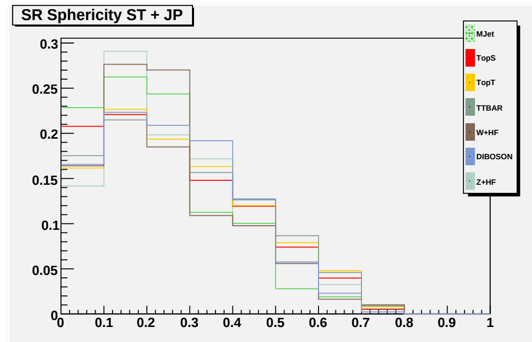

(b) Sphericity

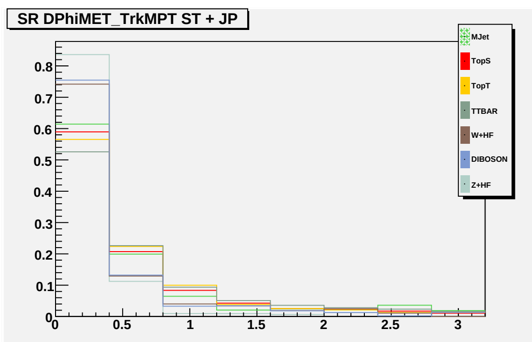

(c) $\Delta\phi(\not{p}_T^{tr}, \not{E}_T)$

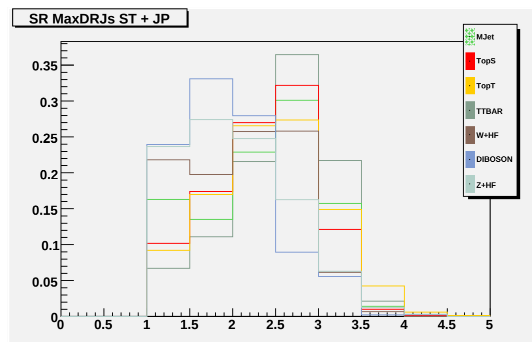

(d) Max($\Delta R(J_i, J_k)$)

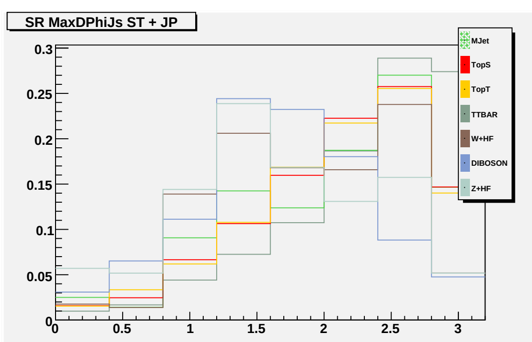

(e) Max($\Delta\phi(J_i, J_k)$)

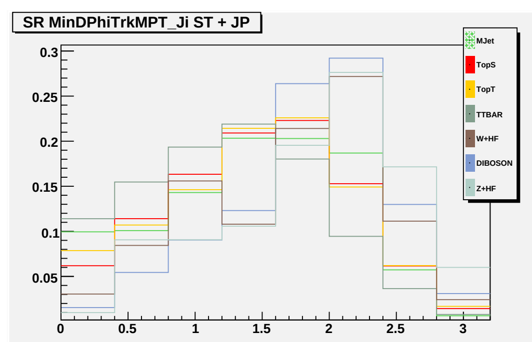

(f) Min($\Delta\phi(\not{p}_T^{tr}, J_i)$)

Figure 65: Signal Region, ST + JP

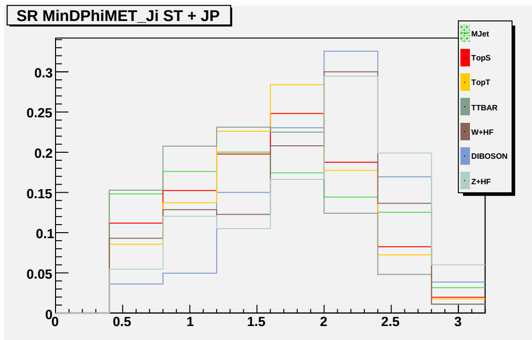

(a) Min($\Delta\phi(\not{E}_T, J_i)$)

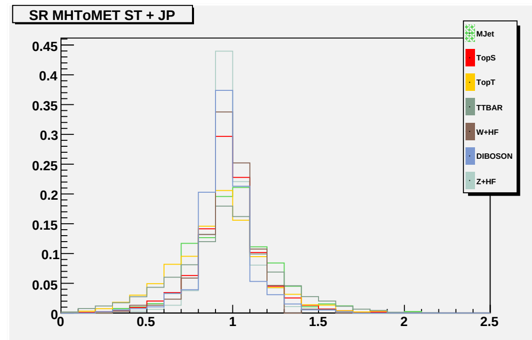

(b) $\not{H}_T/\not{E}_T$

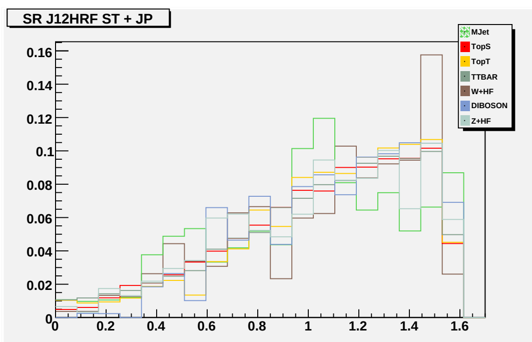

(c) $\Delta\phi(\mathrm{J1/2\ in\ RF, boost})$

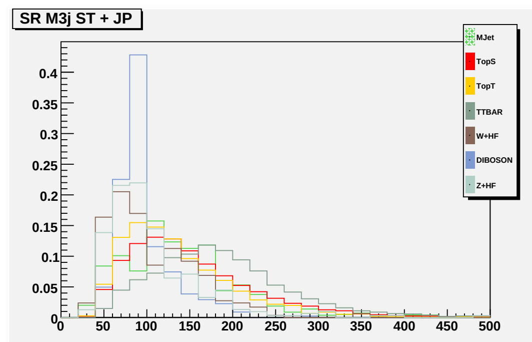

(d) Inv. mass between the two (or three) leading jets

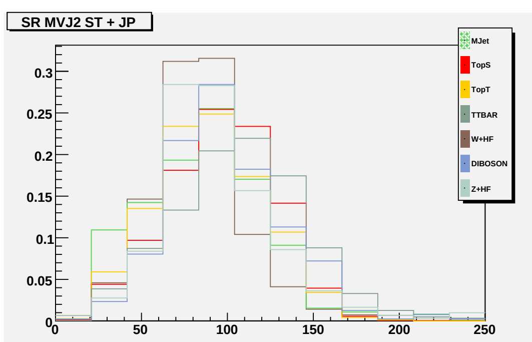

(e) Inv. mass between $\not{E}_T$ and the second leading jet

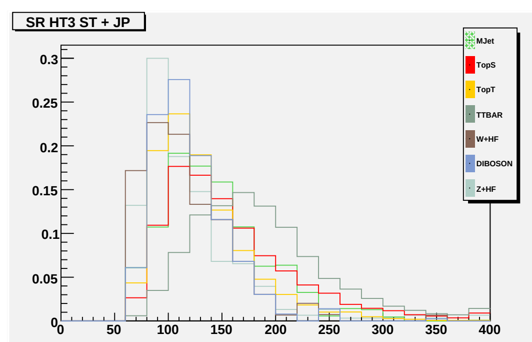

(f) H_T^3

Figure 66: Signal Region, ST + JP

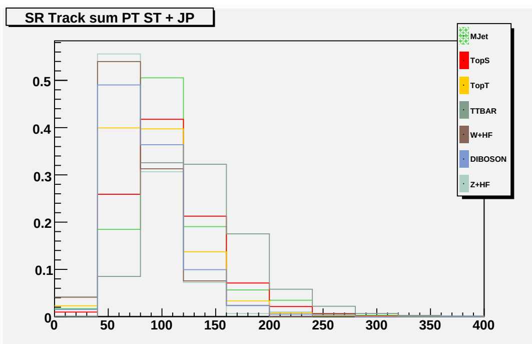

(a) $\sum P_T^{tr}$

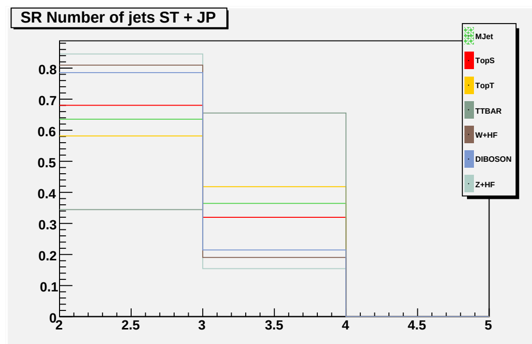

(b) Number of jets

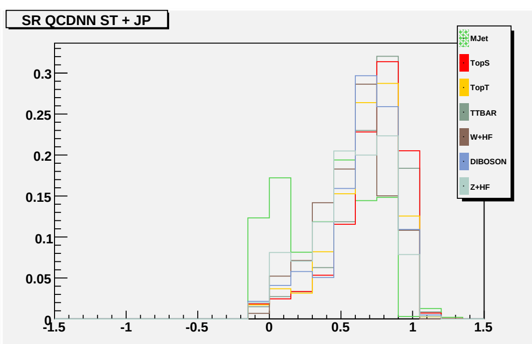

(c) QCDNN

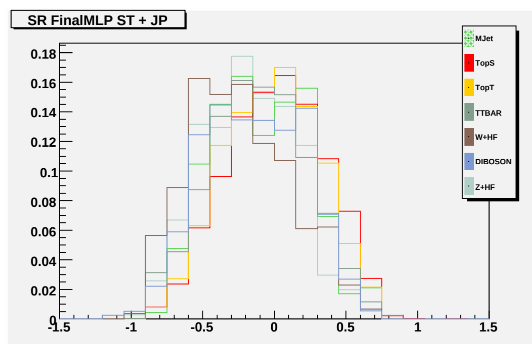

(d) Final MLP Discriminant

Figure 67: Signal Region, ST + JP

B.2 Pre-selection Plots

B.2.1 Excl. Single Tag

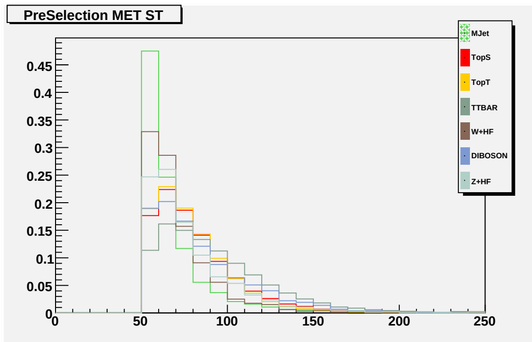

(a) $\not{E}_T$

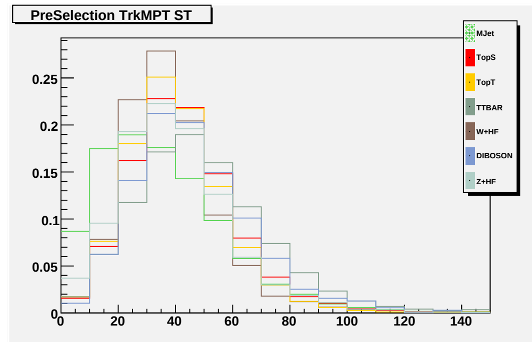

(b) $\not{p}_T^{tr}$

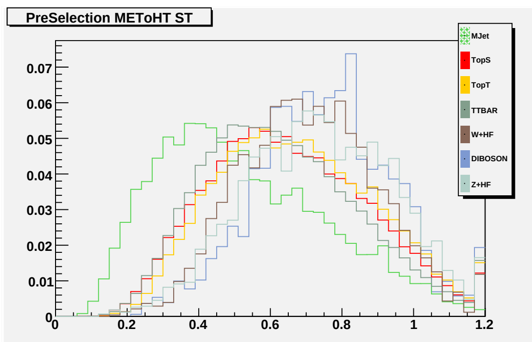

(c) $\not{E}_T/HT$

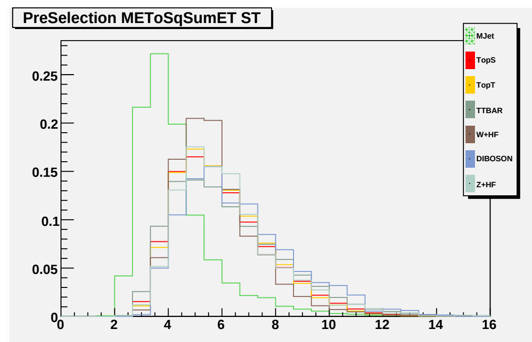

(d) $\not{E}_T$ Signifiance

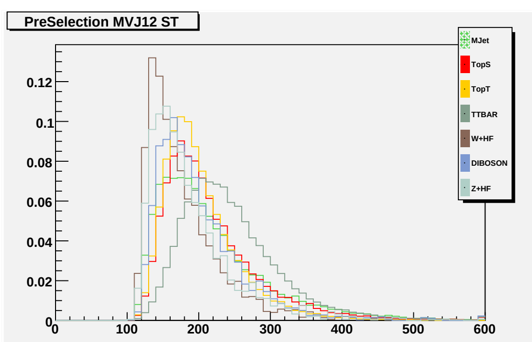

(e) Inv. mass between $\not{E}_T$ and the two leading jets

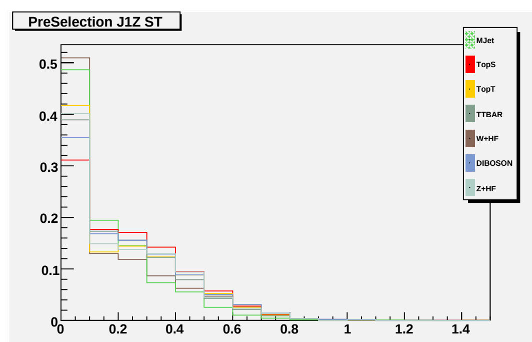

(f) Jet 1 Z

Figure 68: Pre-selection, Excl. Single Tag

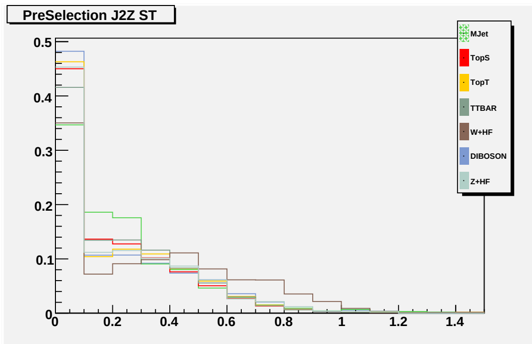

(a) Jet 2 Z

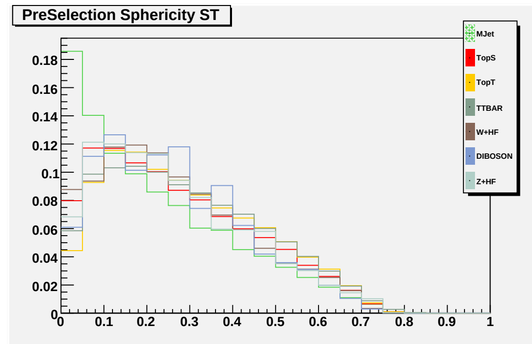

(b) Sphericity

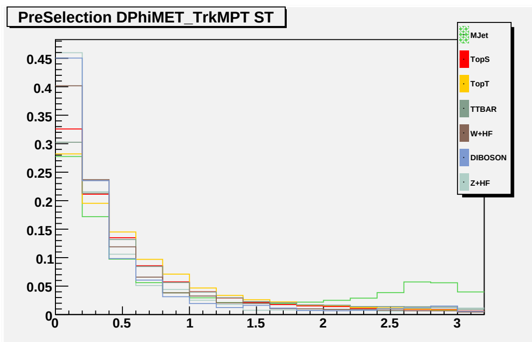

(c) $\Delta\phi(\not{p}_T^{tr}, \not{E}_T)$

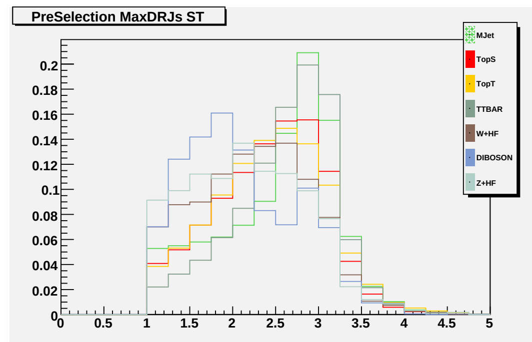

(d) Max($\Delta R(J_i, J_k)$)

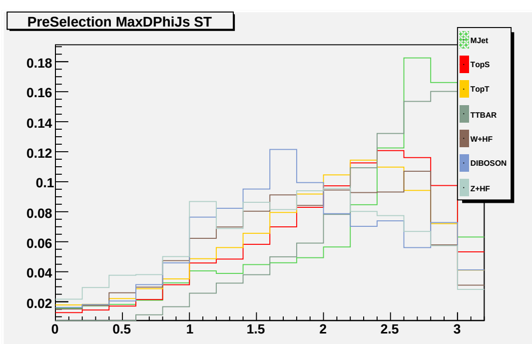

(e) Max($\Delta\phi(J_i, J_k)$)

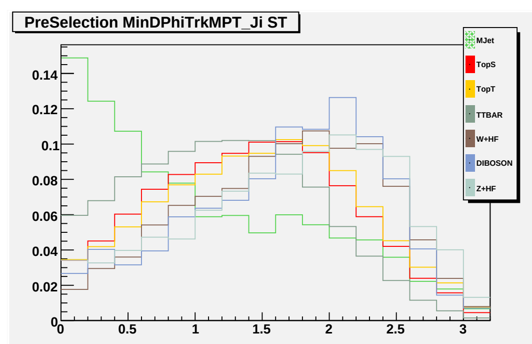

(f) Min($\Delta\phi(\not{p}_T^{tr}, J_i)$)

Figure 69: Pre-selection, Excl. Single Tag

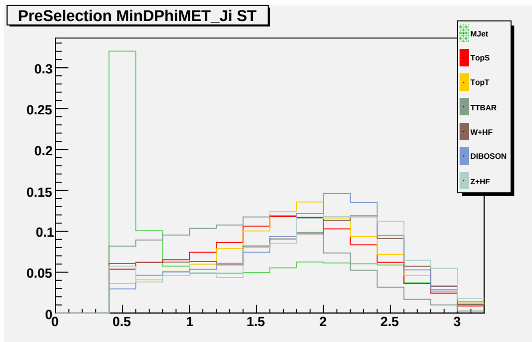

(a) Min($\Delta\phi(\not{E}_T, J_i)$)

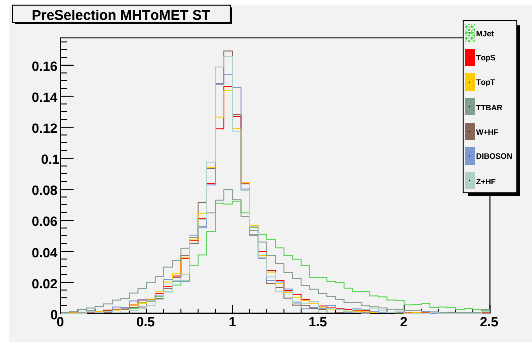

(b) $\not{H}_T/\not{E}_T$

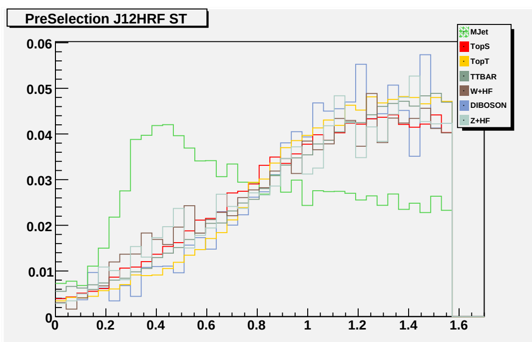

(c) $\Delta\phi(\mathrm{J1/2\ in\ RF, boost})$

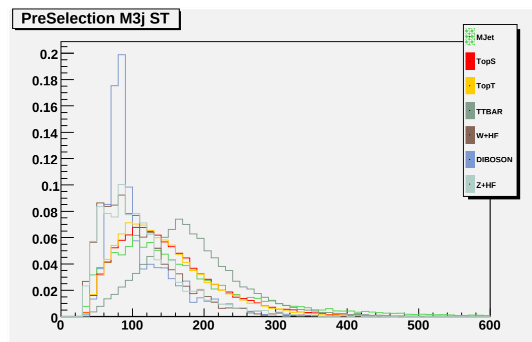

(d) Inv. mass between the two (or three) leading jets

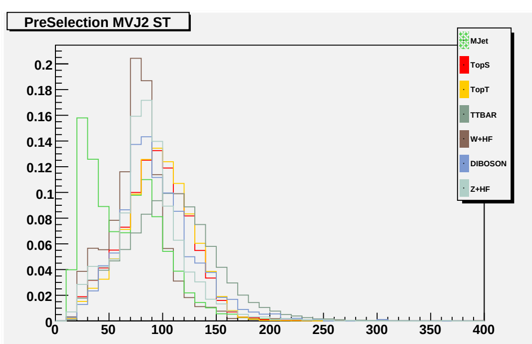

(e) Inv. mass between $\not{E}_T$ and the second leading jet

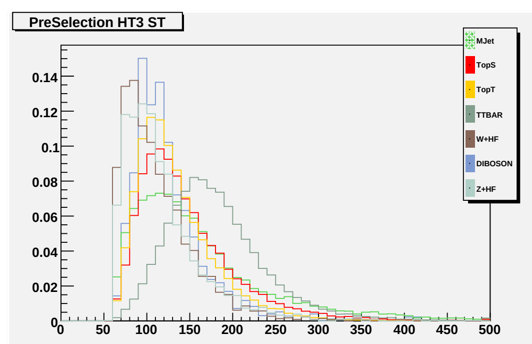

(f) H_T^3

Figure 70: Pre-selection, Excl. Single Tag

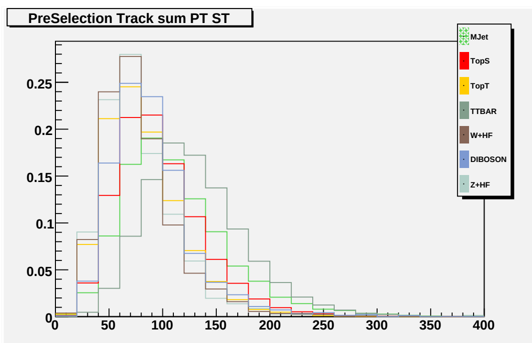

(a) $\sum P_T^{tr}$

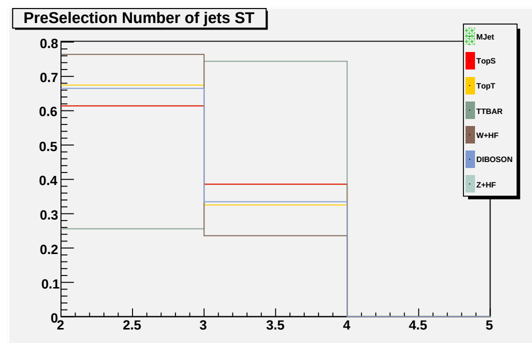

(b) Number of jets

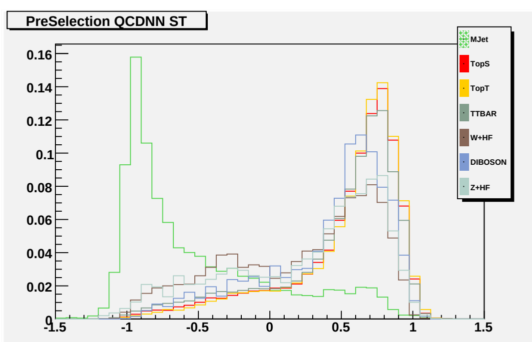

(c) QCDNN

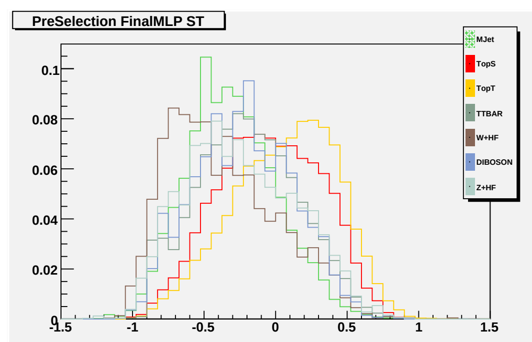

(d) Final MLP Discriminant

Figure 71: Pre-selection, Excl. Single Tag

B.2.2 ST + ST

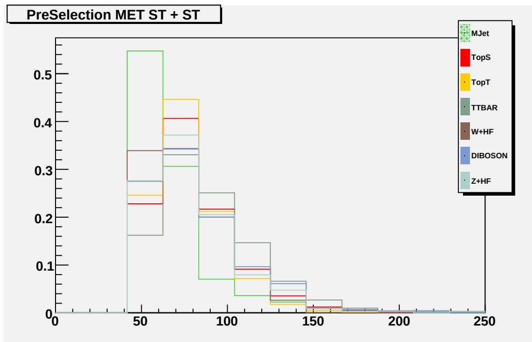

(a) $\not\!\!E_T$

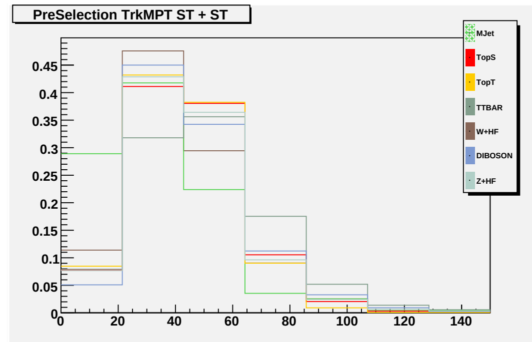

(b) $\not\!p_T^{tr}$

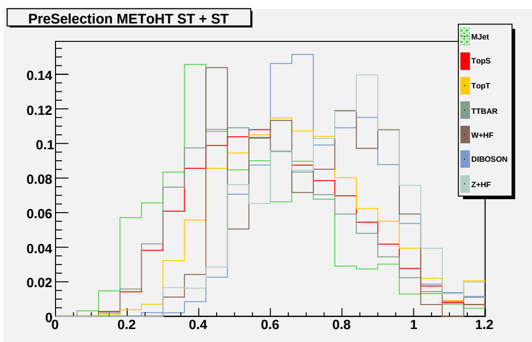

(c) $\not\!\!E_T/HT$

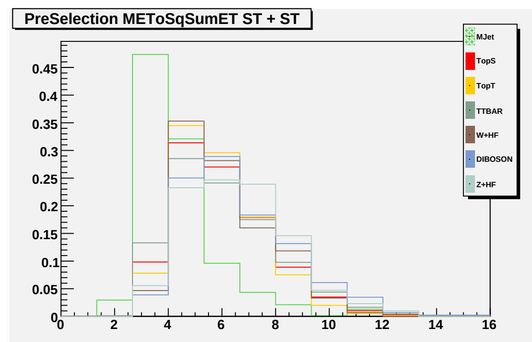

(d) $\not\!\!E_T$ Signifiance

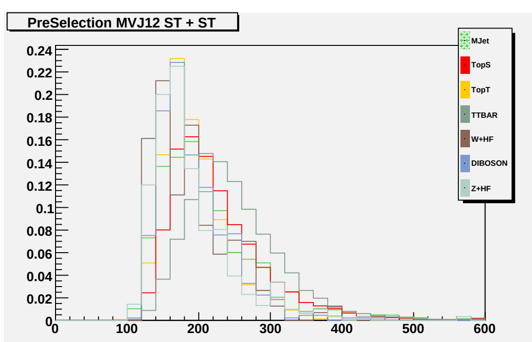

(e) Inv. mass between $\not\!\!E_T$ and the two leading jets

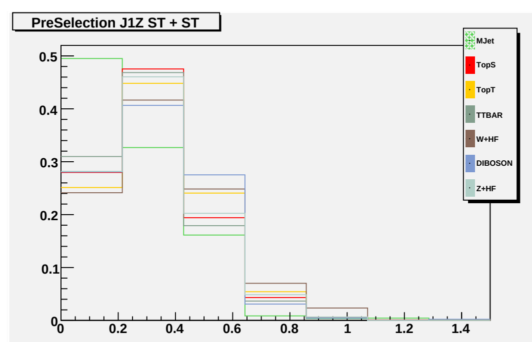

(f) Jet 1 Z

Figure 72: Pre-selection, ST + ST

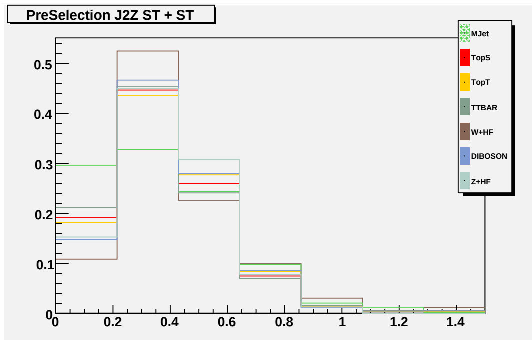

(a) Jet 2 Z

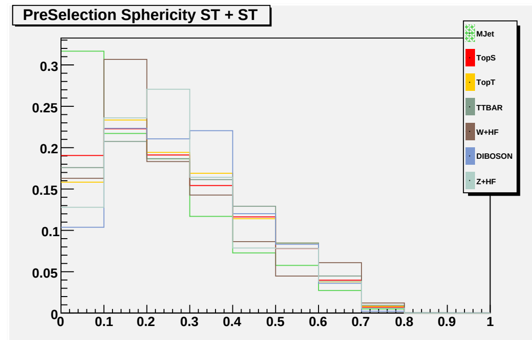

(b) Sphericity

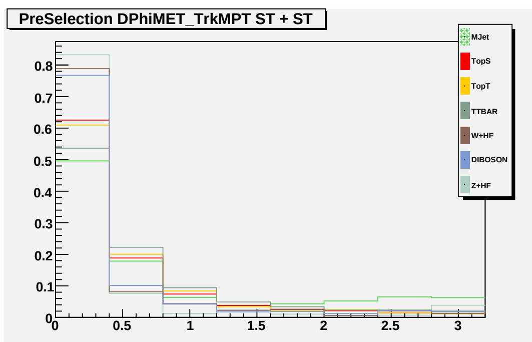

(c) $\Delta\phi(\not{p}_T^{tr}, \not{E}_T)$

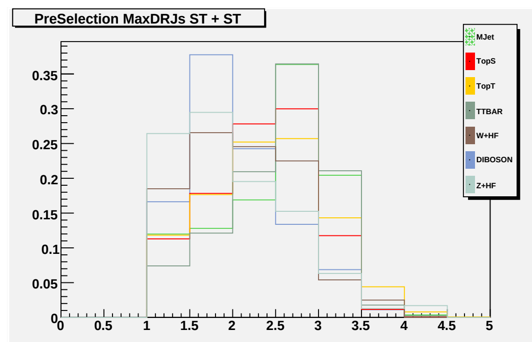

(d) $\mathrm{Max}(\Delta R(J_i, J_k))$

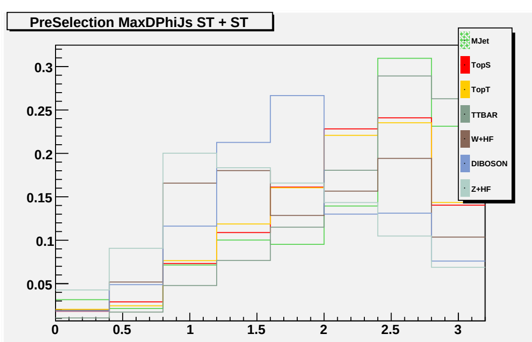

(e) $\mathrm{Max}(\Delta\phi(J_i, J_k))$

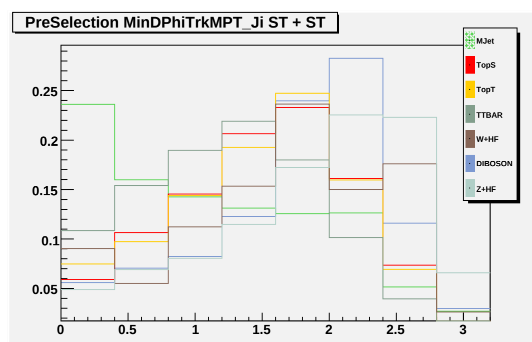

(f) $\mathrm{Min}(\Delta\phi(\not{p}_T^{tr}, J_i))$

Figure 73: Pre-selection, ST + ST

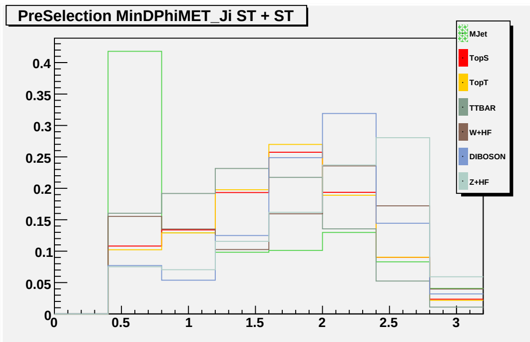

(a) Min($\Delta\phi(\not{E}_T, J_i)$)

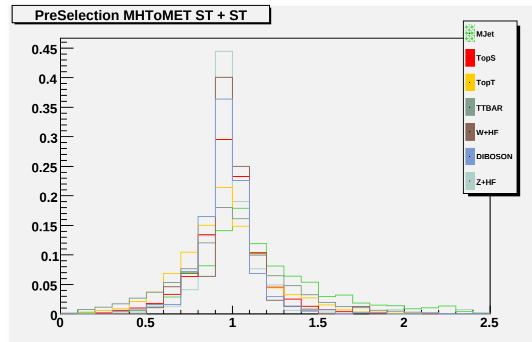

(b) $\not{H}_T/\not{E}_T$

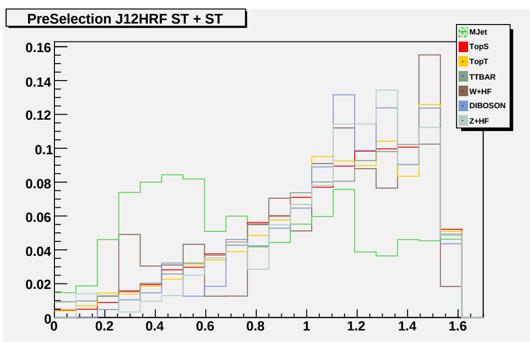

(c) $\Delta\phi$(J1/2 in RF, boost)

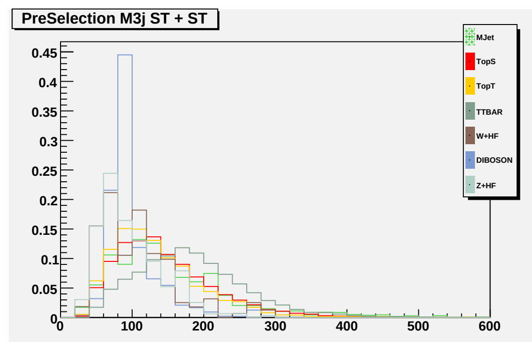

(d) Inv. mass between the two (or three) leading jets

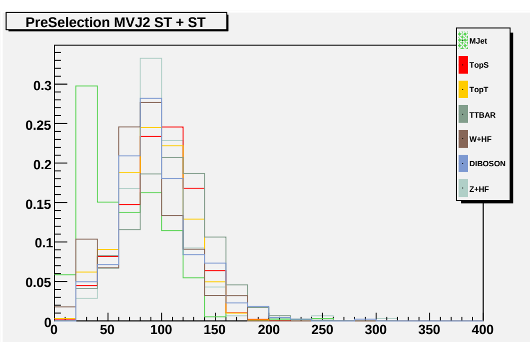

(e) Inv. mass between $\not{E}_T$ and the second leading jet

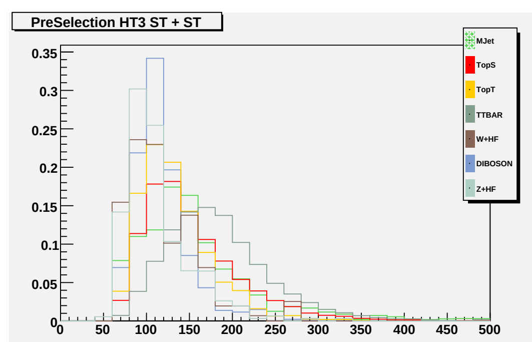

(f) H_T^3

Figure 74: Pre-selection, ST + ST

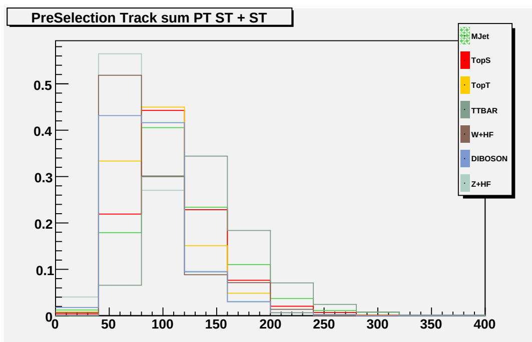

(a) $\sum P_T^{tr}$

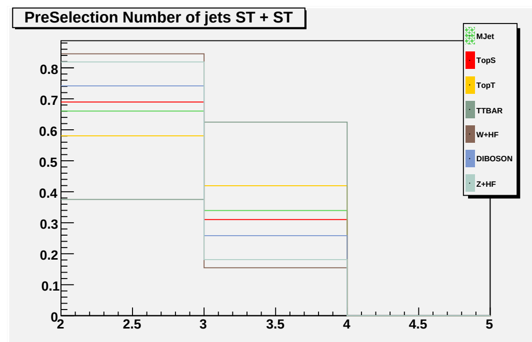

(b) Number of jets

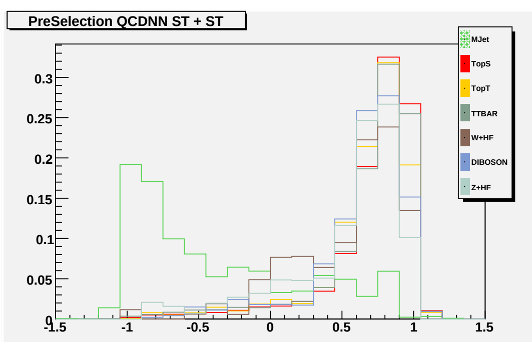

(c) QCDNN

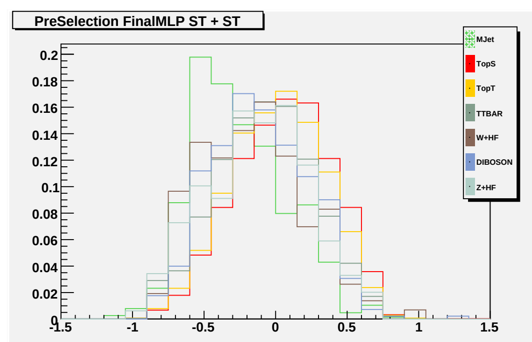

(d) Final MLP Discriminant

Figure 75: Pre-selection, ST + ST

B.2.3 ST + JP

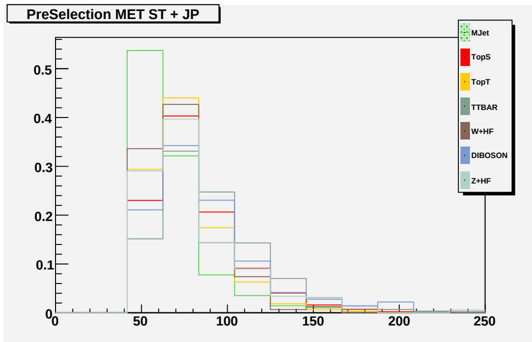

(a) $\not\!\!E_T$

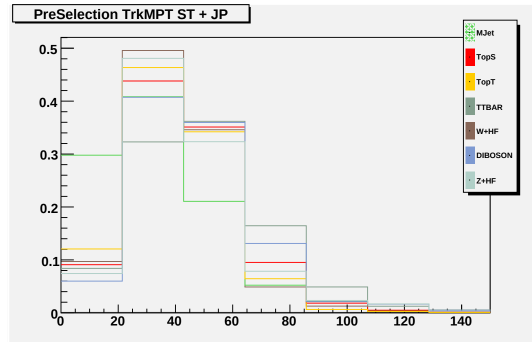

(b) $\not\!p_T^{tr}$

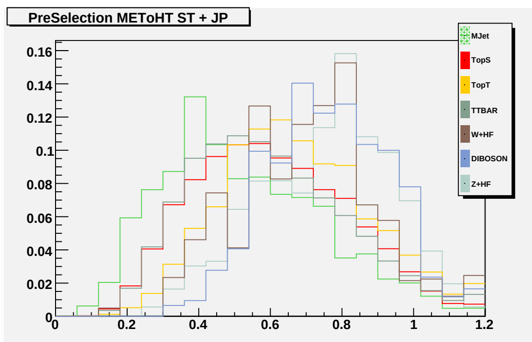

(c) $\not\!\!E_T/HT$

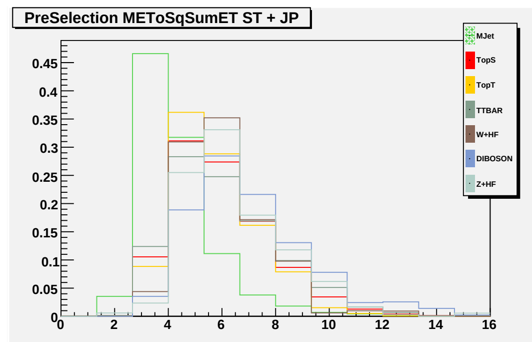

(d) $\not\!\!E_T$ Signifiance

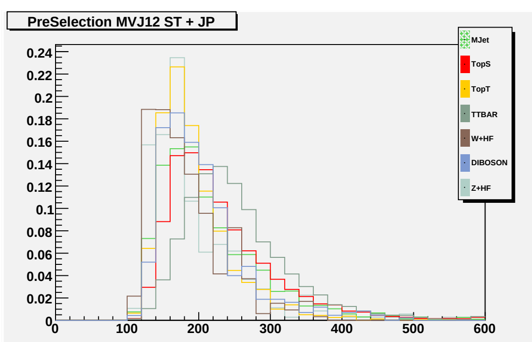

(e) Inv. mass between $\not\!\!E_T$ and the two leading jets

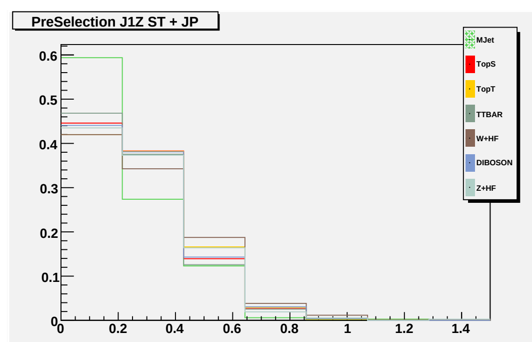

(f) Jet 1 Z

Figure 76: Pre-selection, ST + JP

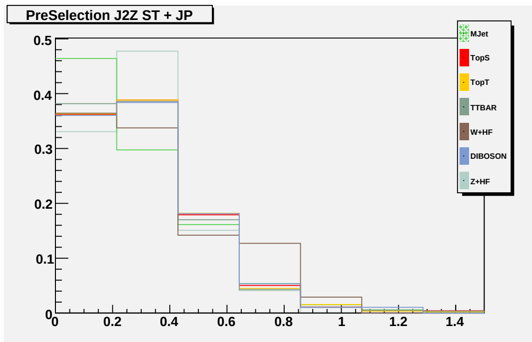

(a) Jet 2 Z

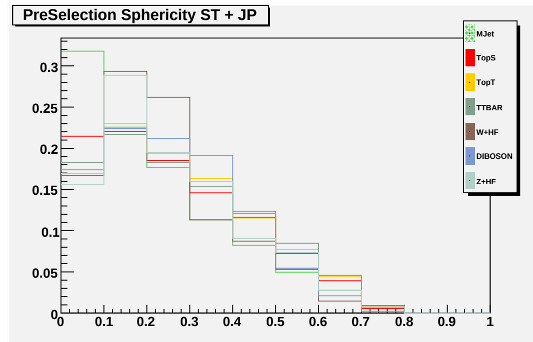

(b) Sphericity

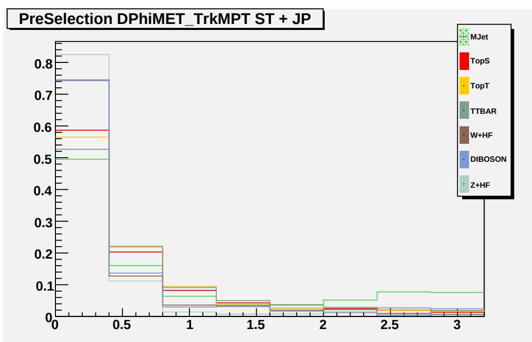

(c) $\Delta\phi(\not{p}_T^{tr}, \not{E}_T)$

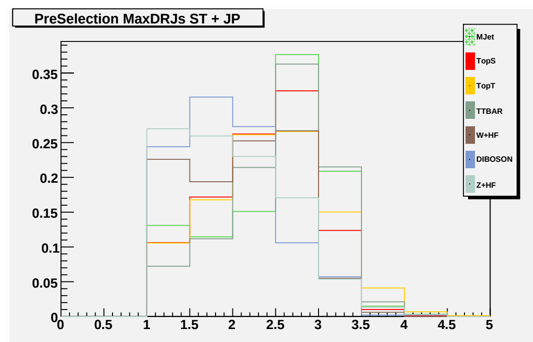

(d) Max($\Delta R(J_i, J_k)$)

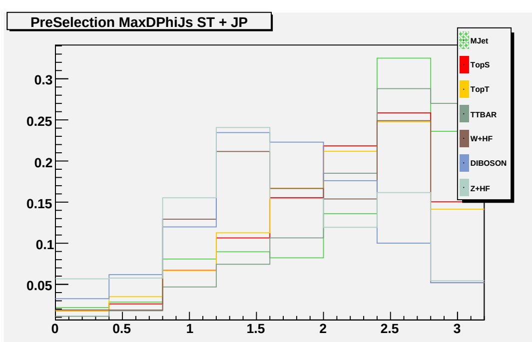

(e) Max($\Delta\phi(J_i, J_k)$)

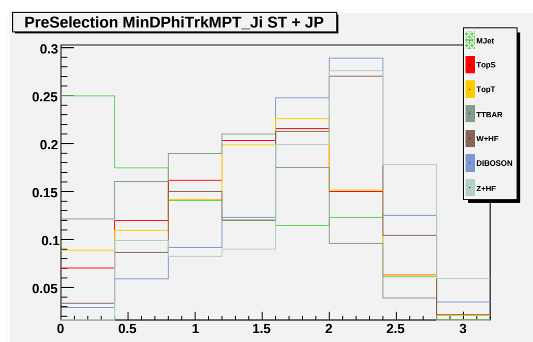

(f) Min($\Delta\phi(\not{p}_T^{tr}, J_i)$)

Figure 77: Pre-selection, ST + JP

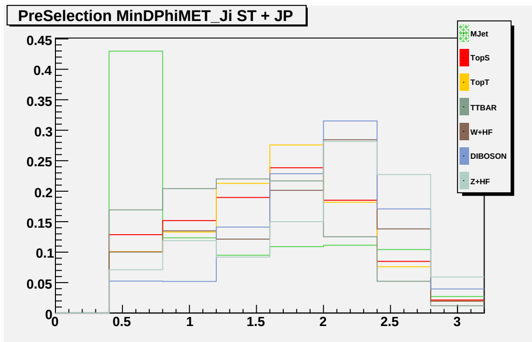

(a) Min($\Delta\phi(\not\!\!E_T, J_i)$)

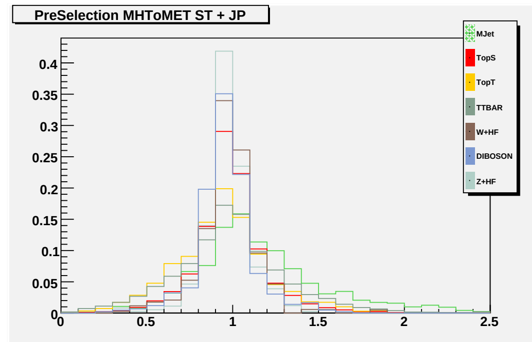

(b) $\not\!\!H_T/\not\!\!E_T$

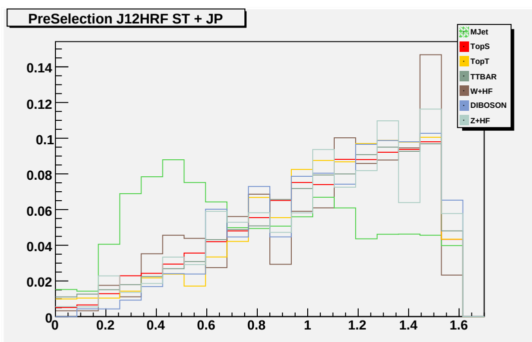

(c) $\Delta\phi(\text{J1/2 in RF, boost})$

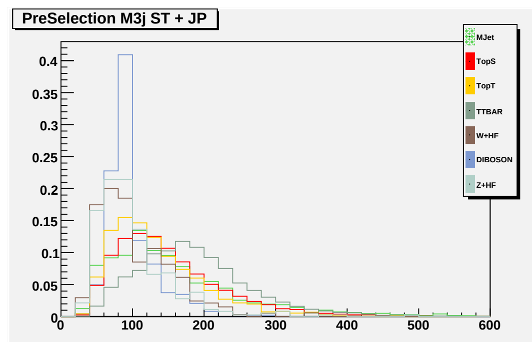

(d) Inv. mass between the two (or three) leading jets

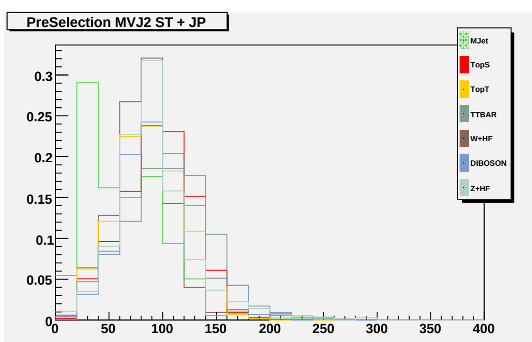

(e) Inv. mass between $\not\!\!E_T$ and the second leading jet

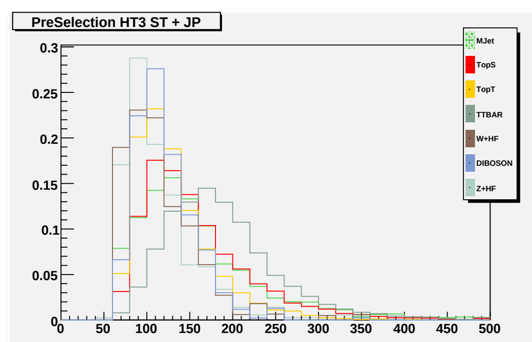

(f) H_T^3

Figure 78: Pre-selection, ST + JP

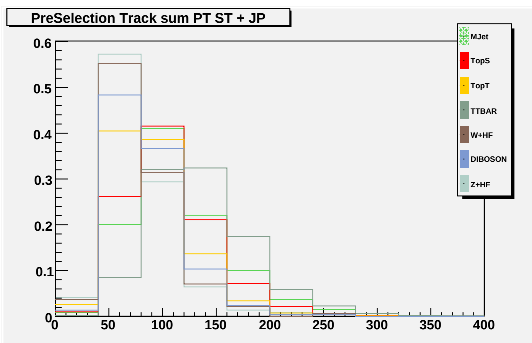

(a) $\sum P_T^{tr}$

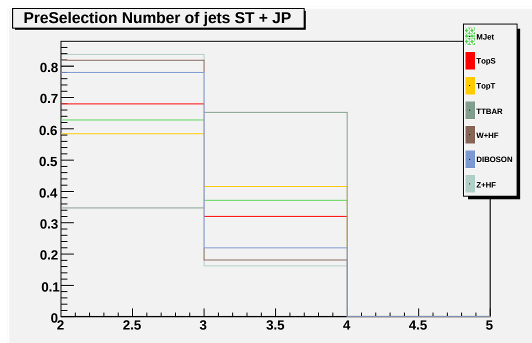

(b) Number of jets

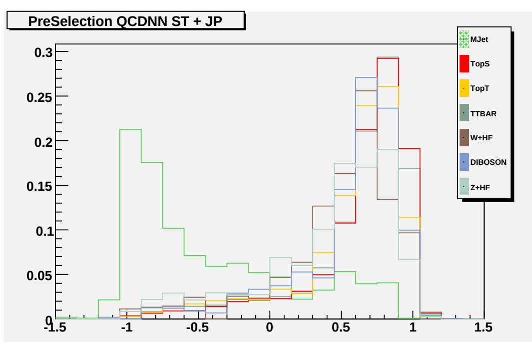

(c) QCDNN

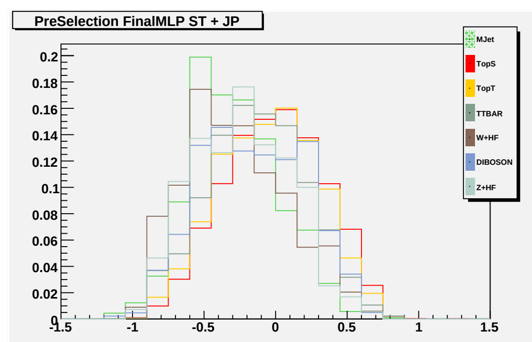

(d) Final MLP Discriminant

Figure 79: Pre-selection, ST + JP

C Shape Systematics Plots

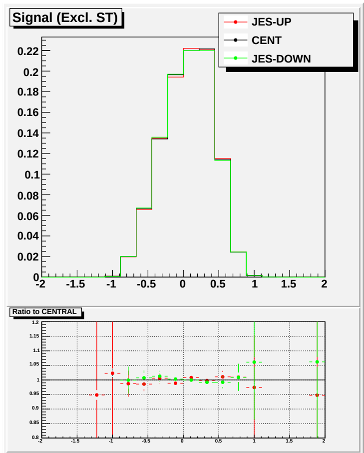

(a) Signal, Excl. ST

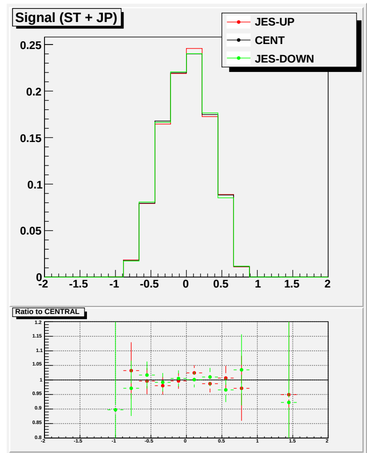

(b) Signal, ST + JP

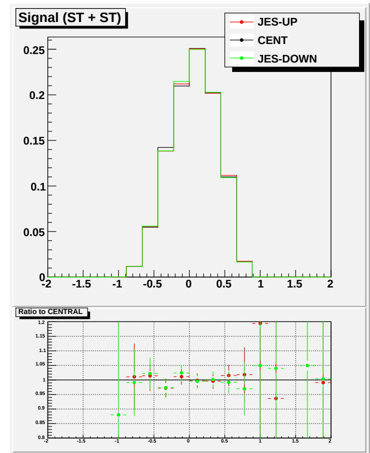

(c) Signal, ST + ST

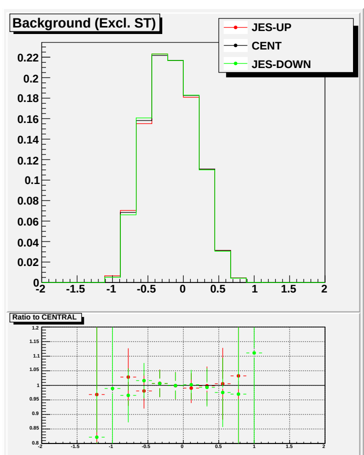

(d) Background, Excl. ST

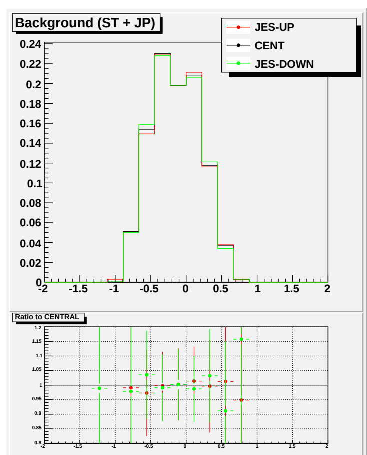

(e) Background, ST + JP

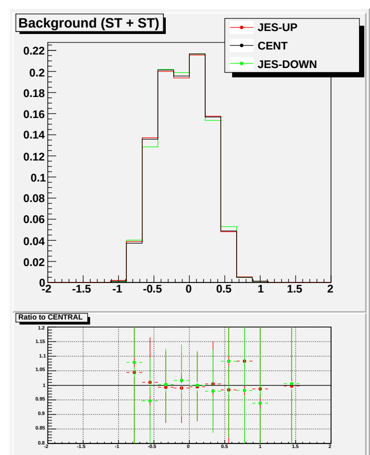

(f) Background, ST + ST

Figure 80: Jet energy scale shape systematic. The lower plot shows the ratio of the shape systematic to the central histogram.

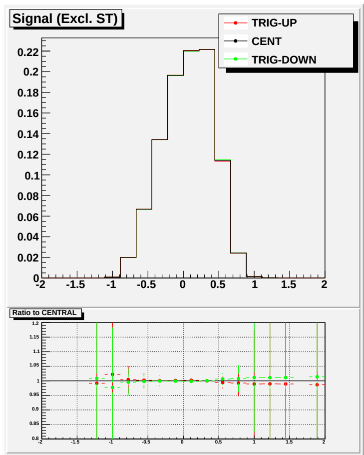

(a) Signal, Excl. ST

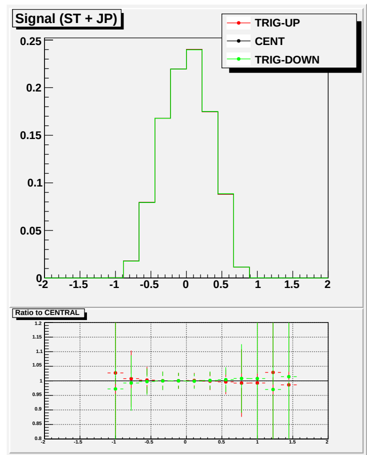

(b) Signal, ST + JP

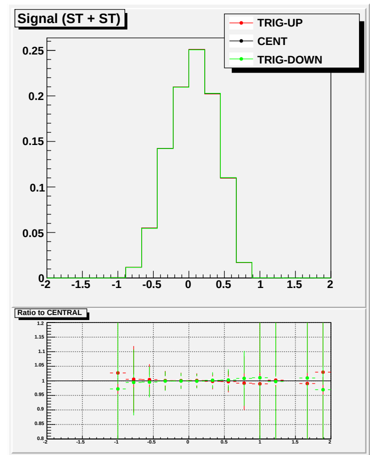

(c) Signal, ST + ST

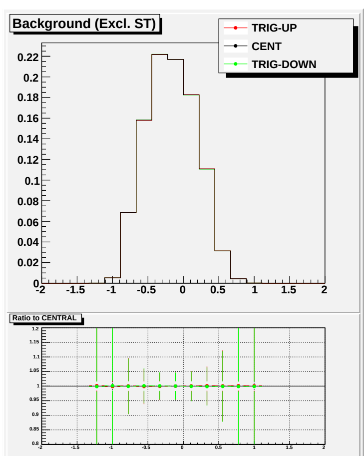

(d) Background, Excl. ST

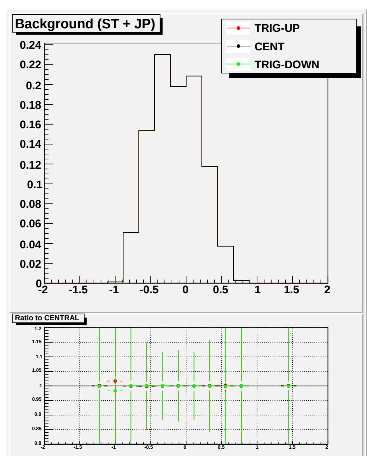

(e) Background, ST + JP

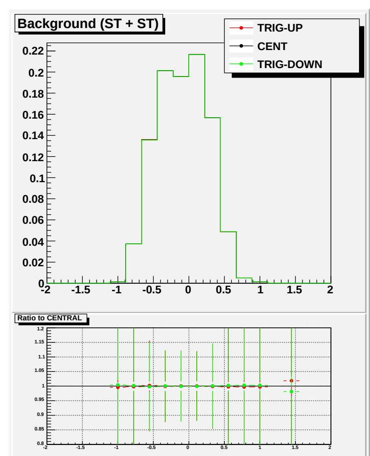

(f) Background, ST + ST

Figure 81: Trigger shape systematic. The lower plot shows the ratio of the shape systematic to the central histogram.

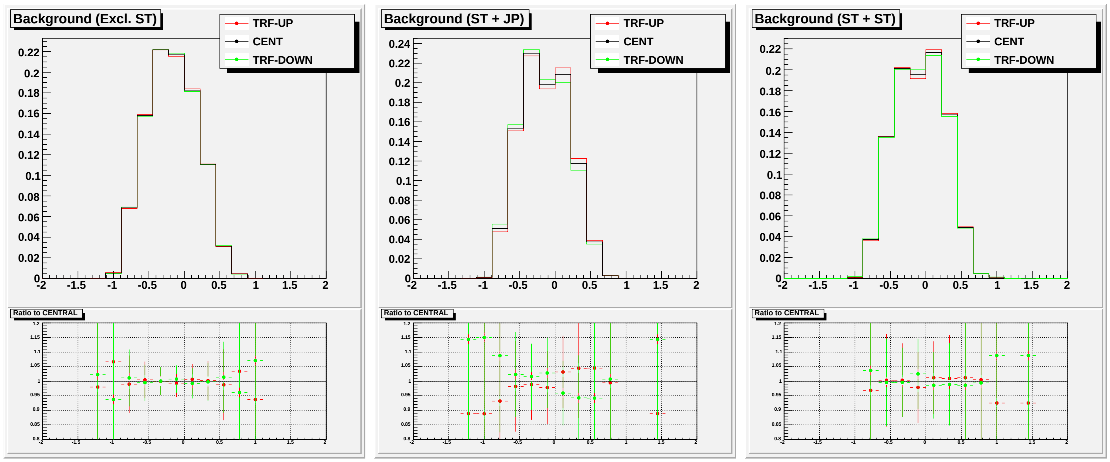

(a) Background, Excl. ST (b) Background, ST + JP (c) Background, ST + ST

Figure 82: Tag Rate Function shape systematic. The lower plot shows the ratio of the shape systematic to the central histogram.

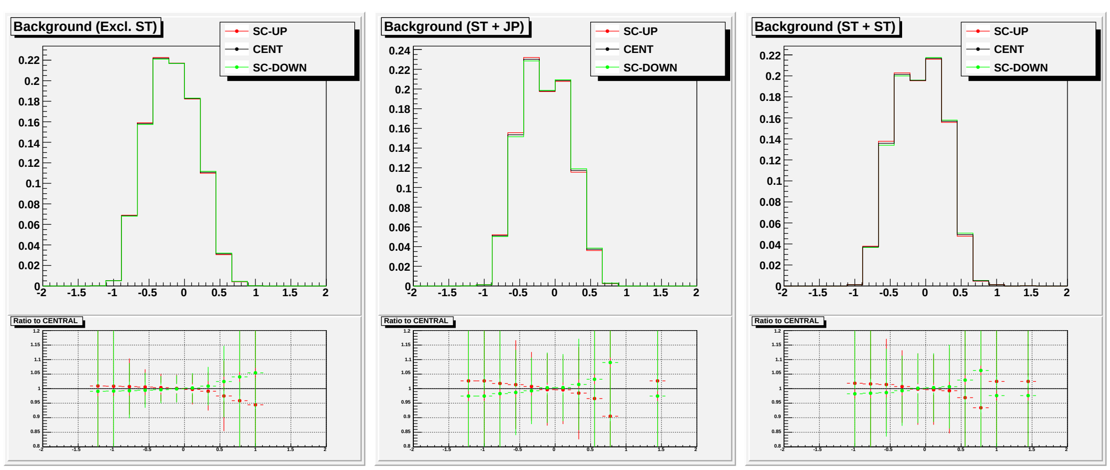

(a) Background, Excl. ST (b) Background, ST + JP (c) Background, ST + ST

Figure 83: Signal contamination shape systematic. The lower plot shows the ratio of the shape systematic to the central histogram.

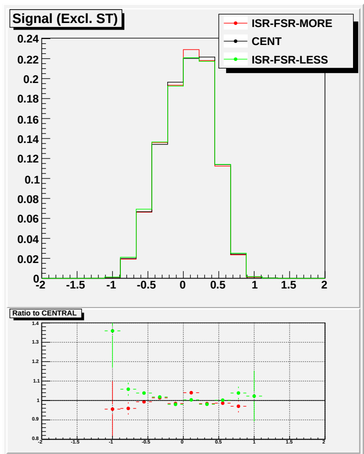

(a) Signal, Excl. ST

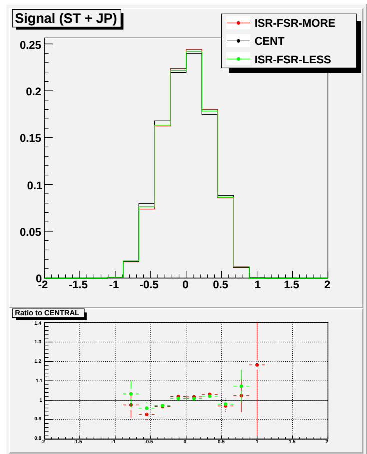

(b) Signal, ST + JP

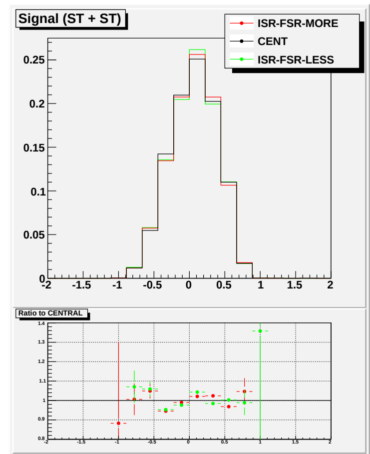

(c) Signal, ST + ST

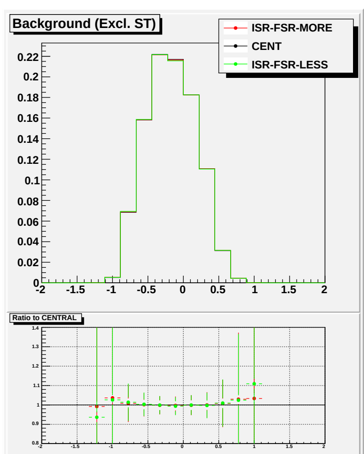

(d) Background, Excl. ST

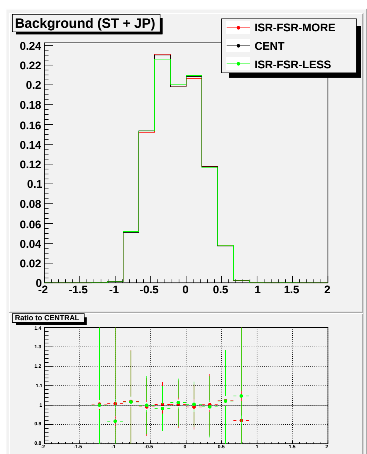

(e) Background, ST + JP

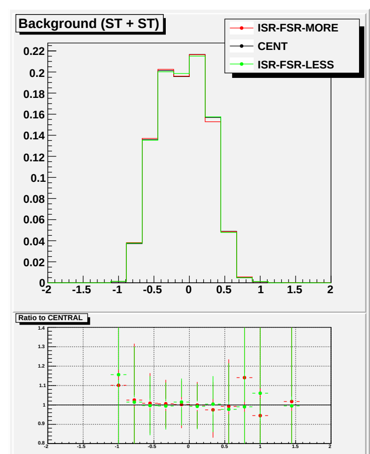

(f) Background, ST + ST

Figure 84: ISR/FSR shape systematic. The lower plot shows the ratio of the shape systematic to the central histogram.

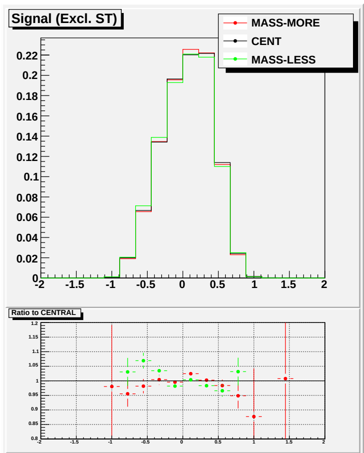

(a) Signal, Excl. ST

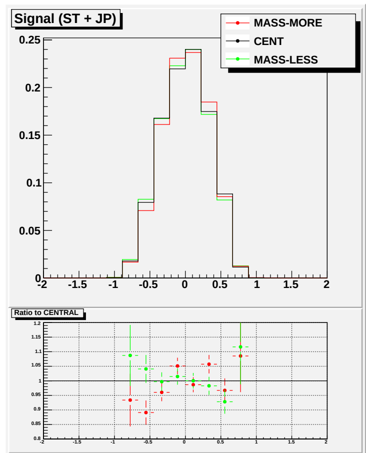

(b) Signal, ST + JP

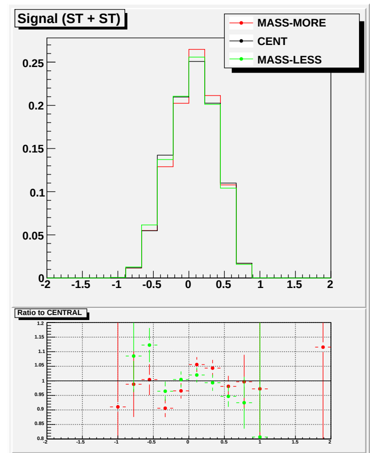

(c) Signal, ST + ST

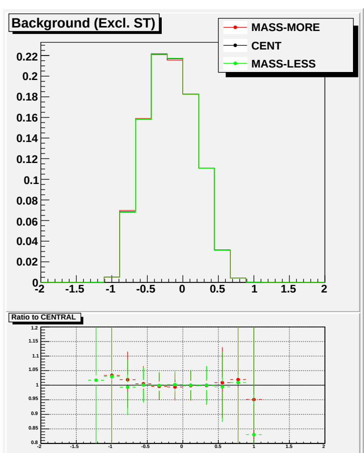

(d) Background, Excl. ST

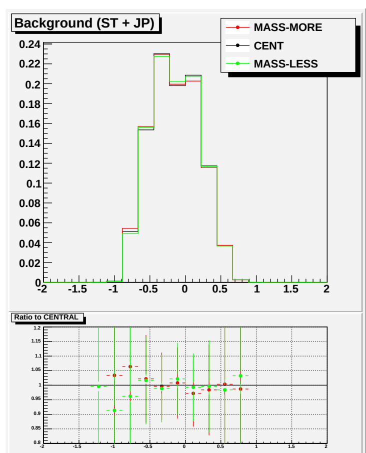

(e) Background, ST + JP

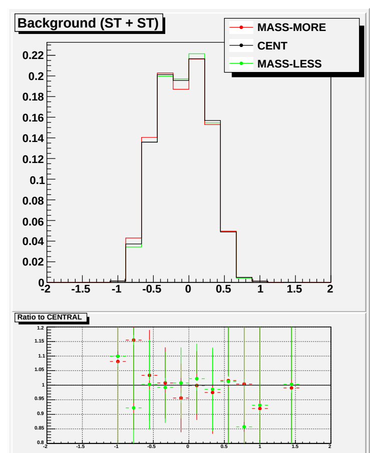

(f) Background, ST + ST

Figure 85: Top mass variation shape systematic. The lower plot shows the ratio of the shape systematic to the central histogram.